Molecular pathways leading to sleep and wakefulness in *Drosophila*

Katerina Christodoulou

Supervisor: Professor Gero Miesenböck

St. Anne's College

University of Oxford

In partial fulfilment of the requirements for the degree of Doctor of Philosophy

Trinity 2021

Acknowledgements

Much like the topic in this thesis, life moves in cycles; it is important to recognise that without the substantial support from people around me, the “cycle” of my PhD would be slow, monotonous, and extremely difficult. Therefore, I would like to acknowledge everyone who has made these past few years a beautiful journey. First and foremost, I would like to thank my supervisor Gero Miesenböck for the opportunity to work in his lab and learn under his guidance. Most importantly for his encouragement during times of struggle, and for teaching me to never give up. I am grateful to Anissa Kempf and Diogo Pimentel for their excellent mentorship, kindness, and patience throughout the years; to Peter Hasenhütl and Eleftheria Vrontou for endless hours devoted to discussion and valuable advice; to Raffaele Sarnataro for his optimism, generous help, advice and support; to Lea Ballenberger for contributing a great deal into setting up a lot of laborious experiments; to Celina Hartmann for her invaluable help with fly work; to Clifford Talbot for his technical expertise and unlimited supply of positive energy. I would also like to acknowledge former and current members of the lab for their help: Laura Chan, Lukas Groschner, and Michael Song for being my first teachers in the lab, and subsequently, Ammerins de Haan for being a saviour in times of molecular biology crisis; Timothy Wong, Alina Krebbers, Laura Garmendia Sanchez, Olof Rorsman, Haram Park, Jan Kropf, Susanne Szydlowski, Giacomo Bertuzzi and Patrick Liu for their constant support and kind words through the years. I am also indebted to Fiona Woods and Ruth Brain for assisting in all lab and administration issues in the most efficient way possible. Lastly, to all the members of the CNCB, who created an inspiring environment where I was surrounded not only by exceptional scientists but also by friends who made it feel like home. The work in this thesis was supported by the Gotch memorial studentship.

To my loving family, whose unconditional support has shielded me through life, and to my little niece, Christina-Anna, whose smile never ceases to brighten up my day.

Declaration

I confirm that this thesis is the product of my own work and has not been submitted for any other academic award at this University or elsewhere.

Abstract

Sleep is a universal and highly conserved phenomenon across species; yet its operational mechanisms remain one of the greatest biological mysteries. In *Drosophila*, sleep homeostasis is largely mediated by the activity of neurons projecting to the dorsal fan-shaped body (dFB). Dopamine promotes wakefulness by inhibiting the activity of dFB neurons, switching them to a silent state. This wake-promoting effect is hypothesised to require the exocytosis of the potassium "leak" channel, Sandman, to the plasma membrane, where it exerts its effects by blunting the firing of the neurons. In the chronically sleep-deprived flies bearing a mutation for the *crossveinless-c (cv-c)* gene, the dFB neurons were previously found in electrical quiescence as well. It is therefore possible that in these mutants, Sandman resides at the plasma membrane of the neurons, reducing their excitability and causing insomnia in the flies. However, the signals responsible for Sandman's recycling to and from the plasma membrane remain elusive.

To visualise the exo-endocytic pathway of Sandman, I attempted to localise the channel with different fluorescent probes and identify proteins acting in the same pathway using genetic interaction experiments. Depletion of Sandman from the dFB neurons rescues the sleep loss of *cv-c* mutants, supporting the notion that insomnia in these flies results from the channel's presence at the plasma membrane. As *cv-c* encodes for a Rho GTPase-activating protein (Rho-GAP) and small GTPases are often regulated by neurotrophin-related pathways, sleep induction involving the Cv-c-Sandman pathway may further couple to the upstream action of neurotrophic molecules.

dFB-restricted interference with Toll-6, a receptor with neurotrophic function, reduces sleep. *Toll-6*/*cv-c* mutants mirror the sleepless phenotype of *cv-c* mutants, suggesting that Toll-6 may signal through Cv-c, conveying sleep pressure to the neurons. A mutation for *Drosophila neurotrophin 1 (DNT1)*, a ligand of Toll-6, also diminishes sleep. RNAi-mediated knockdown of *DNT1* in the R5 neurons, a defined input to the dFB, decreases sleep and abolishes sleep drive encoded by the circuit.

It is proposed here that activity-dependent release of DNT1 from the R5 neurons signals sleep pressure that is transduced by the Toll-6 receptor in the dFB neurons. Activation of the receptor likely feeds into a small GTPase cascade that involves Cv-c and Sandman.

Table of contents

List of figures

All figures excluding experimental data were created with BioRender.com.

- **Figures 1, 2, 16** and **31** aimed to provide illustration of published research (Donlea et al., 2014; Kempf et al., 2019; Pimentel et al., 2016) and of hypotheses described in chapters 2 and 3.
- Two-pore domain K^+ channel schematic in **Figure 3** was inspired and adapted from **(Enyedi & Czirják, 2010)**
- Schematic of dFB neurons in **Figure 8** was inspired and adapted from (Pimentel et al., 2016).
- **Figure 15** was inspired and adapted from the *pCFD6* cloning protocol available at www.CRISPRflydesign.org and described by (Port & Bullock, 2016).

Abbreviations

3IY	3-iodo-tyrosine
6-OHDA	6-Hydroxydopamine
aaRS	tRNA/aminoacyl-tRNA synthetase
ANOVA	Analysis of variance
AOX	Alternative oxidase
Arc	Activity-regulated cytoskeleton-associated protein
ASI	Axon-spine interface
AstA	Allatostatin A
BDNF	Brain-Derived Neurotrophic Factor
BDSC	Bloomington Drosophila Stock Centre
BoNT/C	Botulinum neurotoxin C
BRP	Bruchpilot
Ca-a1D	Ca^{2+}-channel protein α_1 subunit D
CamKII	Calcium/calmodulin-dependent protein kinase II
cDNA	Complementary deoxyribonucleic acid
CRISPR	Clustered Regularly Interspaced Short Palindromic Repeats
CS	Canton-S
Cv-c	Crossveinless-c
DA	Dopamine
DAM	Drosophila activity monitor
DAT	Dopamine transporter
dFB	Dorsal fan-shaped body
DGRC	Drosophila Genomics Resource Centre
DNA	Deoxyribonucleic acid
DNT1	*Drosophila* neurotrophin 1
DNT2	*Drosophila* neurotrophin 2
Dop1R2	Dopamine 1-like receptor 2
DSB	Double strand break
EB	Ellipsoid body
ECL	Extracellular loop
ER	Endoplasmic reticulum
FBS	Fetal bovine serum
GABA	Gamma-aminobutyric acid
Gad1	Glutamic acid decarboxylase 1

GFP	Green fluorescent protein
gRNA	Guide ribonucleic acid
GSK-3β	Glycogen synthase kinase-3β
H_2O_2	Hydrogen peroxide
HDR	Homology-directed repair
HEK	Human embryonic kidney
Hk	Hyperkinetic
HV	Head volume
Inc	Insomniac
IP3R	Inositol trisphosphate receptor
K2P	Two-pore domain potassium channel
KCNK	Potassium Two Pore Domain Channel Subfamily K
LC	Locus coeruleus
LH	Left hemisphere
LTD	Long-term depression
LTP	Long-term potentiation
MES	2-(*N*-morpholino)ethanesulfonic acid
mGluR	Metabotropic glutamate receptor
mRNA	Messenger ribonucleic acid
NA	Noradrenaline
NGF	Nerve growth factor
NGS	Normal goat serum
NH_4Cl	Ammonium Chloride
NHEJ	Non-homologous end joining
NMDAR	N-methyl-D-aspartate receptor
NREM	Non-rapid eye movement
OE-PCR	Overlap extension polymerase chain reaction
PAL	Protocerebral anterior lateral
PAM	Protocerebral anterior medial
PBS	Phosphate buffered saline
p-CREB	Phosphorylated- Cyclic AMP response element-binding protein
PPD	Protocerebral posterior dorsal
PPL	Protocerebral posterior lateral
PPM	Protocerebral posterior medial
Process C	Circadian process
Process S	Homeostatic process

PSD	Postsynaptic density
RH	Right hemisphere
Rho-GAP	Rho-GTPase activating protein
RNAi	Ribonucleic acid interference
ROI	Region of interest
ROS	Reactive oxygen species
Sand	Sandman
SEM	Standard error of the mean
SEP	Somatosensory evoked potentials
Sh	Shaker
SHY	Synaptic homeostasis hypothesis
SOD1	Superoxide dismutase 1
SOG	Subesophageal ganglion
Spz	Spätzle
SWA	Slow wave activity
SWS	Slow wave sleep
T1	Thoracic 1
TALK	TWIK-related alkaline pH-activated K^+channel
TASK	TWIK-related acid-sensitive K^+ channel
THIK	Tandem pore domain halothane-inhibited K^+ channel
TM	Transmembrane domain
TREK	TWIK-related K^+ channel
TRESK	TWIK-related spinal cord K^+ channel
TrkB	Tyrosine receptor kinase B
tRNA	Transfer ribonucleic acid
TrpA	Transient receptor potential cation channel A1
TuBu	Tubercular-Bulbar
TWIK	Tandem of pore domains in a weak inward rectifying K^+ channel
TyrII	Tyramine II (TyrII)
VDRC	Vienna Drosophila Resource Centre
VLPO	Ventrolateral preoptic nucleus
WT	Wild-type
YW	Yellow-white
ZT	Zeitgeber

Chapter 1

SLEEP HOMEOSTASIS IN *DROSOPHILA*

"In the first place, sleep comes on when the power of spirit is drawn apart through the body, part being cast forth has gone away, and part more crowded together has retreated into the depths; for only then the limbs loosen and become flaccid. For there is no doubt that this feeling in us comes about by action of the spirit, and when sleep hinders the feeling so that there is none, then we must suppose that the spirit has been disordered and cast forth without; but not all, for then the body would lie pervaded with the everlasting cold of death; since of course if no part of the spirit were left hidden in the limbs, like fire covered in a heap of ashes, whence could the feeling be suddenly rekindled throughout the limbs and arise like a flame from the hidden fire?"

Lucretius, De Rerum Natura, VI, 916-928

1.1 INTRODUCTION

From mythology to modern literature and cinematography, the enigmatic nature of sleep has captured the interest of various forms of arts throughout the centuries. In his poem De Rerum Natura, Lucretius's description of the induction of sleep reflects the theories of that era on what the physiological cause of sleep may be. Lucretius envisioned that sleep is forced upon species by the depletion of the "pneuma psychikon" (vital spirit) during wakefulness (Lucretius Carus et al., 1924). Others like Aristotle and Galen shared similar views, suggesting that sleep restores the "aesthesis" (sense-perception) or "dynamis" (power) (Eijk & Hulskamp, 2019). Strikingly, these early philosophies retain one fundamental principle that characterises sleep models even today. The one conclusion that all of them arrive to is the unique ability of sleep to restore; may that be the "pneuma psychikon", the "aesthesis" or the "dynamis".

Centuries later, a convergence of work in the fields of chronobiology, neurochemistry, and neurophysiology has eventually led to the establishment of a model called the "two-process model" to explain sleep (Borbély, 1982; Daan et al., 1984). The two-

process model posits that sleep is regulated by two processes that interact with each other: the circadian process (process C) and the homeostatic process (process S). The circadian process C refers to the circadian clock, which is synchronised to the 24h period of the day and whose oscillations reflect the day and night cycles (Borbély et al., 2016). The homeostatic process S reflects the accumulation of sleep debt during wakefulness and its dissipation while sleeping (Borbély et al., 2016). Both processes restart in the morning once the sleep drive has been removed and the circadian clock resets (Borbély et al., 2016). One physiological hallmark of process S is increased slow-wave activity (SWA) during sleep. The "sleep homeostasis" term derives from observations where sleep deprivation is followed by an increased amount of sleep in the following days (rebound sleep) and by increases in the slow wave sleep (SWS) intensity and duration (Borbély et al., 2016). Based on the conceptual framework of the two-process model, modern theories of what the physiological function fulfilled by sleep is, have evolved. One of these theories is summarised below.

1.2 SYNAPTIC HOMEOSTASIS HYPOTHESIS

The synaptic homeostasis hypothesis (SHY) is one of the most prevalent modern hypotheses, stating that sleep is the "the price we pay for plasticity" (Tononi & Cirelli, 2003; Tononi & Cirelli, 2014, 2020). It proposes that during wakefulness, there is an overall increase in the net synaptic strength due to ongoing learning while sleep is required for synaptic renormalisation. In this regard, synaptic potentiation occurs during wakefulness, whereas renormalisation occurs during sleep where the spontaneous activity of the brain is less biased by external stimuli.

Monoaminergic signalling is correlated with wakefulness by virtue of its inhibition to sleep centres in the brain (Saper et al., 2010). Unilateral injection of the neurotoxin 6-hydroxydopamine (6-OHDA) in rats, destroys the catecholaminergic neurons of the locus coeruleus (LC) and abolishes almost completely the expression of immediate early genes such as c-FOS and of the phosphorylated-cyclic adenosine monophosphate response element-binding protein (p-CREB) (Cirelli et al., 1996). In non-lesioned controls, and on the

intact side of lesioned controls, these genes are induced normally after spontaneous waking and following sleep deprivation (Cirelli et al., 1996). In a subsequent study, mRNA levels of the brain-derived neurotrophic factor (BDNF) and activity regulated cytoskeleton-associated protein (Arc) were also increased in the cerebral cortex of rats following the same conditions; spontaneous wakefulness and sleep deprivation (Cirelli & Tononi, 2000). Thus, wakefulness enhances the expression of genes involved in synaptic plasticity and their induction depends on the action of wake-promoting neurotransmission.

Interestingly, in rats, the period of enriched exploratory behaviour is positively correlated with expression of BDNF in the cortex (Huber et al., 2007). The amount of BDNF induction is proportional to the SWA response in the subsequent sleep period as well (Huber et al., 2007). To directly assess whether BDNF manipulations alter SWA, BDNF was injected into the cortex of rats and the intensity of SWA was measured (Faraguna et al., 2008). Injection of BDNF selectively increases SWA during non-REM sleep (NREM) while blocking a BDNF receptor, the receptor tyrosine kinase B (TrKB), attenuates it (Faraguna et al., 2008).

In humans, exposure to a visuomotor learning task is associated with a local increase in SWA in the right parietal cortex, an area known to be involved in the learning paradigm (Huber et al., 2004). Testing of the task after sleep improves the performance of the subjects on the following day. In contrast, arm immobilisation with a sling and bandage decreases motor performance in a reaching task, reduces somatosensory evoked potentials (SEP) and induces a local decrease in SWA (Huber et al., 2006). These changes occurred in the right sensorimotor cortex, an area where SEP peaked before immobilisation (Huber et al., 2006). Engagement in learning paradigms during wakefulness is therefore not only associated with the induction of genes involved in synaptic plasticity but also with local increases in SWA. Thus, SWA architecture can be indicative of changes in synaptic homeostasis.

AMPA receptor trafficking and changes in the phosphorylation status of the receptors are among the best established molecular markers of long term potentiation (LTP) and long term depression (LTD) (Citri & Malenka, 2008). In synaptoneurosomes of

rats, the protein levels of GluR1-containing AMPA receptors, the phosphorylation levels of the GluR1 subunit at Ser 831, and the phosphorylation of Calcium/calmodulin-dependent protein kinase II (CamKII) and Glycogen synthase kinase-3β (GSK3β) in the cortex and hippocampus of rats are all increased during wakefulness (Vyazovskiy et al., 2008).

Accordingly, electrophysiological experiments that measure synaptic strength show increases after wakefulness and decreases after rest (Vyazovskiy et al., 2008). The increase in synaptic strength positively correlates with SWA at the onset of sleep following enforced wakefulness as well (Vyazovskiy et al., 2008). Therefore, the molecular and electrophysiological data imply that wakefulness is associated with an increase in net synaptic strength linked to sleep homeostasis. While this study provides possible molecular candidates underpinning synaptic potentiation during wakefulness, a recent study implicated a synaptic downscaling role for the short isoform of Homer protein, Homer1a (Diering et al., 2017).

In mice, Homer1a expression is increased during sleep and following sleep deprivation in the post-synaptic density (PSD) (Diering et al., 2017). Co-immunoprecipitations demonstrate that once localised in the PSD, Homer1a causes the disassemble of synaptic plasticity receptor complexes formed by Type I metabotropic glutamate receptor (mGluR5) and IP_3 receptors (IP3R) (Diering et al., 2017). Increasing noradrenaline (NA) levels by injecting D-amphetamine at the onset of sleep is enough to block expression of Homer1a in the PSD. In contrast, injecting an adenosine A1 receptor antagonist abolishes the sleep-deprivation induction of Homer1a in the PSD (Diering et al., 2017). An elegant mechanism is thus proposed to explain downscaling.

During wakefulness, when the levels of the wake promoting NA are high (Aston-Jones & Bloom, 1981), the absence of Homer1a from the PSD, allows formation of mGluR5-IP3 receptor complexes and synaptic strengthening (Diering et al., 2017). At the onset of sleep, when NA levels are low and the sleep promoting adenosine (Benington & Heller, 1995; Halassa et al., 2009) is released, Homer1a enters the PSD, disrupting mGluR5-IP3 receptor complexes and leading to mGluR5 independent signalling and synaptic weakening (Diering et al., 2017).

Finally, it was shown using three-dimensional electron microscopy that a large proportion of synapses in layer 2 of primary motor and primary somatosensory cortices of mice weaken during sleep when two parameters were measured: the axon-spine interface (ASI) and the volume of the spine head (HV) (De Vivo et al., 2017). Overall, 80% of the synapses was renormalised during sleep (De Vivo et al., 2017). The scaling was selective in that this 80% encompassed small and medium sized synapses. Synapses that were less likely to go through scaling shared three characteristics: they were large, lacked a recycling endosome and were found in environments crowded by dendritic branches (De Vivo et al., 2017). Addressing each of these features separately will be important in further elucidating the defining characteristics of synaptic remodelling during sleep.

Summarising, SHY proposes that sleep is the state during which synaptic renormalisation occurs, leading to the down-scaling of synapses and to the restoration of cellular energy consumption levels. Once renormalisation of the net synaptic strength is achieved and energy stores are refilled, the connection to the external world can resume (Tononi & Cirelli, 2003; Tononi & Cirelli, 2014, 2020).

1.3 SLEEP HOMEOSTASIS IN *DROSOPHILA*

Despite variations in the duration and timing of sleep, this naturally occurring phenomenon appears to be evolutionarily conserved across species (Keene & Duboue, 2018). Over the years, different parameters and methodologies have been developed to describe sleep architecture in terms of quality and duration in different species. In mammals, behavioural hallmarks that characterise sleep include immobility, a preferred rest posture, an increase in sleep intensity following its disruption and the ability to reverse back to wakefulness following a stimulus (Campbell & Tobler, 1984; Siegel, 2005). *Drosophila* shares a lot of the cardinal features that characterise sleep in mammals. They too, exhibit periods of immobility, state reversibility, and increased arousal thresholds after sleep deprivation (Hendricks et al., 2000; Shaw et al., 2000). Like humans, their sleep also becomes more fragmented with age (Koh et al., 2006) and is regulated by both a circadian and a homeostatic component (Hendricks et al., 2000; Shaw et al., 2000). The circadian clock has been explained in detail by transcriptional feedback loops (Dubowy & Sehgal, 2017); however, the homeostatic component of sleep has been more challenging to decode. The discussion below focuses on the fan-shaped body neurons, a circuit that lies at the core of homeostatic sleep control in *Drosophila*.

Fan-shaped body neurons

A cluster of neurons projecting to a dorsal layer of the fan-shaped body (dFB) of the central complex was the first sleep promoting circuit characterised in *Drosophila;* constitutive activation of the dFB neurons causes flies to sleep more (Donlea et al., 2011). (Donlea et al., 2011). The flies have heightened arousal thresholds and following sleep deprivation they exhibit a sleep rebound as well (Donlea et al., 2011). Taken together, these findings indicate the involvement of these neurons in sleep homeostasis. Remarkably, thermogenetic activation of the dFB neurons acutely induces sleep (Donlea et al., 2011).

Disruption of a Rho-GTPase-activating (Rho-GAP) protein encoded by *crossveinless-c* (*cv-c)*, causes flies to have dramatically fragmented sleep patterns and impairs sleep homeostasis; flies with the mutation are not able to recover the lost sleep

following sleep deprivation (Donlea et al., 2014). Notably, the insomniac phenotype of *cv-c* is mirrored in the electrical excitability of dFB neurons (Donlea et al., 2014). Under physiological conditions, the neurons exist in two electrical states: an electrically active state (ON state) and an electrically quiescent state (OFF state) (Donlea et al., 2014). The input resistance and time constant, two parameters reflecting the intrinsic electrical properties of neurons, are decreased in *cv-c* mutants, which is suggestive of reduced excitability (Donlea et al., 2014). The *cv-c* mutation prevents the dFB neurons from increasing their excitability after sleep loss, further indicating that the neurons are trapped in the OFF state in these flies and that the sleep homeostat is compromised (Donlea et al., 2014).

Dopaminergic input to dFB neurons

Dopamine (DA) is a well-known wake promoting neurotransmitter in flies (Andretic et al., 2005; Kume, 2005; Liu et al., 2012; Pimentel et al., 2016; Ueno et al., 2012). Flies with a disruption in the *dopamine transporter* (*DAT*) gene are severely sleepless (Kume, 2005). Consistent with this finding, flies fed with methamphetamine, display a decrease in their night-time sleep, while an inhibitor of dopamine synthesis (3IY) has the opposite effect, promoting sleep (Andretic et al., 2005).

Dopaminergic neurons in *Drosophila* are distributed among various clusters: the posterior protocerebrum lateral (PPL1, PPL2), protocerebral anterior lateral (PAL), protocerebral posterior medial (PPM1/2, PPM3), protocerebral anterior medial (PAM), subesophagal ganglion (SOG) and thoracic 1 (T1) clusters (Mao & Davis, 2009). Single dopaminergic neurons are also found within PPL3, PPL4, and PPL5 and protocerebral posterior dorsal (PPD) (Mao & Davis, 2009).

Thermogenetic activation of dopaminergic neurons residing in almost all clusters results in diminished night-time sleep (Liu et al., 2012). Restricting the activation to specific dopaminergic neurons that include a single neuron from each PPL1 cluster projecting to the dFB, mimics these results (Liu et al., 2012). In contrast, silencing these neurons,

increases sleep, suggesting that dopamine's wake-promoting effect depends on the PPL1-dFB connection (Liu et al., 2012).

Activating a single neuron from the PPM3 cluster projecting to the dFB neurons reduces sleep as well (Ueno et al., 2012). However, the reduction in sleep is not as severe as the one observed upon activating the majority of dopaminergic clusters (Ueno et al., 2012). It is therefore possible, that other dopaminergic neurons contribute to the wake-promoting effects of dopamine to the dFB, for example neurons from the PPL1 cluster (Liu et al., 2012). Taken together these studies provide anatomical and functional evidence that dopaminergic neurons in the PPL1 and PPM3 clusters project to the dFB neurons, promoting wakefulness.

The dopaminergic input to the dFB was further illuminated by optogenetic activation of dopaminergic neurons that promotes wakefulness by hyperpolarising the dFB neurons (Pimentel et al., 2016). RNA-mediated interference (RNAi) with the expression of Dopamine 1-like receptor 2 (Dop1R2) in the dFB neurons points to this receptor as the mediator of the wake-promoting effect of dopamine (Pimentel et al., 2016). Flies with reduced levels of the receptor sleep more and lack the inhibitory response of dFB neurons to the neurotransmitter (Pimentel et al., 2016).

In addition, the dopamine-mediated switch requires the antagonistic regulation of two potassium channels: the voltage-gated Shaker channel and the "leak" channel, Sandman (Pimentel et al., 2016). Knockdown of Shaker causes flies to sleep less by dampening the activity of dFB neurons, whereas knockdown of Sandman causes an increase in sleep by preventing the switch to the OFF state (Pimentel et al., 2016). As both loss of Sandman and blocking vesicle exocytosis lock the dFB neurons in the ON state, an appealing conjecture is that Sandman's recycling to and from the plasma membrane parallels the OFF to ON transitions of the neurons (Pimentel et al., 2016). Sandman's presence at the membrane is expected to switch the neurons OFF, while its internalisation to promote the shift to the ON state.

Lastly, stimulation of dopaminergic neurons using the ATP-activated cation channel P2X2 or bath application of dopamine to the dFB neurons, inhibits their activity as well (Ni

et al., 2019). Based on the studies above, one way by which the transition to the waking state is achieved in the flies, is by the inhibitory effect of dopamine on the dFB neurons. Recent, advances on the connectome of the central complex, reveal that dopaminergic neurons receive inputs from the dFB neurons as well (Hulse et al., 2020). Thus, comparable to the mammalian sleep physiology, the reciprocal relation between dopaminergic neurons and the dFB resembles the “flip-flop model” of a mutually inhibitory relationship between the sleep promoting ventrolateral preoptic nucleus (VLPO) and monoaminergic populations (Saper et al., 2010). However, whether dFB neurons inhibit dopaminergic neurons to promote sleep and what is the mechanism behind this inhibition remains under investigation.

Mechanisms by which dFB neurons promote sleep

A longstanding theory suggests that the function of sleep is the clearance of reactive oxygen species (ROS) (Reimund, 1994). Loss of function of the *insomniac (inc)* gene causes a short-sleeping phenotype which makes flies susceptible to oxidative stress (Hill et al., 2018). Injecting these mutants with either paraquat, a herbicide that catalyses the production of superoxide anions or feeding them with hydrogen peroxide (H_2O_2), an oxidant involved in the production of highly reactive hydroxyl radicals, causes them to die faster (Hill et al., 2018). Increasing sleep by activating the dFB neurons or by feeding flies with the gamma-aminobutyric acid ($GABA_A$) receptor agonist Gaboxadol rescues the sensitivity to paraquat injection or H_2O_2, suggesting an anti-oxidant role for sleep (Hill et al., 2018).

Interestingly, sleep deprivation alters the redox state of dFB neurons; following a night of sleep deprivation, ROS levels in these neurons are increased (Kempf et al., 2019). Flies with mutations in the *Shaker* channel (Cirelli et al., 2005) or its β-subunit *Hyperkinetic (Hk)* (Bushey et al., 2007) have a short-sleeping phenotype. Because Hk also possesses a binding site for the NADPH cofactor, whose oxidation or reduction can alter the electrophysiological properties of the channel and consequently of dFB neurons, the causal relationship between the two was examined. Indeed, expression of the protein subunit in *Hk* mutants rescues the sleep loss of these flies only if the oxidoreductase activity of the

protein is left intact (Kempf et al., 2019). Thus, redox changes in the dFB neurons are related to the functional activity of Hk.

Consistent with this idea, manipulations that increase or decrease ROS levels in the dFB neurons have opposing effects on sleep (Kempf et al., 2019). Introducing the alternative oxidase (AOX) enzyme and overexpressing antioxidant enzymes such as superoxide dismutase 1 (SOD1) or catalase in dFB neurons causes flies to sleep less. In contrast, increasing oxidation levels with miniSOG, a protein that photogenerates singlet oxygen [$^1O_2$] or expressing a mutant pro-oxidant version of superoxide dismutase 1 (SOD1 A4V) causes flies to sleep more (Kempf et al., 2019). In either case, the increase in sleep could be blocked by removing Hk from the dFB neurons, highlighting again the link between the redox state of the neurons and Hk. Increases in ROS production force the dFB neurons into a state of higher excitability, where high Shaker currents predominate (Kempf et al., 2019). Therefore, accumulation of ROS is one mechanism explaining the transition of dFB neurons from the OFF to the ON state (**Figure 1**).

Finally, excessive sleep deprivation reduces the lifespan of flies and increases oxidation levels also in the gut (Vaccaro et al., 2020). Overexpression of SOD1 in the gut prevents the increase in ROS following sleep deprivation while consumption of antioxidants rescues the shortened lifespan induced by sleep deprivation by clearing ROS (Vaccaro et al., 2020). Distinguishing the effects of the redox state of different tissues on sleep is an interesting avenue of exploration for the future.

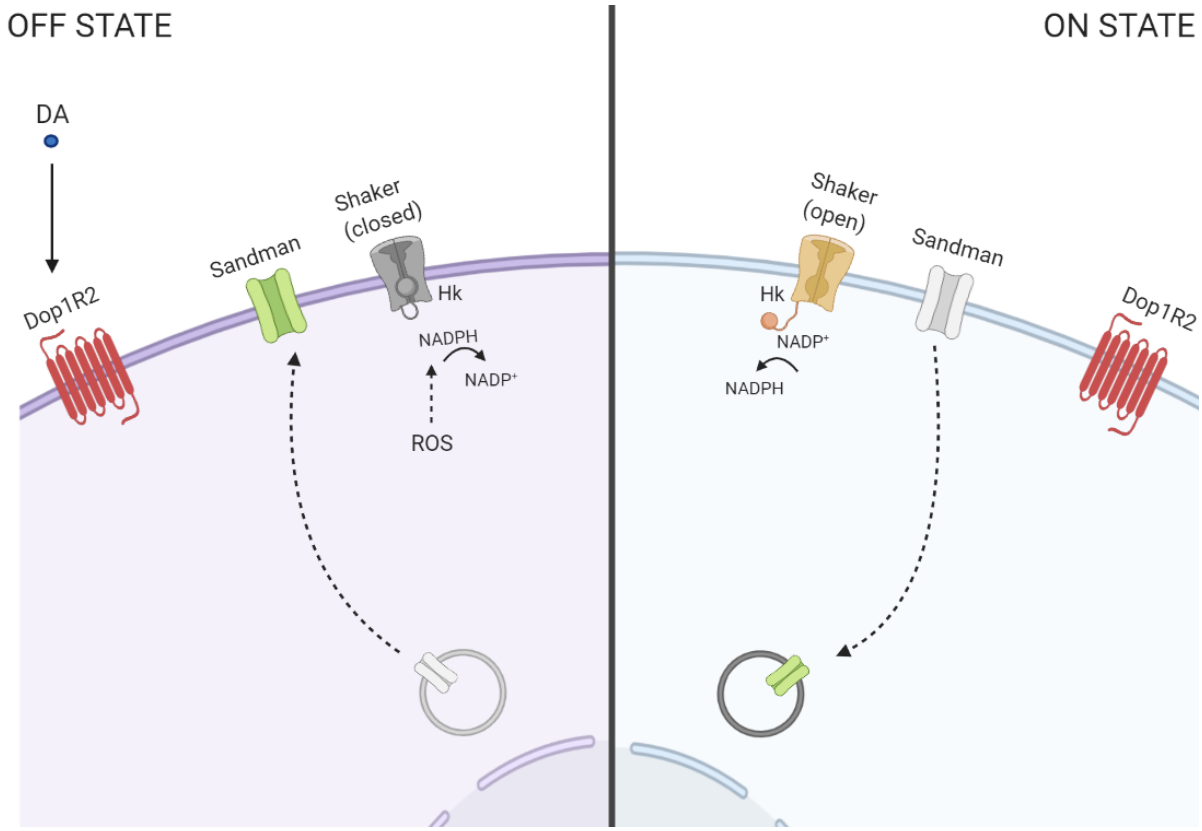

Figure 1: Mechanisms by which the dFB neurons are regulated. In response to dopamine (DA) or under physiological conditions, it is hypothesised that the dFB neurons are maintained in the OFF state, by the presence of Sandman at the plasma membrane (Pimentel et al., 2016). Generation of reactive oxygen species (ROS) during prolonged wakefulness, leads to an increasingly oxidised environment in the neurons. The change in the redox chemistry is sensed by Hyperkinetic (Hk) leading to the exchange of NADPH for NADP+ (Kempf et al., 2019). The oxidation of NADPH eventually increases Shaker currents turning the cells to the ON state. When the cells are in the ON state, NADP+ is reduced back to NADPH, and the sleep pressure generated by ROS is dissipated. The switch to the ON state is also likely to involve the internalisation of Sandman. Figure created with BioRender.com.

R5 neurons generate sleep pressure discharged by the dFB neurons

In the quest of finding circuits capable of generating sleep pressure, the R5 neurons of the ellipsoid body (EB) were identified as an upstream input to dFB neurons (Liu et al., 2016). While thermogenetic activation of dFB neurons induces sleep acutely, activation of the R5 neurons induces “rebound” sleep on the following day, reflecting increases in sleep drive (Liu et al., 2016). Stimulating R5 neurons and measuring subsequent increases in dFB neuron activity led to the hypothesis that the R5 neurons act upstream of the dFB circuit. Conversely, silencing the dFB neurons inhibits the increase in sleep that is normally observed following the thermogenetic activation the R5 neurons, further corroborating this hypothesis (Liu et al., 2016). The encoded sleep need in the R5 neurons requires changes in activity-dependent plasticity such as recruitment of calcium from intracellular stores and an increase in the number of N-methyl-D-aspartate receptors (NMDARs) and active zones (Liu et al., 2016).

R5 neurons exhibit slow-wave oscillations that are reminiscent of the mammalian slow-wave rhythms in the delta band during deep sleep (Raccuglia et al., 2019). This synchronous slow-wave activity appears at late hours of the day during zeitgeber ZT8-12, peaks at ZT13-16 and drops with sleep (Raccuglia et al., 2019). Sleep deprivation causes an increase in delta power, indicating that these oscillations are linked to the fly’s sleep history and therefore to the homeostatic control of sleep (Raccuglia et al., 2019). The synchronisation and power of the oscillations were further shown to depend on NMDAR coincidence detection and input from the tubercular-bulbar neurons (TuBu) neurons (Raccuglia et al., 2019).

Consistent with the findings above, active zone plasticity is indicative of the sleep pressure generated in the R5 neurons (Huang et al., 2020). When sleep need is high, such as in short sleeping mutants, the levels of Bruchpilot (BRP) – a presynaptic active zone marker – are increased (Huang et al., 2020). This finding is reversed when sleep is induced by activation of either the R5 or dFB neurons (Huang et al., 2020). Accordingly, increasing BRP copies (1-4x) increases sleep and sleep rebound in a dosage-dependent manner (Huang et al., 2020). R5-specific knockdown of BRP reduces the homeostatic sleep

rebound following sleep deprivation and restores the BRP-induced sleep during daytime in back to normal levels in 4xBRP flies (Huang et al., 2020). Thus, BRP-driven synaptic plasticity is required for the sleep need encoded by the R5 neurons.

A key component in the regulation of the R5 sleep circuitry is glia. Thermogenetic activation of astroglia, induces “rebound” sleep and elevation of calcium levels (Ca^{2+}) in the R5 neurons (Blum et al., 2021). Activating astroglial cells while silencing the R5 or dFB neurons prevents the transmission of sleep pressure to these circuits (Blum et al., 2021). Thus, astroglia are indicated as an upstream input to the R5 neurons. The astroglial-R5 signalling axis depends on a Ca^{2+} signalling positive feedback loop and the canonical spätzle (Spz)/Toll pathway.

Following conditions of high sleep need such as sleep deprivation, calcium levels Ca^{2+} in astroglia increase (Blum et al., 2021). The increase in Ca^{2+} is mediated by the L-type voltage-gated calcium channel Ca-α1D and causes the upregulation of Tyramine II (TyrII) receptor (Blum et al., 2021). Monoaminergic signalling further increases Ca^{2+} leading to a positive-feedback loop (Blum et al., 2021).

When accumulation of sleep need reaches a sufficient level, the increasingly high levels of Ca^{2+} in astrocytes eventually lead to the secretion of Spz; Spz levels increase following sleep deprivation or thermogenetic activation of the glial cells (Blum et al., 2021). Removing the Toll receptor from the R5 neurons diminishes the Ca^{2+} increases observed upon sleep deprivation in the circuit, pointing to the receptor as the downstream effector of Spz released from astrocytes (Blum et al., 2021). Therefore, this study highlights the transmission of sleep need from glial cells to dedicated sleep circuits. To gain a comprehensive understanding of how sleep is controlled, investigation of the glia contribution to sleep-related mechanisms is critical.

Intriguingly, antennal transection is accompanied by an immediate increase in sleep and the removal of active zones and damaged axons from injured neurons (Singh & Donlea, 2020). The loss in active zones follows the post-injury increase in sleep and is prioritised over axonal removal (Singh & Donlea, 2020). Sleep deprivation on the other hand slows the removal of both components, suggesting that sleep is required for these processes to

occur (Singh & Donlea, 2020). The prioritisation of active zone removal is hypothesised to involve the engulfment action of ensheathing glia (Singh & Donlea, 2020).

Indeed, increases in sleep following antennal ablation are associated with glial innervation of the antennal lobe and the induction of the engulfment receptor Draper (Stanhope et al., 2020). Sleep loss accomplished by activation of dopaminergic neurons, sleep deprivation or sleepless mutants inhibits the induction of Draper (Stanhope et al., 2020). In contrast, inducing sleep with Gaboxadol or by activating the dFB neurons accelerates the engulfment of injured neurons by enhancing expression of Draper (Stanhope et al., 2020).

Downstream targets of dFB neurons

VLPO neurons are well known to inhibit monoaminergic populations by secreting galanin and GABA (Saper et al., 2010; Sherin et al., 1998). Interestingly, depleting the inhibitory neuropeptide allatostatin (AstA) from dFB neurons causes flies to sleep less and to have reduced sleep rebound following sleep deprivation (Donlea et al., 2018). The inhibitory action of allatostatin is facilitated by the AstA-R1 receptor in neurons termed “helicon” neurons due to their shape; these connect the EB and AstA-positive cells in the fan-shaped body (Donlea et al., 2018). Activation of dFB neurons or direct application of AstA silences helicon cells, further validating that they receive inhibitory input from the sleep promoting neurons (Donlea et al., 2018).

From electrophysiological studies it was shown that helicon cells respond to light and are involved in visually-guided movement (Donlea et al., 2018). Therefore, reducing their activity also leads to a decrease in light-induced locomotor activity (Donlea et al., 2018). Conversely, optogenetic activation of helicon cells, restores the locomotor immobility caused by the inhibitory action of dFB neurons (Donlea et al., 2018). Helicon cells, excite the R5 neurons, identifying the functional connectivity between these two neuronal populations as well (Donlea et al., 2018). Following stimulation of helicon cells, flies sleep significantly more the day after, which is reminiscent of the sleep pattern following activation

of the R5 neurons (Donlea et al., 2018). Taken together, these findings led to the conception of an autoregulatory loop.

It is hypothesised that during wakefulness, light activates helicon cells which in turn excite the R5 neurons. There, activity-dependent plasticity generates sleep pressure that is conveyed to the dFB neurons through either direct or indirect connections eventually switching the neurons to the electrically active state. dFB neurons release the inhibitory allatostatin to the helicon cells, decreasing their responses to light, and pausing activity. Thus, the sleep pressure generated by the R5 neurons is dissipated, putting flies to sleep (Donlea et al., 2018).

Finally, octopamine, like dopamine, was characterised as a wake promoting signal in flies (Crocker & Sehgal, 2008; Crocker et al., 2010). Blocking GABAergic transmission in the dFB neurons by RNAi-mediated knockdown of glutamic acid decarboxylase 1 (Gad1) inhibits the induction of sleep following thermogenetic activation of these neurons (Ni et al., 2019). Based on anatomical and functional connectivity studies, the neurons downstream of this inhibition are hypothesised to be octopaminergic neurons (Ni et al., 2019). However, further investigation is needed to strengthen this conclusion. The emerging picture from the above studies suggests that dFB neurons might promote sleep by inhibiting sensory pathways directly or by inhibiting wake-promoting neurotransmission.

In conclusion, the fan-shaped body can be compared to an actuator of sleep, which likely involves the integration of several upstream inputs and their translation into the physiological manifestations of sleep. It discharges sleep pressure accumulated from other sleep promoting circuits and from cell-intrinsic mechanisms, is inhibited by wake-promoting signals and in turn inhibits sensory pathways. Further characterisation of the molecular mechanisms operating within the dFB neurons, and their connections is crucial for understanding how these lead to state transitions. Such questions are addressed and discussed in the next two chapters.

Chapter 2

DEVELOPMENT OF TOOLS TO VISUALISE THE TRAFFICKING OF SANDMAN

2.1 INTRODUCTION

Like a conductor in an orchestra, the sleep homeostat must ensure that several components act in concert to fine-tune the sleep-wake cycle: tight regulation of genetic and molecular machinery, transitions in electrical excitability and integration of synaptic/non-synaptic inputs. In *Drosophila*, this homeostat lies within approximately a dozen cells in each hemisphere that project to the dorsal fan-shaped body (dFB) of the central complex; referred to here as the dFB neurons. Thermogenetic activation of dFB neurons puts flies to sleep (Donlea et al., 2011). Based on a series of experiments (Donlea et al., 2014; Donlea et al., 2018; Kempf et al., 2019; Pimentel et al., 2016), the dFB neurons were found to exist in at least two physiologically electrical states: an electrically active state (ON state) and an electrically quiescent state (OFF) (Donlea et al., 2014). Following conditions of high sleep need, such as sleep deprivation the neurons switch ON (Donlea et al., 2014).

The OFF state is regulated by dopamine; dopaminergic neurons from the PPL1 and PPM3 clusters project to the dFB neurons where they signal arousal (Liu et al., 2012; Ueno et al., 2012). Optogenetic activation of dopaminergic neurons and direct application of dopamine to the dFB neurons, switches them to the OFF state, promoting wakefulness. Both means of dopamine application elicited a locomotor response (Pimentel et al., 2016). The switch from electrical activity to quiescence requires the dopamine receptor (Dop1R2) and is modulated at least by the antagonistic regulation of two potassium channels: the voltage-gated potassium channel Shaker and the two-pore domain potassium channel, Sandman (Pimentel et al., 2016). dFB-restricted interference with Shaker reduces the excitability of the neurons promoting wakefulness. In contrast, depletion of Sandman from the dFB neurons disables the switch to the OFF state promoting sleep. Blocking vesicle exocytosis using the botulinum neurotoxin C (BoNT/C) traps the neurons in the electrically

active state as well, pointing to a key role of membrane trafficking in the regulation of Sandman.

Taken together, these results led to the conception of a model, where Sandman is internalised when the dFB neurons are electrically active and translocates to the plasma membrane in response dopamine (**Figure 2**). Surface expression of Sandman is hypothesised to silence the neurons promoting wakefulness. Therefore, two tiers can be targeted to lock the dFB neurons in the ON state: upregulation of Shaker's currents or Sandman's internalisation. While one of the signals causing the former has been explained at least in part by the accumulation of reactive oxygen species (ROS) with waking time (Kempf et al., 2019), the signal that causes the latter remains unknown. The aim of this study was to visualise the putative endo-exocytic cycling of Sandman and identify the molecular pathways that control the endocytic leg of the cycle.

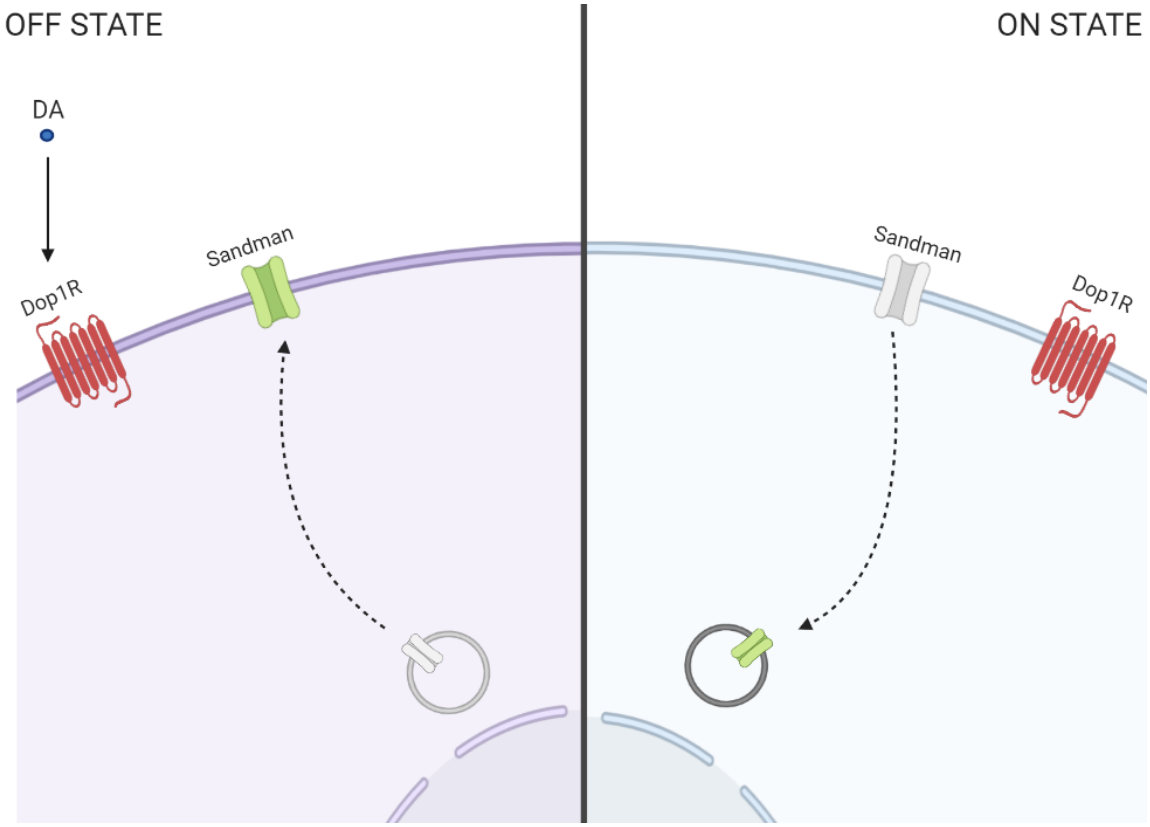

Figure 2: Sandman's envisioned recycling during the sleep-wake cycle. Under physiological conditions or in response to dopamine (DA), it is hypothesised that Sandman translocates to the plasma membrane to switch the neurons OFF by blunting their firing. When the neurons tilt to the ON state, Sandman is internalised in the cells, but the signals responsible for its endocytosis remain unknown**.** Figure created with BioRender.com.

2.2 RESULTS

Generation of *sand-pHluorin* constructs

To gain an optical report of the channel's recycling, I attempted to fuse Sandman with a pH-sensitive version of the green fluorescent protein (GFP), the super-ecliptic pHluorin (Miesenböck et al., 1998; Sankaranarayanan et al., 2000). Due to its pH sensitivity, the super-ecliptic pHluorin provides an excellent tool for visualising the trafficking of receptors and ion channels. At the acidic pH inside vesicles (pH<6), protonation of the chromophore quenches the pHluorin signal whereas its deprotonation following exocytic events restores fluorescence emission (Miesenböck et al., 1998; Sankaranarayanan et al., 2000). The properties of the pHluorin, requires the fluorophore to be inserted in extracellular regions of the channel that are exposed to pH changes in the cell.

Sandman is part of the two-pore domain K^+ (K2P) channel family which is further subdivided into 6 subfamilies: TWIK (Tandem of pore domains in a weak inward rectifying K^+ channel), TASK (TWIK-related acid-sensitive K^+ channel), TREK (TWIK-related K^+ channel), TRESK (TWIK-related spinal cord K^+ channel), TALK (TWIK-related alkaline pH-activated K^+channel) and THIK (Tandem pore domain halothane-inhibited K^+ channel) (Enyedi & Czirják, 2010). The human ortholog of Sandman is the potassium two-pore domain channel subfamily K member 18 (KCNK18) which is a TRESK channel ("The Alliance of Genome Resources: Building a Modern Data Ecosystem for Model Organism Databases," 2019). However, the major structural features of K2P channels are conserved across the 6 subfamilies. These are: two intracellular N-and C-termini, four transmembrane domains (TM1-TM4), four extracellular loops (ECL1-4), two pore domains (P1-P2) and a long extracellular loop between TM1 and P1 (Enyedi & Czirják, 2010). Thus, using overlap-extension polymerase chain reaction (OE-PCR), constructs with insertions of the super-ecliptic pHluorin at different positions of the four extracellular loops of Sandman were generated (**Figure 3**). The constructs are referred to here as *sand-pHluorin*; these were first cloned into a vector containing a *CMV* promoter suitable for mammalian cell culture

and later subcloned into a *UAS* vector to study the channel's localisation and functionality both *in vitro* and *in vivo*.

A

ATGTCCTCCCGACGCAGCTCCTTCAGGCGGAGGGAGAAGCCGGCCTTCGAGCGCTTTAAGGACCACTGCCGCCACTTCA
CGGCGTTCATGTTCAGCAACGTGGGCATCATTCTACTGGTCACATTTTATATTATCGGCGGAGCGTTCATATTCCAGAGCA
TC1GAGATTTTC2GAGTACGAGCGGCTCAAGTCGGAGAAGCCGCACCGGTTTATAGCACGGAACTTCAGTGGCGAGTGCC
TCAGCCGCATATGGGAGTTGACGGCGGAGAACATCAGCTTCTTCGACCACCACGCCTACAGGAGACGGGTGAACGATGT
GCTTCTGGATTATCAGAGGGCCATAGTGAAAAAGCAGCT3GAAGGGACCCGAC4GTGGAGCAGTGGAGCTTCTCCGGAG
CTTTTCTCTACTCACTGACGGTGATCACGACCATCGGGTACGGGAACATTACGCCGCACTCCGAGTGCGGAAAGCTGGTG
ACCATTCTATATGCGATAATTGGCATGCCGCTGTTCTTGCTCTACCTGTCCAACATT1GGAGAC2GTCCTG3GCCAAG4TCC
TTC5AAGTGGATATACTCGAAGGTGTGCCTATGTCGCATCTGCCCCGGCGTGGCCAAGCGCCGGATAATCCGCGAGAGAC
GAAAAATGCGACAGTTGGCCAGAGCGCTCCAGATGCACGACATGGAGAATGCCCGGGGAAGCAGCAGCTACACTAGCAC
CAGCAGTACCACCTCCTCCAACAGCAGCAGTAGCGAATACACCAGAAGTTCCCGCCAGAGTTCCAGCCTCGTGGATATTC
AGTACACCGAGTCTGATTCGGATATCGAGCGGGAAATACGCGGCAGCACGGATGAAATTACAGTGCCAGTCACTGTGTGC
GTCTTCGTTATGGTCGGGTATATCCTGTGGGGTGCGCTGCTCTTCGGT1CGTTGG2GAGGAC3TGGAAC4TATCTG5GATG
GG6AGCTACTTCTGCCTTATATCGCTCAGCAGCATTGGATTTGGCGATCTG1GTGCCA2GGCGAT3CGTGTG4ATAACT5GC
CGAC6AGGGAT7AAGGTGGAGGTTAGCTTCATTCTCTGCGCCATATATCTGCTGCTCGGCATGGCCGTGATTGCCATGTG
CTTCAATTTGATGCAGGAGCAGGTCGTTCACAACATTCGGGCGATCAAGCGGGGATTCAAGGCCTGCTTTCGGTGCCGCA
CCTCCTAG

B

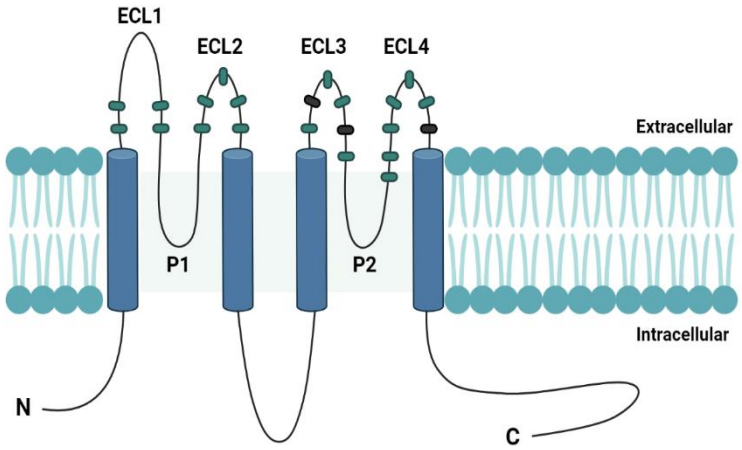

Figure 3: Insertion sites of the super-ecliptic pHluorin into Sandman. (A) Coding sequence of *sandman*. Domain predictions by Phobius and Uniprot are denoted by colour; Blue: N- and C-termini, yellow: extracellular loops (ECL1-4), grey: part of ion channel domain, red: predicted pore domain motifs (P1 and P2), green: transmembrane domains, purple: intracellular loop. Numbers indicate the positions where pHluorin insertion was attempted. Red colour indicates successful cloning in these positions. **(B)** Schematic representation of the channel's structure: rectangles indicate the positions where insertion of the super-ecliptic pHluorin was attempted. Green colour indicates successful cloning in these positions. Figure created with BioRender.com.

Localisation of Sand-pHluorin in HEK-293T cells

The *sand-pHluorin* constructs were first transfected to human embryonic kidney (HEK) cells and imaged live with a plasma membrane stain (CellMask Deep Red) (**Figure 4**). In all cases, the pHluorin signal was observed mainly intracellularly. Immunostaining of the endoplasmic reticulum (ER) with a KDEL antibody in cells transfected with one of the constructs (*CMV-sand:ECL2_1*), suggests that the channel is most likely retained there (**Figure 5B**). However, whether this is due to misfolding or because protein partners essential for its trafficking to the membrane are lacking from HEK cells, has not been identified.

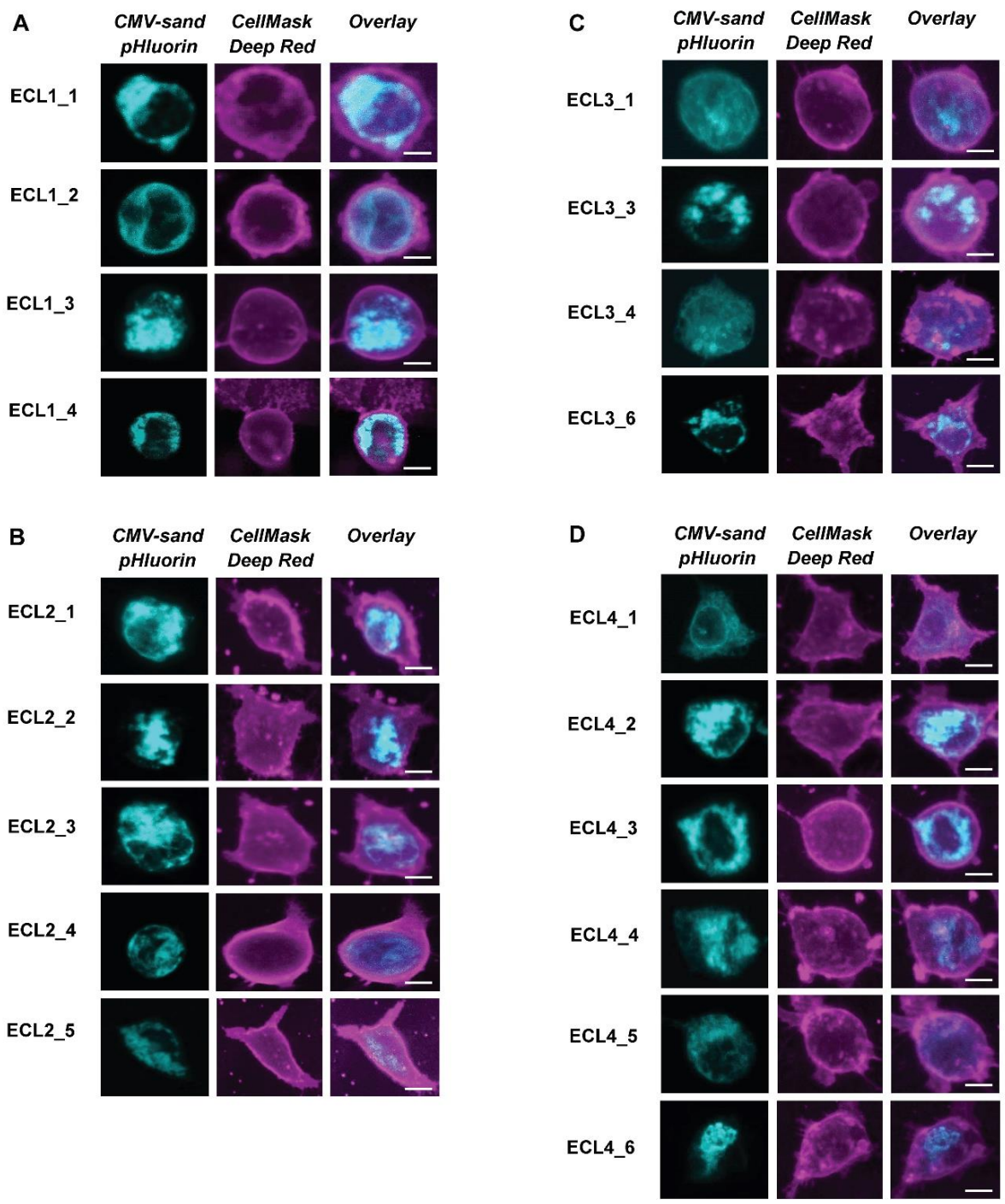

Figure 4: Localisation of Sand-pHluorin in HEK-293T cells. HEK cells were transfected with constructs carrying the pHluorin in **(A)** the first, **(B)** the second, **(C)** the third and **(D)** the fourth loops of Sandman and live imaged with confocal microscopy. Sand-pHluorin is indicated in cyan and the plasma membrane stain (CellMask Deep Red) in magenta. Scale bar = 5µm.

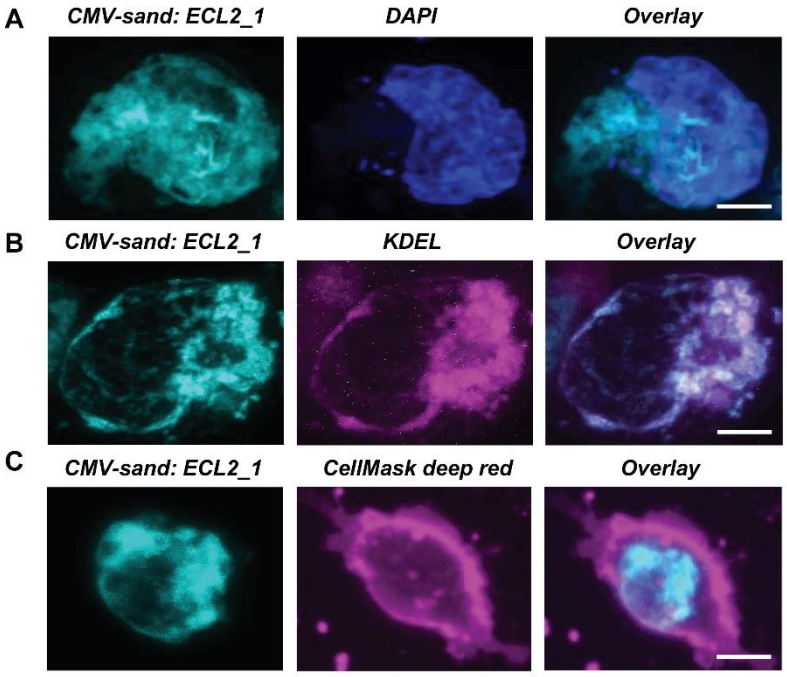

Figure 5: Sand-pHluorin is retained in the ER in HEK-293T cells. HEK cells were transfected with *CMV-sand:ECL2_1* and stained with **(A)** DAPI solution to reveal the nucleus (blue), **(B)** a KDEL antibody to reveal the ER (magenta) and **(C)** CellMask Deep Red solution to visualise the plasma membrane (magenta). Scale bar = 5µm.

Localisation of Sand-pHluorin in dFB neurons and the corresponding sleep amount in flies

As HEK cells might not be equipped with the cellular machinery required to promote the exocytosis of Sandman to the membrane, the *sand-pHluorin* inserts were subcloned into *UAS*-containing vectors and injected into flies. Behavioural studies have shown that knockdown of the channel in the dFB neurons promotes sleep (Pimentel et al., 2016). Therefore, its overexpression was expected to have the opposite outcome. Using the *UAS/GAL4* system, a dFB-specific *GAL4* line (*R23E10-GAL4*), restricted the expression of *UAS-sand-pHluorin* constructs to this population of cells. While some flies injected with the constructs did not show any alteration in their sleep patterns, others did show a decrease in their total amount of sleep compared to their parental controls (**Figure 6D**, **Figure 7C** and **Figure 7D**).

The next step was to determine whether in those cases the channel localises correctly at the plasma membrane of dFB neurons. To achieve this, *UAS-sand-pHluorin* insertions were driven in the dFB neurons using *UAS-CD4-tdTomato; R23E10-GAL4* and stained with a GFP antibody to visualise the pHluorin. The tdTomato marker was co-expressed in the neurons to label the plasma membrane. However, the localisation of the channel suggested that it is most likely retained intracellularly, or that a very small proportion is present at the membrane (**Figure 6A, Figure 6B, Figure 7A** and **Figure 7B)**. In most cases, the dFB neurons presented an unhealthy morphology as well: the shape of the usually round nucleus was deformed. In two cases, where the pHluorin was inserted into the second extracellular loop of Sandman (*UAS-sand:ECL2_4* and *UAS-sand:ECL2_5*), fluorescence was visible throughout the cell.

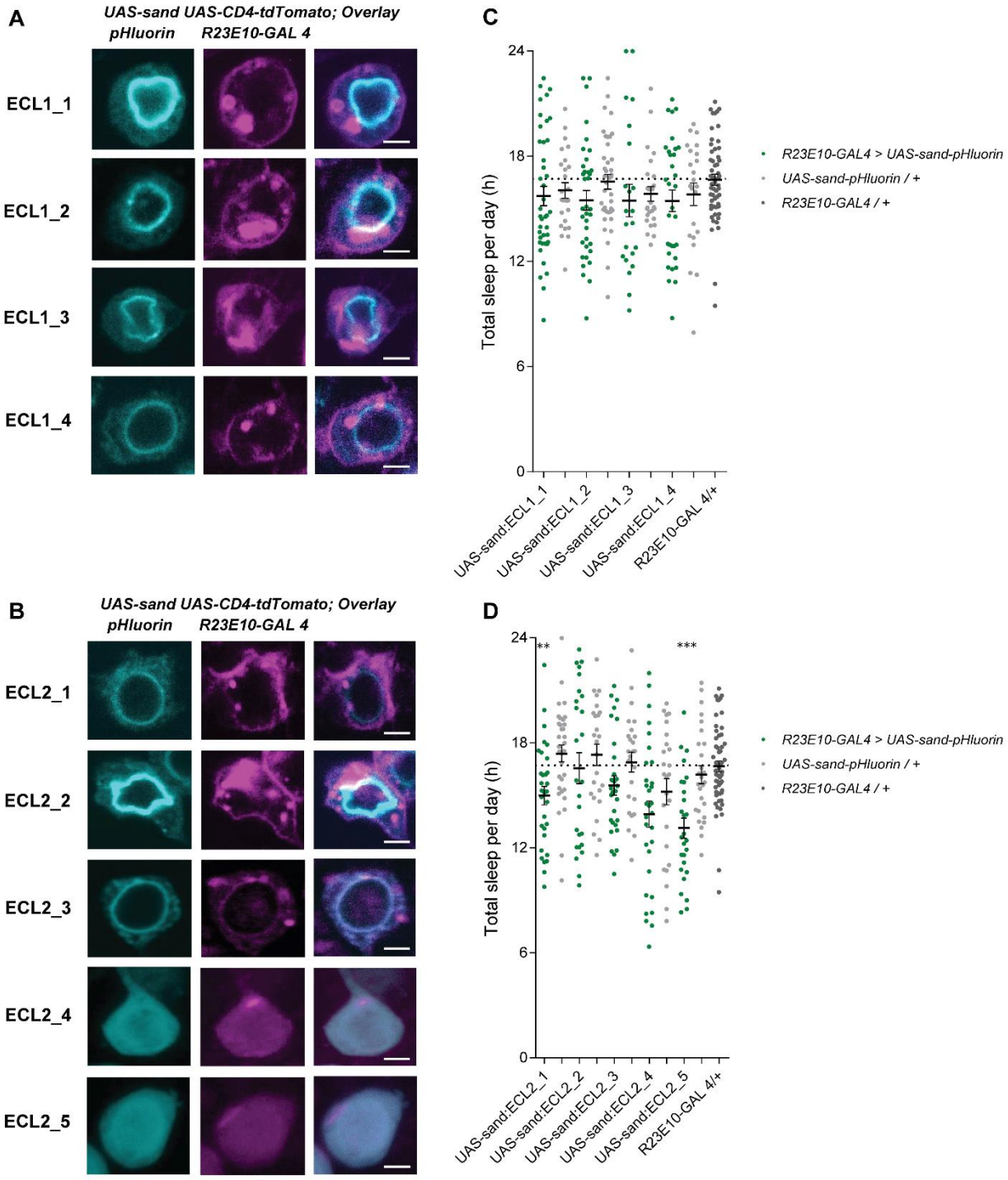

Figure 6: Localisation of Sand-pHluorin in dFB neurons and the corresponding amount of sleep in flies. Immunostaining of dFB neurons co-expressing a membrane tdTomato marker and pHluorin in **(A)** the first and **(B)** second loops of Sandman. Sand-pHluorin is shown in cyan while the tdTomato marker in magenta. Scale bar = 10µm. **(C)** and **(D)** Total amount of sleep in flies expressing the pHluorin in the first and second loops of Sandman in the dFB neurons. *UAS-sand-pHluorin* constructs were driven to the dFB neurons by the *R23E10-GAL4* (green). Parental controls are indicated by the grey (*UAS-sand-pHluorin/+*) and dark grey (*R23E10/+*) colours. Overexpressing the channel in the dFB neurons results in a significant decrease in sleep in two cases where the pHluorin was inserted into Sandman's second loop; *UAS-sand:ECL2_1*: $F_{(2, 116)} = 7.064$, p=0.0013 and *UAS-sand:ECL2_5*: $F_{(2, 106)} = 17.42$, p<000.1. One-way ANOVA with *Holm-Sidak's* multiple comparisons test. The asterisks denote significant differences from both parental controls in the pairwise *post hoc* comparisons. Mean ± SEM, n=27-55.

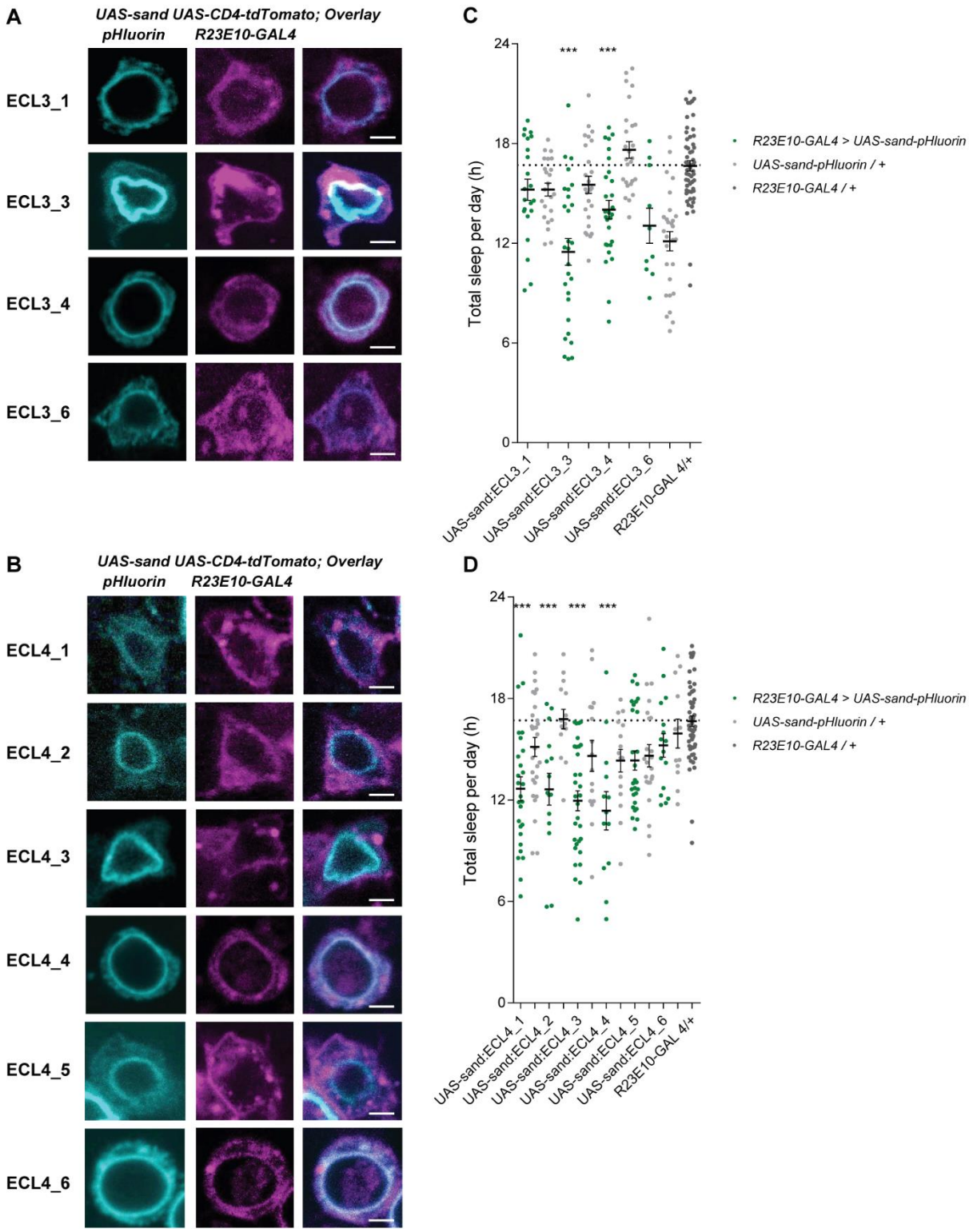

Figure 7: Localisation of Sand-pHluorin in dFB neurons and the corresponding amount of sleep in flies. Immunostaining of dFB neurons co-expressing a membrane tdTomato marker and pHluorin in **(A)** the third and **(B)** fourth loops of Sandman. Sand-pHluorin is shown in cyan while the tdTomato marker in magenta. Scale bar = 10µm. (**C)** and **(D)** Total amount of sleep in flies expressing the pHluorin in the third and fourth loops of Sandman in the dFB neurons. As above, *UAS-sand-pHluorin* constructs were driven to the dFB neurons by the *R23E10-GAL4* (green). Parental controls are indicated by the grey (*UAS-sand-pHluorin/+*) and dark grey (*R23E10-GAL4/+*) colours. Overexpressing the channel in dFB neurons decreases sleep in six cases where the pHluorin was inserted into the third and fourth loops of Sandman; *UAS-sand:ECL3_3*: $F_{(2,\ 105)} = 28.12$, p<000.1, *UAS-sand:ECL3_4*: $F_{(2,\ 106)} = 14.89$, p<000.1, *UAS-sand:ECL4_1*: $F_{(2,\ 108)} = 17.28$, p<000.1, *UAS-sand:ECL4_2*: $F_{(2,\ 82)} = 14.97$, p<000.1, *UAS-sand:ECL4_3*: $F_{(2,\ 81)} = 26.52$, p<000.1 and *UAS-sand:ECL4_4*: $F_{(2,\ 81)} = 21.26$, p<000.1.One-way ANOVA with *Holm-Sidak's* multiple comparisons test. Asterisks denote significant differences from both parental controls in the pairwise *post hoc* comparisons. Mean ± SEM, n=16-55.

Live imaging of dFB neurons expressing Sand-pHluorin

As an insertion of the pHluorin in the 2nd loop of Sandman correlates with fluorescence throughout the cell and a reduction in sleep (**Figure 6B** and **Figure 6D**), flies expressing Sand:ECL2_5 in the dFB neurons were further chosen for two-photon live imaging. Dopamine is one of the neurotransmitters known to mediate the switch from sleep to wakefulness (i.e., the dFB neurons switch to the OFF state). This switch is hypothesised to be facilitated by the exocytosis of Sandman to the plasma membrane (Pimentel et al., 2016). Therefore, dopamine application, is expected to result in an increase in the pHluorin signal, as a larger proportion of the channel should be localised at the plasma membrane and the pHluorin tag would be exposed to a more basic environment.

Dopamine injection onto the dendritic tufts of dFB neurons was used to allow for temporally and anatomically confined application (**Figure 8**). Delivery of the neurotransmitter (10mM) was achieved through repeated pressure pulses using a Picospritzer. To capture exocytotic events, flies co-expressing Sand:ECL2_5 and the tdTomato membrane marker in the dFB neurons were used. The signals for the pHluorin and the tdTomato marker were split into green and red channels respectively and ratiometric analysis was performed to compute the green-to-red ratio. However, following dopamine application, an increase in the pHluorin signal was not detected in either the somatic, dendritic, or axonal compartments of the neurons (**Figure 9**).

An additional way of testing whether the channel localises on the plasma membrane, was acidic treatment. As the pHluorin tag is pH-sensitive, its fluorescence is expected to be quenched in the presence of acidic solutions. Thus, following dopamine stimulation, the extracellular solution was exchanged with acidic ones (pH ~ 5 and pH ~ 3). Conversely, treatment with ammonium chloride (NH_4Cl) was used to alkalinise vesicles; uncharged NH_3 can cross membranes and bind intracellular protons (H^+) causing an rise in the internal pH (Roos & Boron, 1981). The total fluorescence from the pHluorin tagged channel can therefore be revealed. However, a quenching in the signal following acidic treatment was not observed (**Figure 10A**) and application of NH_4Cl did not elicit an increase

in the green-to-red ratio (**Figure 10B**). As both treatments did not alter the fluorescence ratio, it is most likely that the channel is retained intracellularly.

In the flies imaged above (*UAS-CD4-tdTomato;R23E10-GAL4/UAS-sand:ECL2_5*), the pHluorin signal is visible throughout the somata of the dFB neurons. Consequently, fluorescence alternations in response to dopamine might be difficult to distinguish. Therefore, flies with another insertion (*UAS-sand:ECL3_3*) that caused a reduction in sleep when expressed in the dFB neurons, but where the pHluorin signal was largely inside the cell were imaged as well. It is possible exocytic events would be more accessible to detect in this case. Once again however, there was no significant difference in the green-to-red ratio following dopamine application (**Figure 11**). Therefore, it has proven very challenging to visualise the trafficking of the channel using the Sand-pHluorin flies.

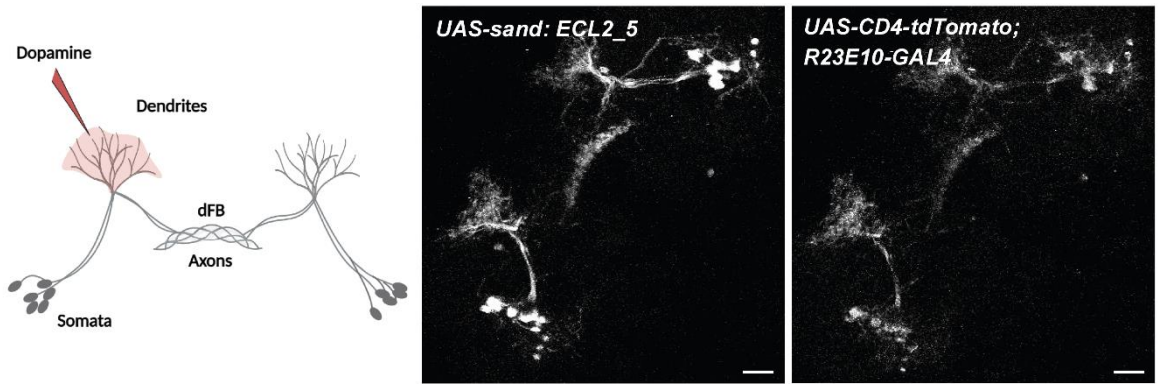

Figure 8: Experimental setup for live imaging of dFB neurons expressing Sand:ECL2_5. Dopamine injection was targeted onto one of the dendritic tufts of dFB neurons in flies co-expressing the plasma membrane tdTomato marker and Sand:ECL2_5. Scale bar = 5µm. dFB schematic created with BioRender.com.

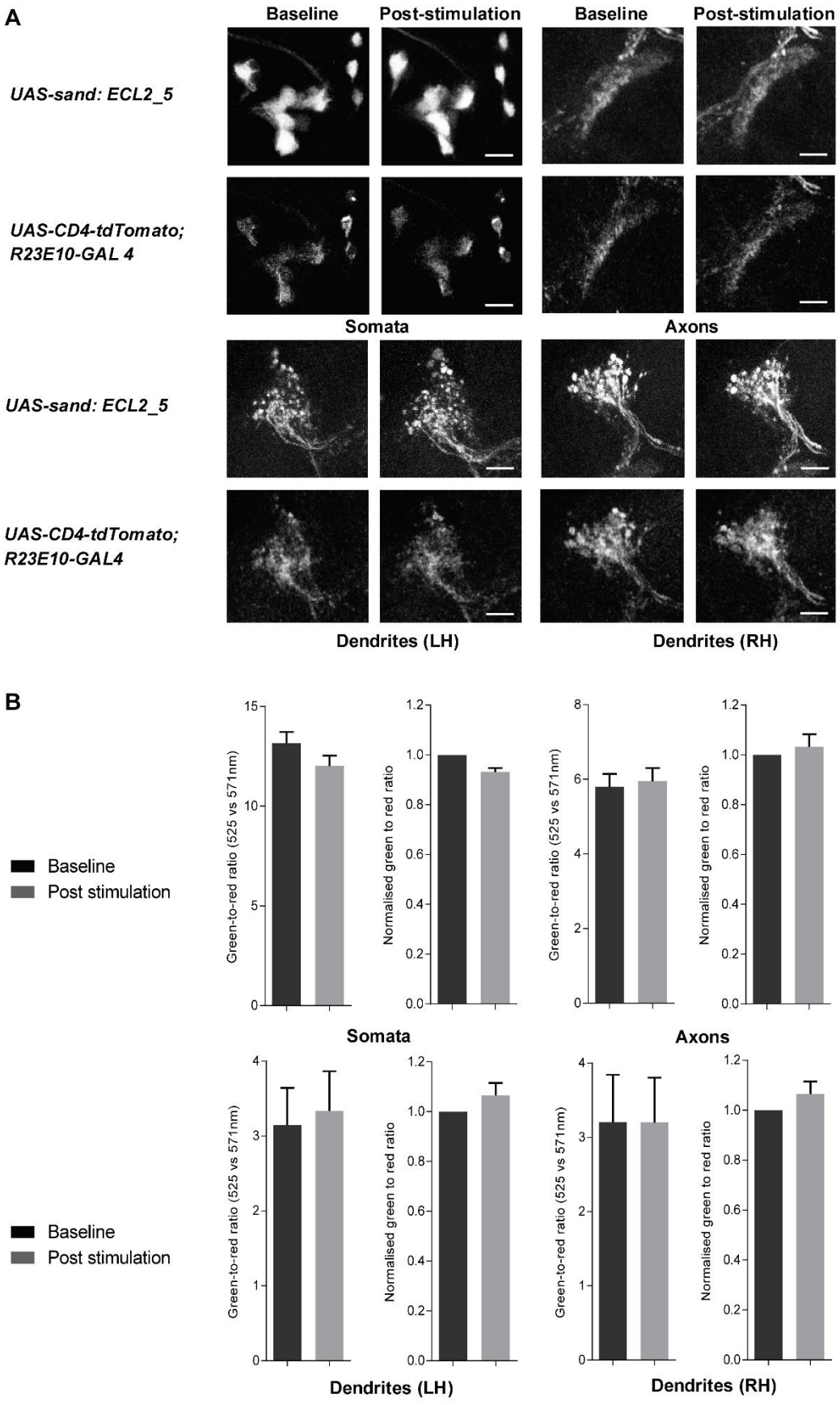

Figure 9: Ratiometric analysis following dopamine stimulation of dFB neurons expressing Sand:ECL2_5. (A) The different compartments of dFB neurons (somata, axons and dendrites) were imaged prior and after dopamine stimulation to determine fluorescence changes in response to the neurotransmitter. LH = left hemisphere, RH= right hemisphere. Scale bar = 1µm **(B)** Ratiometric analysis of the super-ecliptic pHluorin and tdTomato marker fluorescence. No significant changes were detected following the injection of dopamine (paired t-test, n=10 flies).

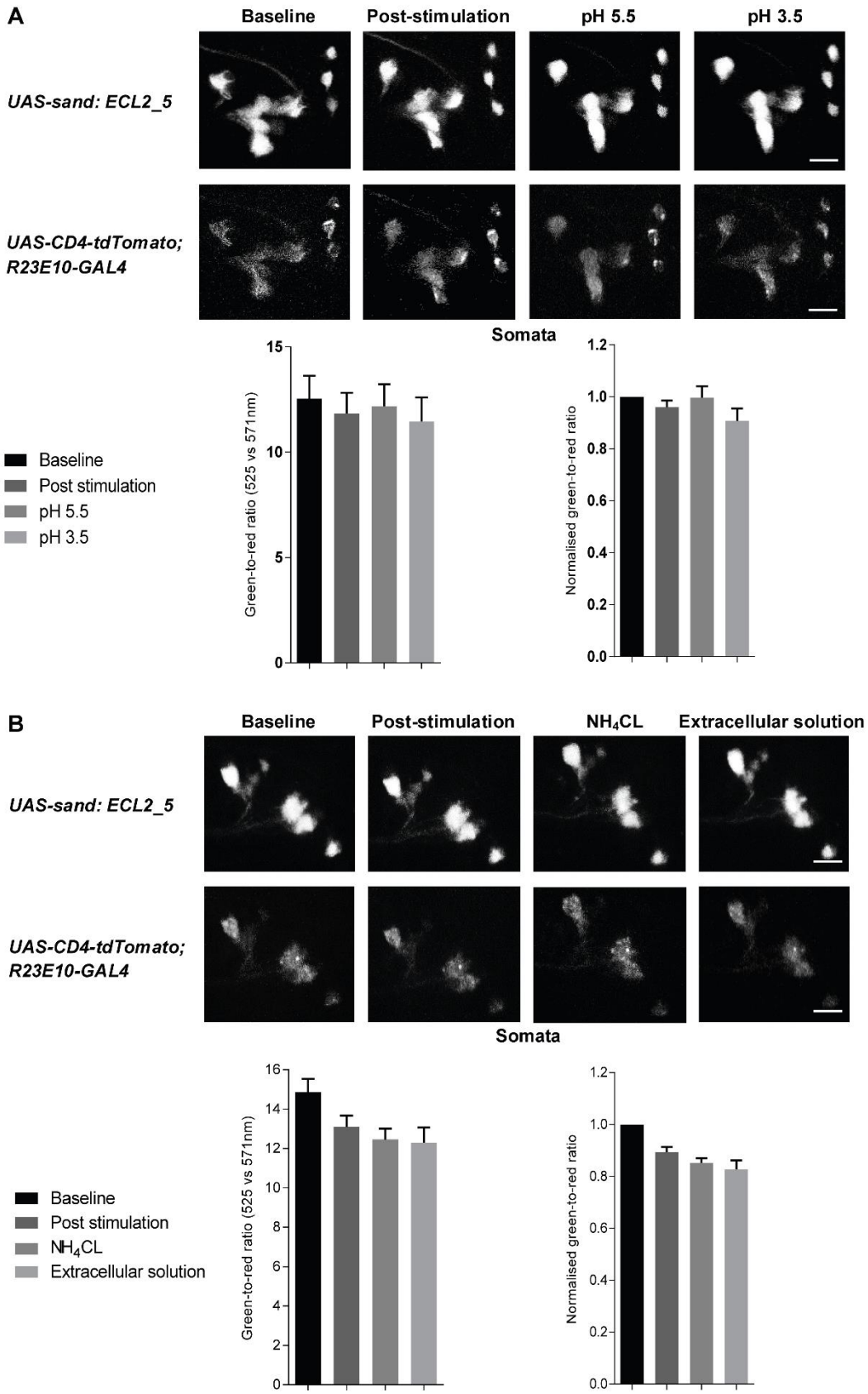

Figure 10: Ratiometric analysis following acidic and ammonium chloride treatment in dFB neurons expressing Sand:ECL2_5. (A) Following dopamine stimulation, the dFB neurons were subjected to acidic treatment with extracellular solutions of pH 5.5 and pH 3.5. The images show representative examples of the somata, after each condition. Scale bar = 1µm. No significant changes were detected (One-way ANOVA, n=10 flies). **(B)** To reveal the maximum pHluorin signal, the brains were exposed to ammonium chloride (NH_4CL) after dopamine stimulation. Scale bar = 1µm. No increase in the pHluorin signal is detected compared to baseline conditions (One-way ANOVA, n=5 flies).

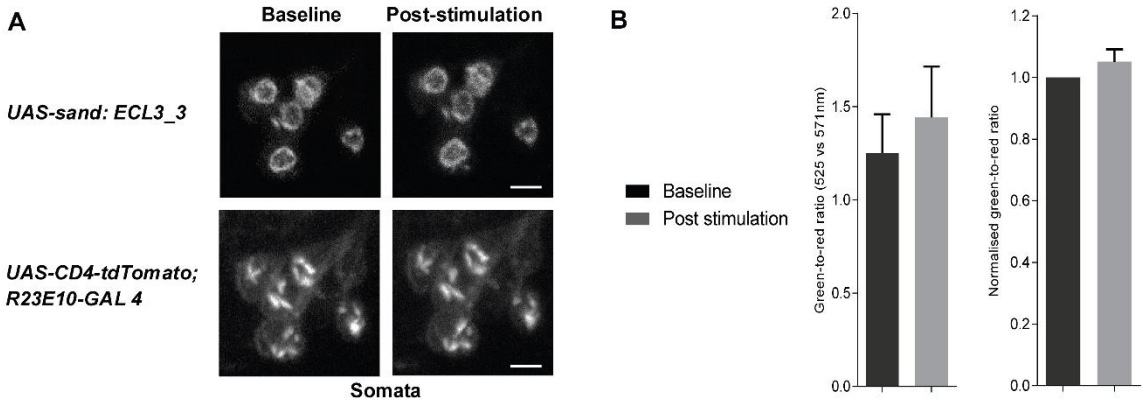

Figure 11: Ratiometric analysis following dopamine stimulation in dFB neurons expressing Sand:ECL3_3. (A) The somata of dFB neurons in flies expressing Sand:ECL 3_3 were imaged before and after DA stimulation to determine fluorescence changes. Scale bar = 1µm **(B)** Ratiometric analysis of super-ecliptic pHluorin and tdTomato marker fluorescence. No significant changes were detected (paired t-test, n=5 flies).

Overexpression of Sandman in the dFB neurons

Due to the insertion of the pHluorin in the extracellular loops of Sandman, it is possible that the folding and/or function of the channel has been disrupted. For this reason, the channel was further tagged with GFP and Venus at the N-terminus (*UAS-GFP-sand* and *UAS-venus-sand*). An untagged version of the channel (*UAS-sand*) was also generated. To test whether the dFB-driven, overexpressed channel preserves its function, the total amount of sleep in flies expressing these constructs was measured. In all three cases, there was no significant change (**Figure 12**). Staining in flies expressing GFP-Sand in the dFB neurons shows that, as in the case of Sand-pHluorin flies, it is not clear whether the channel resides at the membrane (**Figure 13**).

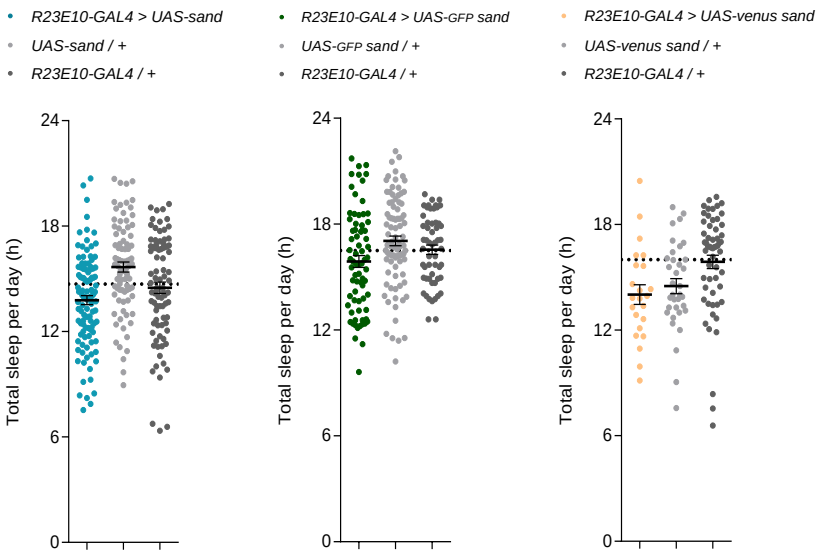

Figure 12: Total amount of sleep in flies overexpressing Sandman. Overexpression of Sandman alone (*UAS-sand*) (cyan) or with GFP (*UAS-GFP-sand*) (green) and Venus (*UAS-venus-sand*) (orange) in the dFB neurons using the *R23E10-GAL4* line does not alter the total amount of sleep (one-way ANOVA). Mean ± SEM, n=23-87.

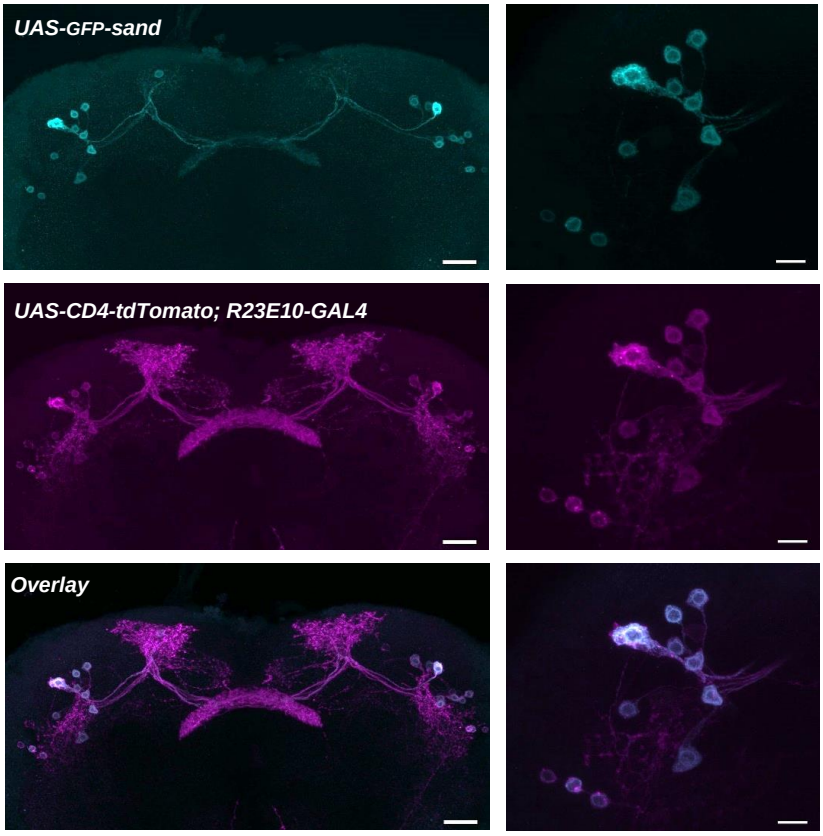

Figure 13: Localisation of GFP-Sand in the dFB neurons. Immunostaining of flies co-expressing GFP-sand (cyan) and a tdTomato plasma membrane marker (magenta) in the dFB neurons. Scale bar = 25µm. Panels on the right show a zoom on the dFB cell bodies. Scale bar = 10µm.

Cv-c and Sandman are likely to act in the same pathway during the sleep-wake cycle

As an alternative way of investigating the trafficking of Sandman, its interaction with another protein involved in regulating sleep in the dFB neurons was examined. *crossveinless-c (cv-c)* is a gene encoding for a Rho-GTPase-activating (Rho-GAP) protein whose mutation disrupts sleep by preventing the dFB neurons from reaching the ON state (Donlea et al., 2014). Therefore, it is conceivable that the mutation clamps the neurons in the OFF state by preventing the internalisation of Sandman. If Sandman interacts with Cv-c during its recycling, its loss from the pathway is expected to rescue the insomnia of these flies. To address this question, an RNAi line targeting *sandman (sandman^{RNAi})* in the dFB neurons was inserted in the *cv-c* mutant background, where a rescue of the *cv-c* sleep loss was observed (**Figure 14**). The sleep amount of *cv-c* mutant flies is restored back to baseline levels when *sandman^{RNAi}* is introduced into the background. These data demonstrate the requirement of Sandman at the membrane where it reduces the excitability of the neurons.

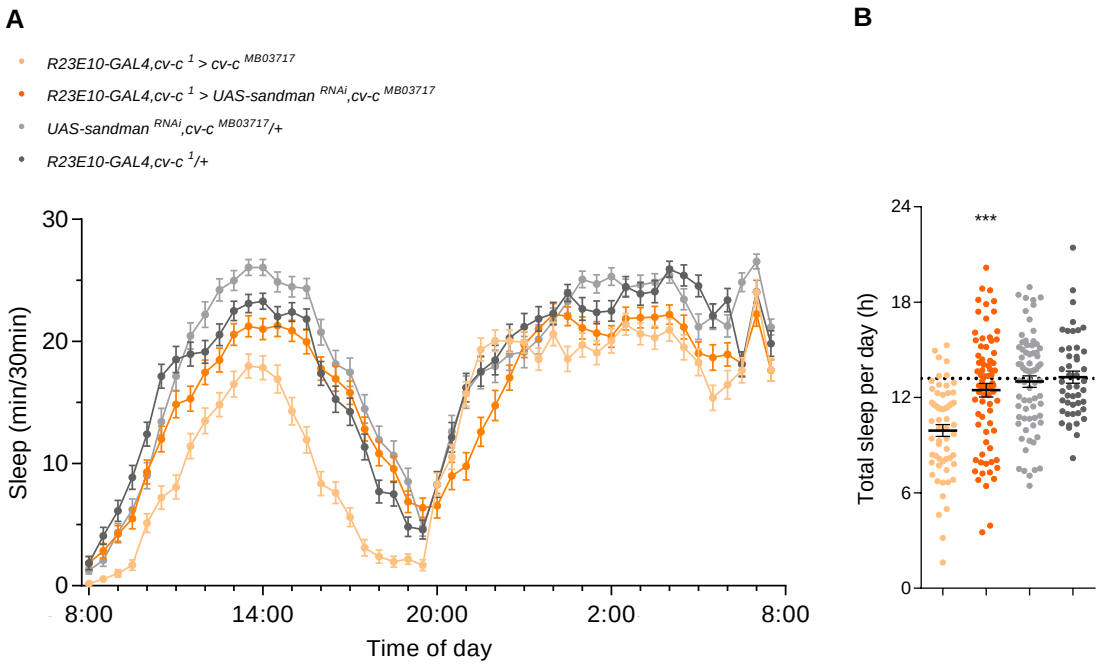

Figure 14: Loss of Sandman in the dFB neurons rescues the insomniac phenotype of *cv-c* mutant flies. **(A)** Sleep (minutes per 30 minutes) of flies expressing *R23E10-GAL4*-driven *sandman^{RNAi}* in the *cv-c* mutant background (dark orange). *R23E10-GAL4, cv-c^{1}/cv-c^{MB03717}* flies are shown in light orange and controls (*R23E10-GAL4, cv-c^{1}/+* and *UAS-sandman^{RNAi}, cv-c^{MB03717}/+*) are shown in grey. **(B)** *R23E10-GAL4, cv-c^{1}/cv-UAS-sandman^{RNAi},cv-c^{MB03717}* flies sleep as much as control flies: $F_{(3, 369)} = 29.43$, $p<0.001$. One-way ANOVA with *Holm-Sidak's* multiple comparisons test. Asterisks denote where there are significant differences between the *R23E10-GAL4, cv-c^{1}/cv-c^{MB03717}, sandman^{RNAi}* and any other group. Mean ± SEM, n=77-101.

Generation of a cell-specific *sandman* CRISPR knockout

To overcome common limitations often faced by RNA-mediated interference such as off-target effects and insufficient knockdown, a cell-specific CRISPR knockout of the gene was generated as well for future studies. To engineer such a knockout, guide RNA (gRNA) sequences were cloned into a *UAS* vector *(pCFD6)* (Port & Bullock, 2016). Because targeting of more than one gRNA increases the probability of a knockout (Port & Bullock, 2016), four different gRNA sequences were selected and constructs bearing two (2X), three (3X) or four (4X) gRNAs were generated (**Figure 15**). These constructs will be used in combination with *UAS-Cas9; R23E10-GAL4* lines to test whether endognous knockout of *sandman* in the dFB neurons recapitulates the phenotype obtained with RNAi.

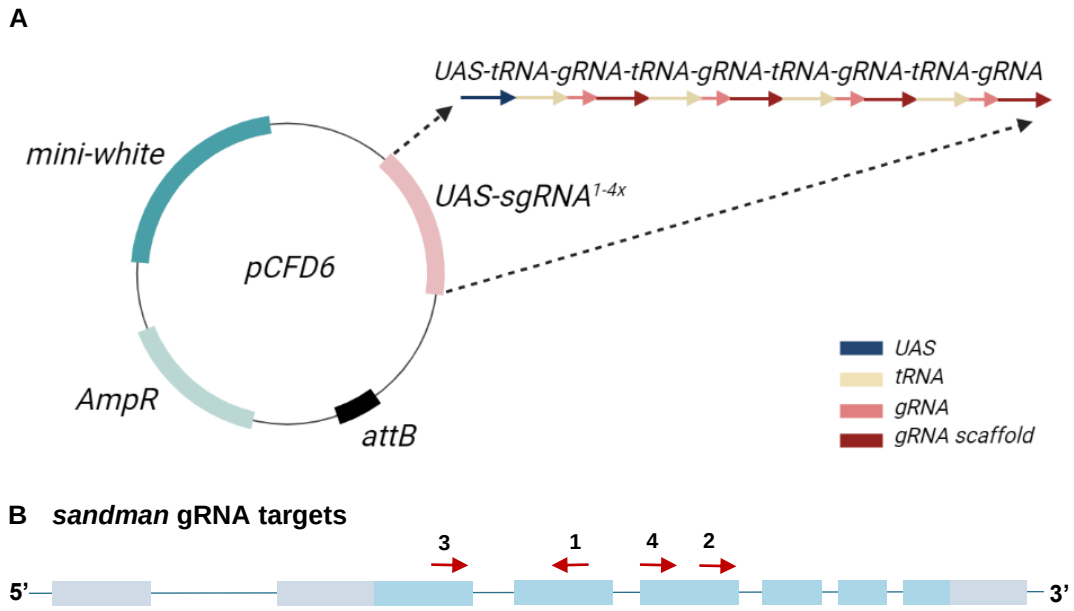

Figure 15: gRNA design for *sandman*. (A) Different gRNA sequences for *sandman* were cloned into a *UAS* vector for the generation of a cell-specific knockout. The transfer RNA sequences *(tRNA)* within the RNA scaffold facilitate the processing and excision of multiple gRNAs as a single transcript (Port & Bullock, 2016; Xie et al., 2015). The *attB* site is used for site-specific integration of the plasmid using the PhiC31 system (Bischof et al., 2007). *Ampicillin-resistance (AmpR)* refers to the selection marker used for cloning and *mini-white* is used for the identification of transformants. **(B)** *sandman* transcript showing the sites of gRNA targets. Diagram created with BioRender.com.

2.4 DISCUSSION

Dopamine's inhibitory effects on the dFB neurons switches them to electrical quiescence (OFF) (Pimentel et al., 2016). Loss of the two-pore domain potassium channel Sandman from the dFB neurons, lifts this inhibition (Pimentel et al., 2016). Similarly, blocking vesicle exocytosis prevents the switch to the OFF state (Pimentel et al., 2016). Thus, it is hypothesised that Sandman is stored in intracellular vesicles when the neurons are electrically active and translocates to the plasma membrane when the neurons switch OFF. To visualise the recycling of the channel, Sandman was first tagged with a pH-sensitive version of GFP, the super-ecliptic pHluorin.

Due to the pH-sensitivity of the pHluorin, it was first attempted to fuse the fluorophore at extracellular sites of the channel (**Figure 3**). The first extracellular loop of K2P channels is crucial for the functionality of the channel as it provides insensitivity to potassium channel blockers and mediates the efflux of K+ to the extracellular environment (Zuniga & Zuniga, 2016). Therefore, only four pHluorin insertions were targeted at the first loop. When transfected to HEK cells (**Figure 4)**, the channel localised in intracellular compartments of the cell, suggesting that either the molecular machinery required for its exocytosis is lacking in these cells or that the channel is retained due to misfolding. Indeed, co-localisation between an ER marker (KDEL) and the channel, favours the second interpretation (**Figure 5**).

To test whether the pHluorin-tagged channel maintained its physiological function *in vivo*, the *sand-pHluorin* inserts were subcloned into *UAS* vectors and injected to flies. Because loss of Sandman in the dFB neurons causes flies to sleep more (Pimentel et al., 2016), its overexpression is expected to decrease sleep. Indeed, in some cases a decrease in the total amount of sleep is observed (**Figure 6** and **Figure 7**). To correlate the behavioural phenotype with the appropriate localisation of the channel, the dFB neurons were stained with a GFP antibody to visualise the pHluorin and a tdTomato plasma membrane marker was co-expressed (**Figure 6** and **Figure 7**). However, as in the HEK cells, the channel was largely retained in the cell interior, or present in a small proportion at the plasma membrane. The behavioural phenotype in many cases could therefore be

attributed to improper folding of the channel and cytotoxic effects on dFB neurons. One insertion that revealed fluorescence throughout the cell and was associated with a decrease in sleep when expressed in the dFB neurons (*UAS-sand:ECL2_5*) was further chosen for live imaging.

Dopamine injection at the dendrites of dFB neurons is hypothesised to promote the channel's exocytosis (Pimentel et al., 2016). Consequently, expression of Sandman at the cell surface is expected to correlate with an increase in the pHluorin signal due to exposure of the fluorophore at a more basic pH. Following dopamine application, such an increase in the pHluorin signal was not observed in either the dendrites, axons or somata of the dFB neurons (**Figure 9**).

One explanation for the lack of changes in the pHluorin signal, could be the time-course of the experiment. Scans were acquired 5min following the application of the neurotransmitter. The experimental design predicts that dopamine will cause the sustained presence of the channel at the plasma membrane. However, dopamine's inhibitory effects on the dFB neurons can occur within seconds following its application (Pimentel et al., 2016). Further the decay time of the pHluorin signal (Sankaranarayanan & Ryan, 2000) and the endocytosis rate of the channel may operate in very short timescales as well. Therefore, changes in the pHluorin signal could be missed due to transient effects of dopamine, the speed of the channel's endocytosis and/or the decay time of the pHluorin's signal. Taking these parameters into consideration, an ideal imaging setting would be time-lapse imaging during dopamine stimulation. However, because dopamine delivery using a Picospritzer introduces movement, it has not been possible to use this approach.

As the pHluorin is pH-sensitive, acidic treatment serves as a second way of determining whether the channel resides at the surface (Sankaranarayanan et al., 2000). Alternatively, treatment with ammonium chloride (NH_4Cl) reveals the total fluorescence of the pHluorin signal by elevating the vesicle pH (Sankaranarayanan et al., 2000). Given that both manipulations did not correlate with any change in the fluorescence ratio (a decrease or an increase respectively) it is most likely that the pHluorin tagged channel is retained in subcellular compartments of the cell (**Figure 10**). Another possibility is that the fluorophore

is cleaved from the channel during post-translational modifications resulting in abnormal fluorescence distribution (Ashby et al., 2004). If this is true, the unchanged fluorescence ratio can be explained, as the fluorophore alone will not respond to the neurotransmitter. To test for this possibility, a western blot can be used to detect the recombinant protein.

The sensitivity of the pHluorin signal detection depends largely on two parameters: the proportion of the channel at the plasma membrane and the pH of intracellular organelles (Sankaranarayanan et al., 2000). Thus, optimum conditions for the imaging include a well-acidified cell interior and a large proportion of Sandman at the plasma membrane. As the pHluorin signal from the flies imaged above (*UAS-CD4-tdTomato;R23E10-GAL4*/*UAS-sand:ECL2_5*) is visible everywhere, and dopamine application does not induce a significant increase in the pHluorin signal these conditions are not met. Therefore, even if a change in the fluorescence signal occurs, it is challenging to detect.

An insertion which also led in a decrease in sleep when expressed in the dFB neurons but where the pHluorin signal was mainly observed intracellularly (*UAS-sand:ECL 3_3*) was also selected for imaging to test whether an increase in the exocytic events/pHluorin signal would be easier to detect. However, also in this case, no increase in the fluorescence ratio was observed (**Figure 11**). Finally, four additional constructs with flexible linkers at each site before and after the tag insertion, were also generated but presented the same morphology as the rest of the constructs.

Given the very small extracellular sites offered by the structure of the channel and the large size of the pHluorin protein, there is a high probability that insertion of the tag impairs the correct folding and function of Sandman. An alternative way to live-image the recycling of Sandman in the future could be with bio-orthogonal amino acid tagging. This technology utilises tRNA/aminoacyl-tRNA synthetase (aaRS) pairs that facilitate the incorporation of unnatural amino acids in the protein of interest (Wang et al., 2001). The unnatural amino acids, often act as reporters of subcellular localisation and trafficking events due to their specific properties (Wang et al., 2001). For example, properties such as photo-responsiveness in the presence of the unnatural amino acid can be a valuable tool for monitoring translocation events (Chatterjee et al., 2013). Using the *UAS/GAL4* system

in *Drosophila* these amino acid incorporations can be tissue-specific as well (Bianco et al., 2012).

Due to the obstacles faced with the pHluorin constructs, additional tools to study the trafficking of the channel were generated: N-terminal GFP and Venus tags as well as an untagged version. Flies overexpressing the channel do not show a decrease in their sleep pattern (**Figure 12**). Thus, it is possible that overexpression overwhelms the physiological regulation of the channel or that there is a saturation point whereby an increased number of Sandman molecules will not affect the state of the dFB neurons and the sleep behaviour of the insect. Staining of the N-terminal GFP-tagged flies showed that Sandman is expressed ubiquitously in the dFB neurons but as in the case of Sand-pHluorin flies, it is not clear what proportion of the channel is present at the membrane (**Figure 13**). Thus, it cannot be concluded whether the lack of sleep phenotype relates to the correct localisation of the channel. It is also noteworthy that auxiliary proteins such as 14-3-3, COP1 and p11 mediate the trafficking of the channel by binding to the N- and C-termini of K2P channels (Mathie et al., 2010). Therefore, tagging of the channel at these sites is not ideal either.

As an alternative way of investigating the trafficking of the channel, its interaction with another protein previously implicated in regulating the excitability of dFB neurons was studied. *cv-c* encodes a Rho-GAP protein whose mutation in the dFB neurons causes flies to be insomniac by clamping the neurons in electrical quiescence (Donlea et al., 2014). It is hypothesised that *cv-c* mutation likely causes surface expression of Sandman, enhancing the leak currents that maintain the OFF state and causing the insomnia observed in these flies. To test this possibility, flies with a *sandman* knockdown (*sandman*^{RNAi}) in the dFB neurons were recombined with flies carrying mutations in the *cv-c* gene. Indeed, loss of Sandman in the *cv-c* mutant background rescues the sleep loss of theses flies, possibly due to the channel's internalisation switching the neurons to the ON state (**Figure 14**). These experiments provide the first evidence that the two proteins may interact in the same pathway. Future measurements of the electrophysiological properties of the dFB neurons in flies carrying *cv-c* mutations and a *sandman* knockdown are

essential to further support this finding; if *cv-c* mutation prevents the internalisation of Sandman, an upregulation of the leak current in these flies is expected.

Lastly, as any tool, RNA interference suffers from certain limitations, most notably unwanted off-target effects and insufficient knockdown of the target due to residual gene expression (Svoboda, 2020). The type II CRISPR/Cas9 technology overcomes these limitations by reducing the amount of off-target effects and leading to permanent gene disruption (Jinek et al., 2012; Ran et al., 2013). To achieve this, the Cas9 nuclease from *S. pyogenes* is guided to the targeted genomic locus by a guide RNA sequence and induces a double-stranded break (DSB) that is repaired by either the non-homologous end joining (NHEJ) or the homology directed repair (HDR) pathways (Jinek et al., 2012). These pathways are exploited to generate knockouts and to introduce precise repair templates generating knock-ins. Coupled to the *UAS/GAL4* and *GAL80^{ts}* systems in *Drosophila*, these knockouts and knock-ins can be directed in a tissue-specific manner and switched on at will (Port et al., 2020). Cell specific CRISPR KO versions of Sandman with two, three or four gRNA sequences were therefore generated (**Figure 15**) but remain to be tested.

In conclusion, the work described in this chapter aimed to develop tools to visualise and identify the trafficking pathway of the K2P channel Sandman and by extension its role in pathways related to sleep and wakefulness. Overexpression of Sandman with different fluorophores most likely interferes with the appropriate localisation and function of the channel. However, preliminary genetic interaction experiments between Sandman and Cv-c suggest that the two proteins act in the same pathway during the sleep-wake cycle of *Drosophila* (**Figure 16**). Future studies involving candidate upstream or downstream components of this pathway are critical in further characterising sleep mechanisms, as discussed in the next chapter (**Chapter 3**).

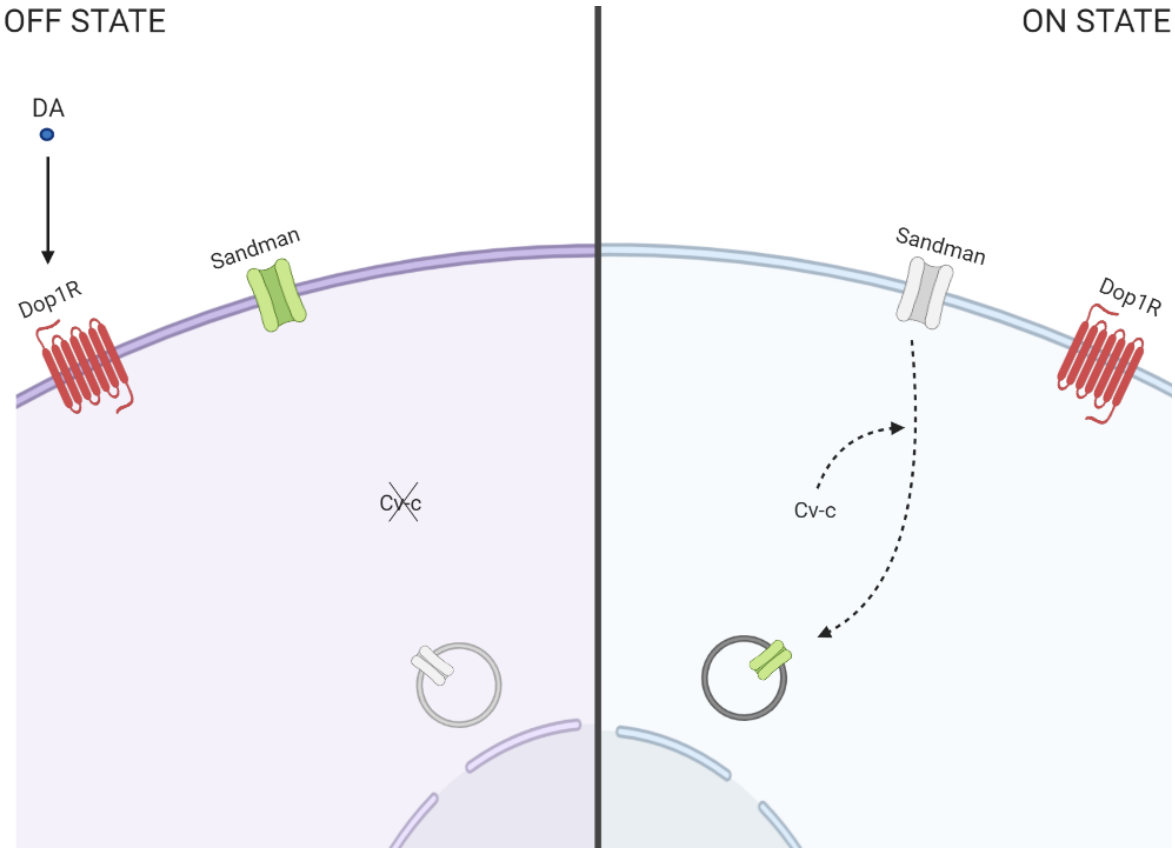

Figure 16: Cv-c and Sandman are proposed to act in the same pathway during the sleep-wake cycle of *Drosophila*. It is hypothesised that in *cv-c* mutants, the dFB neurons are locked in an electrically silent state because the mutation of the Rho-GAP prevents the internalisation of Sandman. As a result expression of Sandman at the plasma membrane retains electrical quiescence. Figure created with BioRender.com.

Chapter 3

TOLL RECEPTORS AS REGULATORS OF SLEEP PRESSURE

3.1 INTRODUCTION

The concept that sleep is regulated by somnogens dates to the early 20th century and the experiments of Legendre and Pieron and of Ishimori; these investigators showed that the infusion of cerebrospinal fluid from sleep-deprived dogs to non-deprived ones would cause the latter group to fall asleep (Ishimori, 1909; Kubota, 1989; Legendre & Piéron, 1907). An explanation for the phenomenon invoked the existence of endogenous substances with hypnagogic effects. To date, many sleep-inducing molecules have been identified, including growth factors (Brown et al., 2012).

In rats, the expression of brain-derived neurotrophic factor (BDNF), a growth factor that is well-characterised to modulate activity-dependent plasticity is induced by wakefulness or following sleep deprivation in several brain regions such as the cortex, thalamus and the hippocampus (Cirelli & Tononi, 2000). Similarly, the levels of receptor tyrosine kinase B (TrkB), through which BDNF exerts its effect, are elevated under the same conditions (Cirelli & Tononi, 2000). Accordingly, injecting BDNF into the cortex of rats increases slow-wave activity (SWA) during sleep - a marker commonly used to asses sleep homeostasis (Faraguna et al., 2008). Conversely, blocking TrkB leads to the opposite outcome, attenuating SWA compared to animals injected with vehicle (Faraguna et al., 2008).

The amount of time rats engage in exploratory behaviour, is also proportional to the induction of BDNF levels and SWA (Huber et al., 2007). The higher the BDNF inductions, the stronger is SWA response in the subsequent sleep period (Huber et al., 2007). In humans as well, a single polymorphism within the BDNF gene enhances cognitive performance and accounts for differences in SWA (Bachmann et al., 2012). Individuals with a Val/Val over a Val/Met substitution show better response accuracies in memory tasks and higher activity in the delta range (Bachmann et al., 2012).

Evidence for the existence of neurotrophin orthologs in *Drosophila* has been lacking for many years. From early studies, Spätzle (Spz), a protein well characterized for its effects in development and immunity through the Toll receptor, was identified to contain a cysteine-knot domain comparable to nerve growth factor (NGF) (DeLotto & DeLotto, 1998). However, due to the domain similarity to the *Horseshoe crab* coagulogen (Mizuguchi et al., 1998), a possible neutrotrophin role for this protein seemed unlikely. Initial BLAST searches for neurotrophins revealed no clear orthologues of these trophic factors in *Drosophila* and *C. elegans* (Rubin et al., 2000). Their absence was attributed to the small size of the insect and worm brains that was assumed not to require plastic interactions to adjust cell number and organ formation (Jaaro et al., 2001).

Eventually, two paralogues of the Spz family, spz2 and spz5 - renamed to *Drosophila* neurotrophin 1 (DNT1) and *Drosophila* neurotrophin 2 (DNT2) respectively - were the first proteins characterised in *Drosophila* to execute essential neurotrophic functions: targeted innervation of neurons and regulation of neuronal survival and numbers (Zhu et al., 2008). DNT1 and DNT2 are expressed in target cells during embryonic stages and the central brain during the adult stage. Their loss of function is associated with increased apoptosis and the axonal misrouting and mistargeting of neurons (Zhu et al., 2008).

The receptors downstream of these secreted proteins belong to the Toll receptor family and include Toll-6 and Toll-7 (McIlroy et al., 2013). The two receptors exhibit neurotrophic function as well by regulating neuronal survival and motor axon targeting (McIlroy et al., 2013). Genetic interaction studies showed that apoptosis caused by *DNT1* mutants can be rescued by overexpressing the *Toll-7* receptor while apoptosis caused by *DNT2* mutants is rescued when overexpressing the *Toll-6* receptor (McIlroy et al., 2013). Thus, it is proposed that Toll-7 and Toll-6 are the downstream receptors for DNT1 and DNT2 respectively (McIlroy et al., 2013). However, binding of the ligands to the receptors is promiscuous; co-immunoprecipitation from S2 cells suggest that both receptors could bind either ligand (Foldi et al., 2017).

Neurotrophins often signal through small GTPases to exert their effects (Reichardt, 2006). An example involves the peripheral nervous system myelination, a process dependent partly on Schwann cell migration. Neurotrophin 3 (NT3) acts through the receptor tyrosine kinase C (TrkC), initiating a Rac1 and cdc42 cascade that activates the c-Jun N-terminal pathway, stimulating Schwann cell migration (Yamauchi et al., 2003). BDNF, on the other hand, acts on the $p75^{NTR}$ receptor to inhibit Schwann cell migration through RhoA mediated-signalling (Yamauchi et al., 2004). Therefore, due to their multiple targets, neurotrophins and downstream GTPases are strong candidates for the regulation of several biological processes.

Importantly, Toll-6 and Toll-7 localise to layers of the fan-shaped body (McIlroy et al., 2013), a major sleep-promoting structure in the fly (Donlea et al., 2014; Donlea et al., 2018; Donlea et al., 2011; Pimentel et al., 2016). *cv-c* is gene encoding for a Rho-GAP whose mutation locks the dFB neurons into an electrically silent state and produces flies with fragmented sleep patterns (Donlea et al., 2014). Switching or retaining the dFB neurons to the OFF state, is hypothesised to require Sandman at the plasma membrane (Pimentel et al., 2016). Genetic interaction experiments described in the previous chapter provide preliminary evidence to support this theory. As neurotrophins are capable of signalling through GTPases, a plausible hypothesis is that sleep pressure is reflected in the activity-dependent release of neurotrophins and transduced in the fan-shaped body by Toll-receptors upstream of Cv-c and Sandman. The aim of this chapter was to investigate if a Toll receptor signals sleep pressure in the dFB neurons through the Cv-c-Sandman pathway, inducing sleep.

3.2 RESULTS

Sleep amount in flies with RNAi-mediated knockdown for Toll receptors in the dFB neurons

To identify whether Toll receptors regulate sleep in the dFB, RNAi lines targeting *Toll* genes were restricted to the dFB neurons using the *R23E10-GAL4* line. The knockdown of four receptors (Toll-8, Toll-2, Toll-5, and Toll-6) in the sleep promoting-circuit causes a reduction in the total amount of sleep (**Figure 17**). Because Toll-6 is one of the two receptors with established neurotrophic function and multiple RNAi lines directed against the gene produce the same phenotype, subsequent experiments have focused on this receptor.

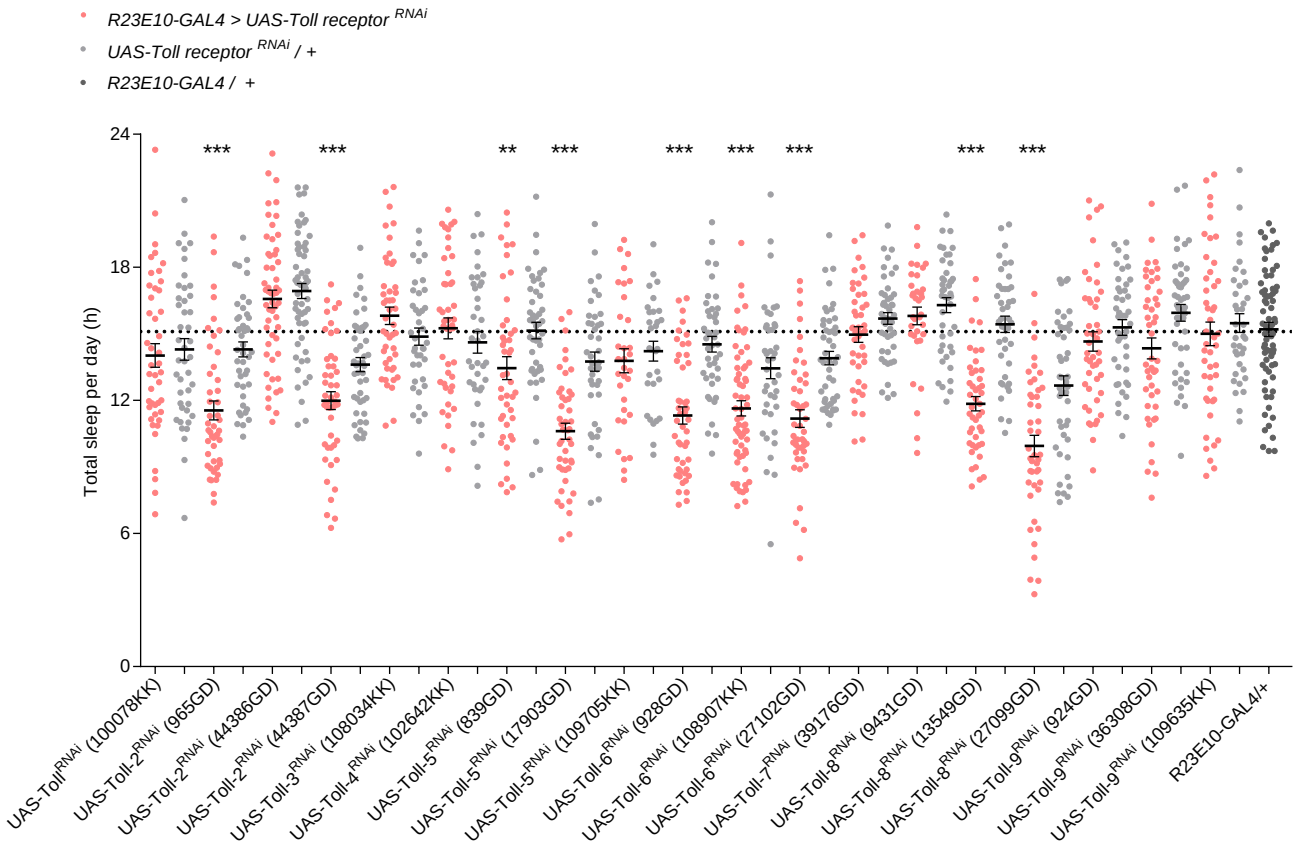

Figure 17: Sleep amount in flies with RNAi lines targeting *Toll* receptors in the dFB neurons using *R23E10-GAL4*. RNAi lines targeting *Toll* receptors were driven in the dFB neurons by the *R23E10-GAL4* line (pink). The *UAS-Toll receptor/+* and *R23E10-GAL4/+* parental controls are shown in grey and dark grey respectively. Knockdown of *Toll* receptors in the dFB causes a reduction in sleep compared to controls in the following cases; *UAS-Toll-2^{RNAi} (965GD)*: $F_{(2, 158)}$ = 27.60, p<0.0001, *UAS-Toll-2^{RNAi} (44387GD)*: $F_{(2, 161)}$ = 22.69, p<0.0001, *UAS-Toll-5^{RNAi} (839GD)*: $F_{(2, 157)}$ = 5.874, p=0.0035, *UAS-Toll-5^{RNAi} (17903GD)*: $F_{(2, 156)}$ =42.52, p<0.0001, *UAS-Toll-6^{RNAi} (928GD)*: $F_{(2, 158)}$ = 34.00, p<0.0001, *UAS-Toll-6^{RNAi} (108907KK)*: $F_{(2, 172)}$ = 27.90, p<0.0001, *UAS-Toll-6^{RNAi} (27102GD)*: $F_{(2, 160)}$ = 35.41, p<0.0001, *UAS-Toll-8^{RNAi} (13549GD)*: $F_{(2, 155)}$ = 31.80, p<0.0001 and *UAS-Toll-8^{RNAi} (27099GD)*: $F_{(2, 157)}$ = 45.24, p<0.0001. One-way ANOVA with *Holm-Sidak's* multiple comparisons test. Asterisks denote significant differences between dFB-driven RNAi lines for the receptors and both parental controls. Mean ± SEM, n = 42-71.

Depletion of the Toll-6 receptor from dFB neurons decreases sleep

To further establish the effect of Toll-6 receptor knockdown in dFB neurons, two *GAL4* lines (*R23E10-GAL4* and *R84C10-GAL4*) that label the dFB neurons and three RNAi lines targeting the gene were used (**Figure 18** and **Figure 19**). Expressing *Toll-6^{RNAi}* under the control of both dFB-specific *GAL4* lines reduces the total amount of sleep of the flies (**Figure 18B** and **Figure 19B**). Decreases in the sleep bout durations were observed with one *R23E10-GAL4*-driven *Toll-6^{RNAi}* line (928GD) during day time (**Figure 18D**) and two *R23E10-GAL4*-driven *Toll-6^{RNAi}* lines (928GD and 27102GD) during night-time (**Figure 18E**). Under the *R84C10-GAL4* control, a decrease in sleep bout duration was observed with all three RNAi lines targeting *Toll-6* during the day (**Figure 19D**) and a tendency during the night was also apparent (**Figure 19E**). Overall, these data suggest that flies with reduced levels of the receptor are likely defective in maintaining their sleep. To exclude that the observed decrease in sleep is due to hyperactivity, the activity of the flies during waking periods was also assessed (**Figure 18C** and **Figure 19C**). As this parameter was not significantly different in flies expressing *Toll-6^{RNAi}* driven with either *GAL4* line and control flies, the possibility was rejected. Flies with a *R23E10-GAL4*-driven *Toll-6^{RNAi}* line (928GD) also showed prolonged latency to sleep onset (**Figure 18F**).

Due to the developmental roles that Toll receptors fulfil it was also essential to exclude that the reduction in sleep in Toll-6 deficient flies is the result of developmental defects. To this end, the *R23E10-GAL4* line was combined with the temperature - sensitive *tubP-GAL80^{ts}* repressor, which allows expression of the *GAL4* (and therefore of the transgene) only at the permissive temperature of 31°C (**Figure 20**). Compared to flies raised at 18°C, adult-onset induction of *Toll-6^{RNAi}* in the dFB neurons at 31°C, decreases sleep suggesting that the phenotype observed under normal temperature conditions is not due to developmental abnormalities (**Figure 20A** and **Figure 20B**).

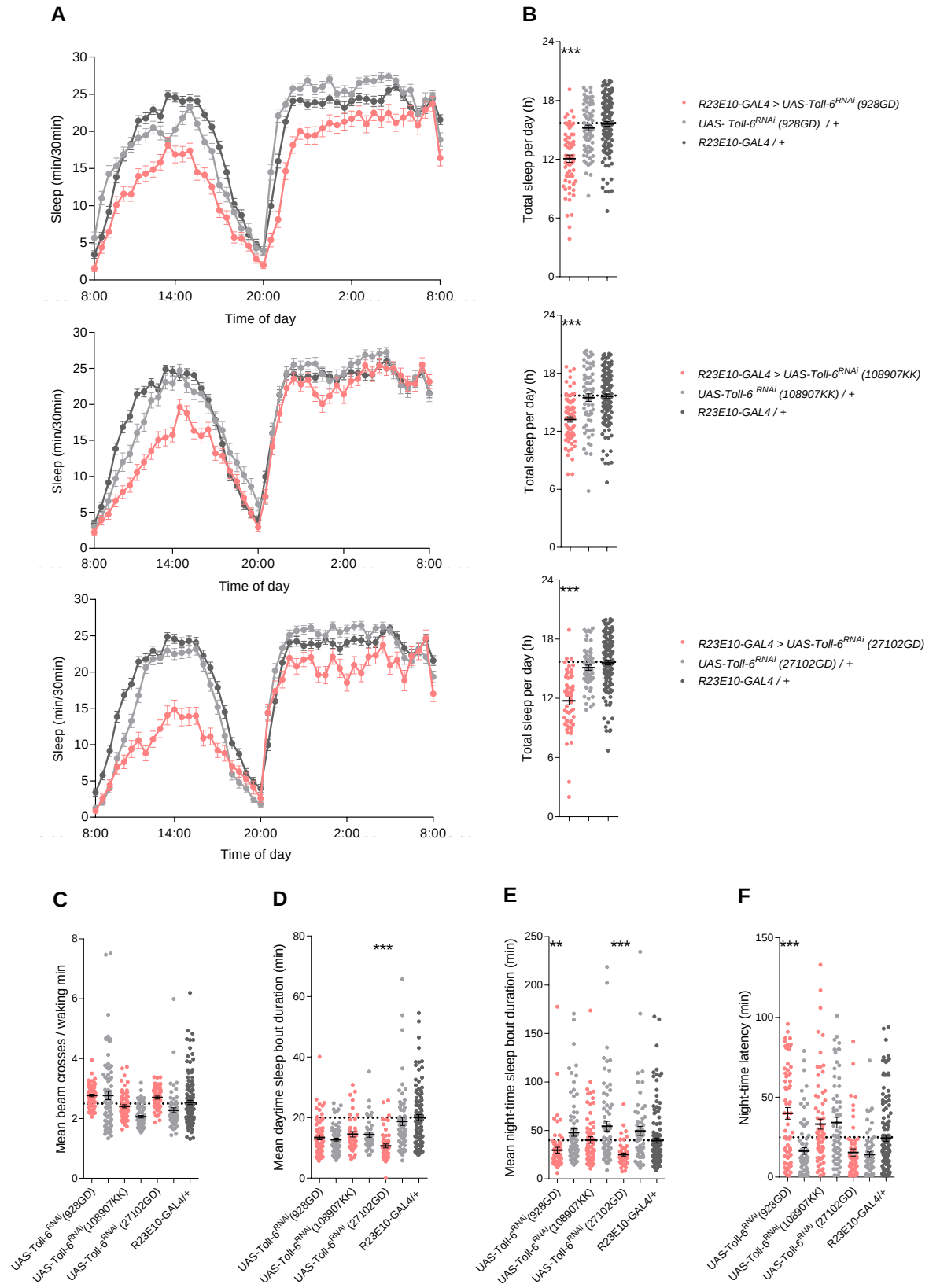

Figure 18: dFB-restricted interference with *Toll-6* using *R23E10-GAL4*. (A) Sleep (minutes per 30 minutes) of flies expressing *R23E10-GAL4*-driven RNAi lines targeting*Toll-6* (pink) and of *UAS-Toll-6^{RNAi}*/+ and *R23E10-GAL4*/+ parental controls, shown in grey and dark grey respectively. **(B)** Flies with *R23E10-GAL4*-driven *Toll-6^{RNAi}* have reduced sleep compared to parental controls; 928GD: $F_{(2, 276)} = 39.79$, $p<0.0001$, 108907KK: $F_{(2, 273)} = 19.76$, $p<0.0001$, and 27102GD: $F_{(2, 253)} = 44.50$, $p<0.0001$. **(C)** *R23E10-GAL4*-driven *Toll-6^{RNAi}* flies are not hyperactive compared to their parental controls. **(D)** The mean sleep bout duration of flies expressing *R23E10-GAL4*-driven *Toll-6^{RNAi}* was reduced in one case during daytime; 27102GD: $F_{(2, 253)} = 20.37$, $p<0.0001$ and **(E)** in two cases during night-time; 928GD: $F_{(2, 276)} = 6.803$, $p=0.0013$) and 27102GD: $F_{(2, 253)} = 10.92$, $p<0.0001$ **(F)** The sleep latency of flies with *R23E10-GAL4*-driven *Toll-6^{RNAi}* is also longer in the case of one RNAi line; 928GD: $F_{(2, 276)} = 20.29$, $p<0.0001$. **(B-F)** One-way ANOVA with *Holm-Sidak's* multiple comparisons test. Asterisks denote significant differences between *R23E10-GAL4*-driven RNAi lines for *Toll-6* and both parental controls. Mean ± SEM, n=58-137.

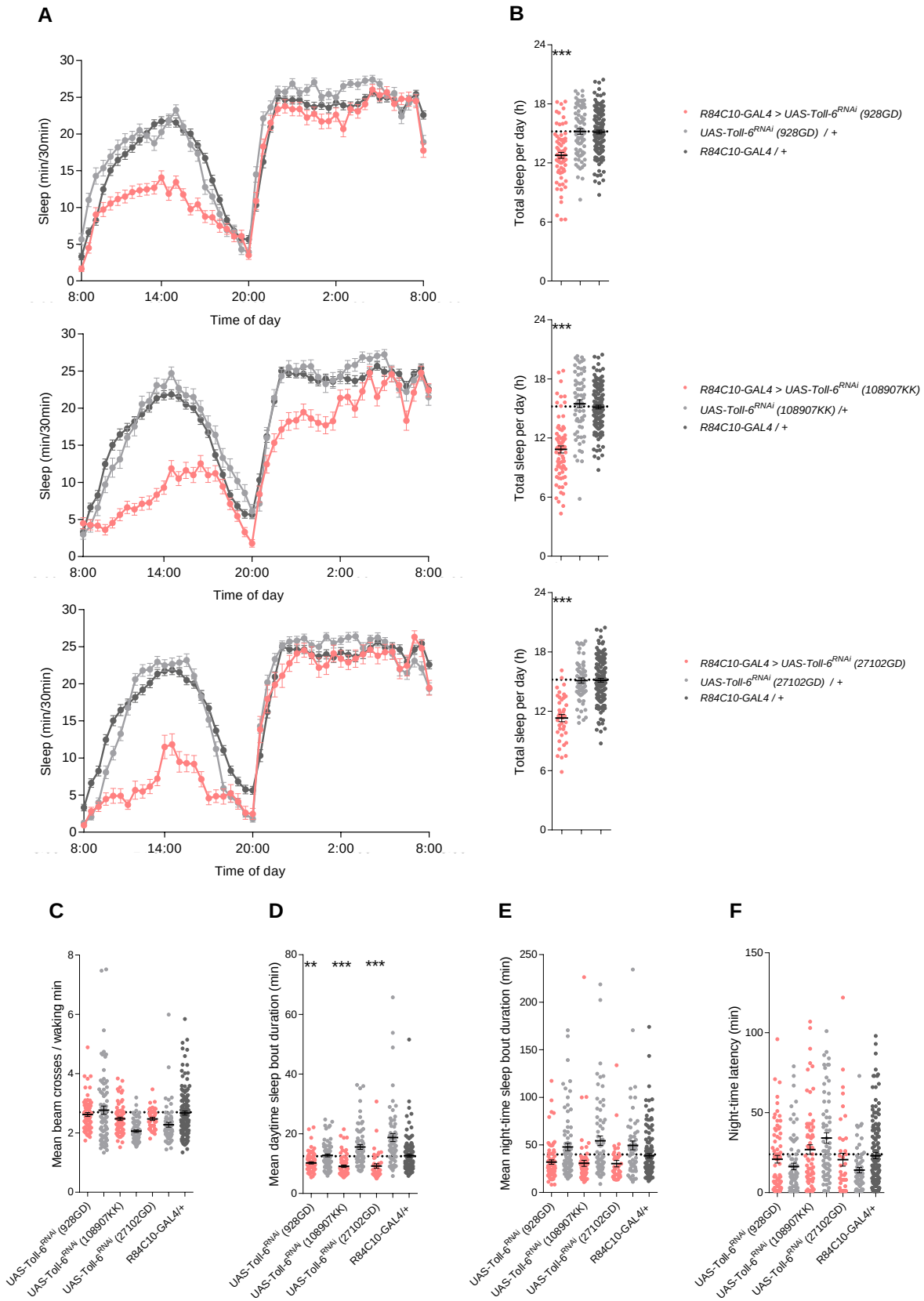

Figure 19: dFB-restricted interference with *Toll-6* using *R84C10-GAL4*. (A) Sleep (minutes per 30 minutes) of flies expressing *R84C10-GAL4*-driven RNAi lines targeting *Toll-6* (pink) and of *UAS-Toll-6^{RNAi}*/+ and *R84C10-GAL4*/+ parental controls, shown in grey and dark grey respectively. **(B)** Flies with *R84C10-GAL4*-driven *Toll-6^{RNAi}* have reduced sleep compared to parental controls; 928GD: $F_{(2, 293)} = 27.04$, $p<0.0001$, 108907KK: $F_{(2, 282)} = 71.66$, $p<0.0001$, 27102GD: $F_{(2, 246)} = 50.02$, $p<0.0001$. **(C)** Activity during waking periods does not differ between *R84C10-GAL4*-driven *Toll-6^{RNAi}* flies and their parental controls. **(D)** During daytime, the mean sleep bout duration of all *R84C10-GAL4*-driven *Toll-6^{RNAi}* flies was reduced; 928GD: $F_{(2, 293)} = 7.645$, $p = 0.0006$, 108907KK: $F_{(2, 282)} = 26.19$, $p<0.0001$ and 27102GD: $F_{(2, 246)} = 25.91$, $p<0.0001$, while **(E)** no significant difference in the night-time mean sleep bout durations was observed. **(F)** No differences in sleep latency were detected between genotypes. **(B-F)** One-way ANOVA with *Holm-Sidak's* multiple comparisons test. Asterisks denote significant differences between *R84C10-GAL4*-driven RNAi lines for *Toll-6* and both parental controls. Mean ± SEM, n=41-145.

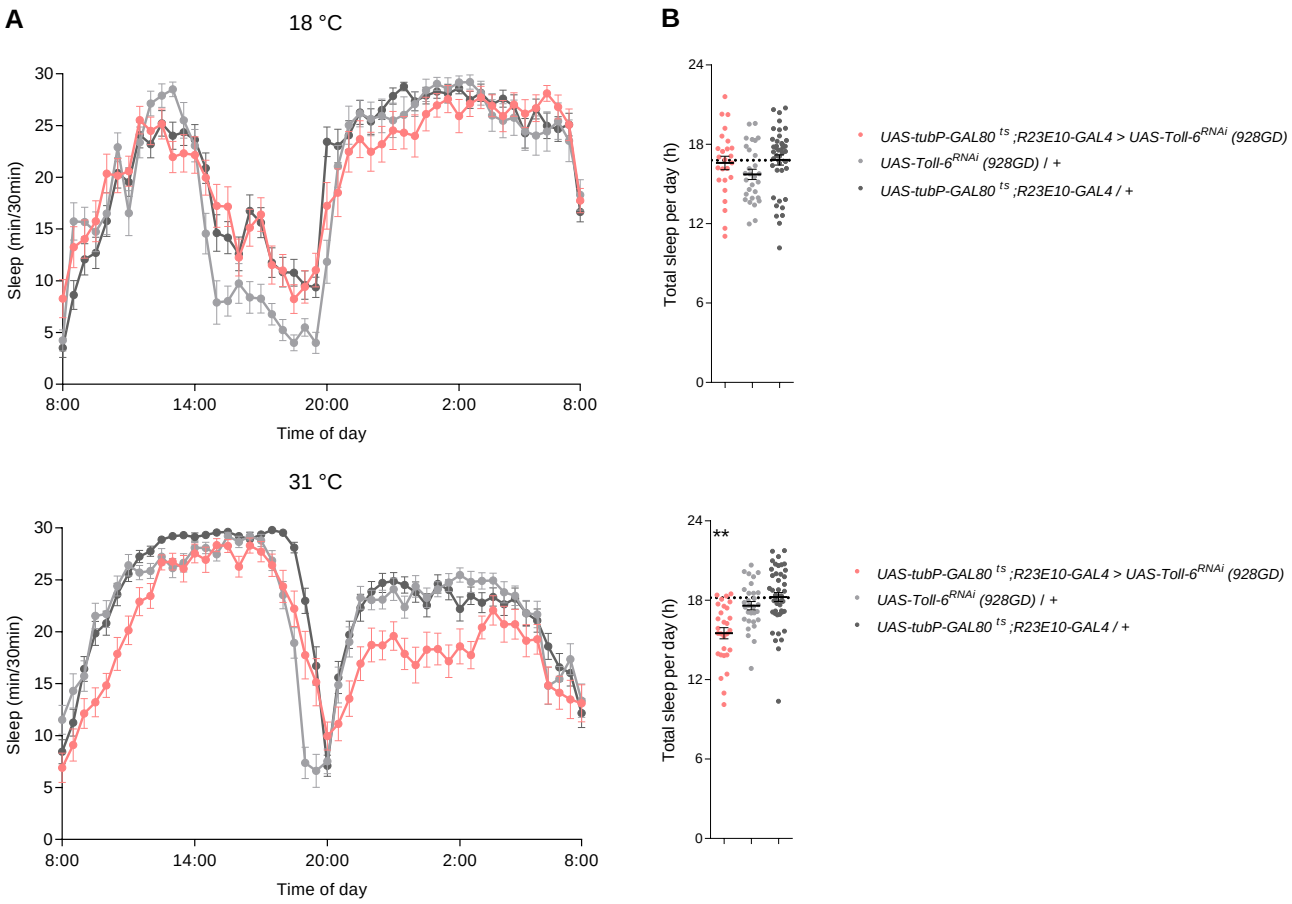

Figure 20: Adult-onset induction of *Toll-6^{RNAi}* in the dFB neurons using the temperature-sensitive *GAL80^{ts}* repressor. (A) Sleep (minutes per 30 minutes) of flies expressing *Toll-6^{RNAi}* in the dFB neurons (pink) and of parental controls, raised at 18°C or 31°C. The *UAS-Toll-6^{RNAi}/+* and *UAS-tubP-GAL80^{ts};R23E10-GAL4/+* parental controls are shown in grey and dark grey respectively. **(B)** The total amount of sleep in flies with dFB-driven *Toll-6^{RNAi}* is reduced only at 31°C compared to parental controls. Two-way ANOVA with *Holm-Sidak's* multiple comparisons test, interaction of genotype x temperature: $F_{(2, 192)} = 7.139$, $p = 0.0010$. Mean ± SEM, n=25-44.

Toll-6 mutation reduces sleep

Mutants for *Toll-6* (*Toll-6*^{MI02127}) generated by a transposon insertion disrupting the sequence of the gene were tested as well, in two genetic backgrounds: yellow-white *(yw)* and Canton-Special *(CS)*. The *yw* background is the genetic background of the mutants and the *CS* background the commonly used wild-type *(wt)* background. *Toll-6* homozygous mutant flies (*Toll-6*^{MI02127}/*Toll-6*^{MI02127}) exhibited a dramatic sleep loss (**Figure 21B** and **Figure 22B**), decreased sleep bout durations that were more prominent during night-time (**Figure 21E** and **Figure 22E**) and increased night-time sleep latencies (**Figure 21F** and **Figure 22F**) compared to controls in both backgrounds. Compared to controls in the *wt* background, the homozygous *Toll-6* mutant flies were more active (**Figure 22C**); this might be due to the genetic background differences.

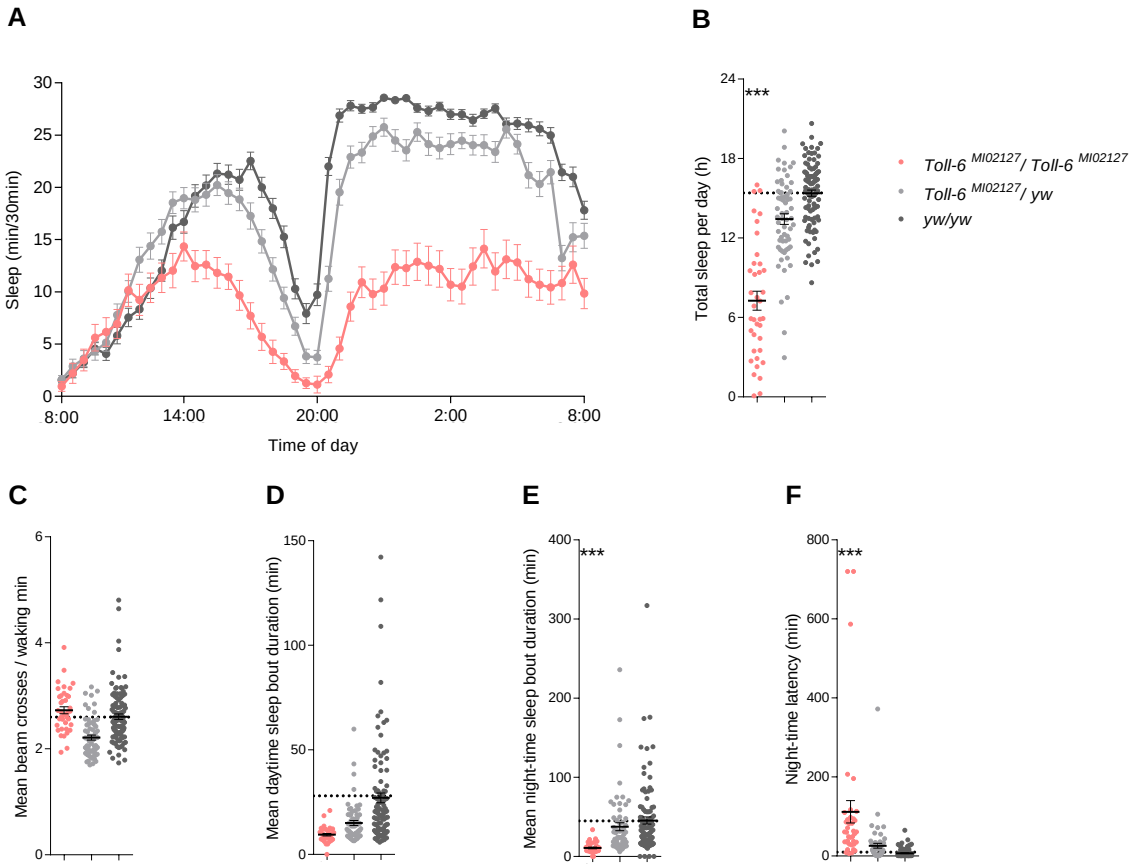

Figure 21: Sleep architecture of *Toll-6*^{MI02127} mutants in the *yw* background. (A) Sleep (minutes per 30 minutes) of *Toll-6*^{MI02127} homozygous mutant flies (pink) and of heterozygous (*Toll-6*^{MI02127}/*yw*) and *yw* controls shown in grey and dark grey respectively. **(B)** The total amount of sleep in *Toll-6*^{MI02127} homozygous mutant flies is reduced compared to controls: $F_{(2, 199)} = 94.62$, $p<0.0001$. **(C)** *Toll-6*^{MI02127} homozygous mutant flies are equally active to the *yw* control flies but not the *Toll-6*^{MI02127}/*yw* heterozygous flies. **(D)** During daytime, both *Toll-6*^{MI02127} homozygous and heterozygous mutants tend to sleep less. **(E)** In contrast, during night-time, only *Toll-6*^{MI02127} homozygous mutants show a defect in maintaining their sleep: $F_{(2, 199)} = 11.12$, $p<0.0001$. **(F)** The night-time sleep latency was also increased in *Toll-6*^{MI02127} homozygous mutants: $F_{(2, 199)} = 23.83$, $p<0.0001$. **(B-F)** One-way ANOVA with *Holm-Sidak's* multiple comparisons test. Asterisks denote significant differences between *Toll-6*^{MI02127} homozygous mutants and both controls. Mean ± SEM, n=38-64.

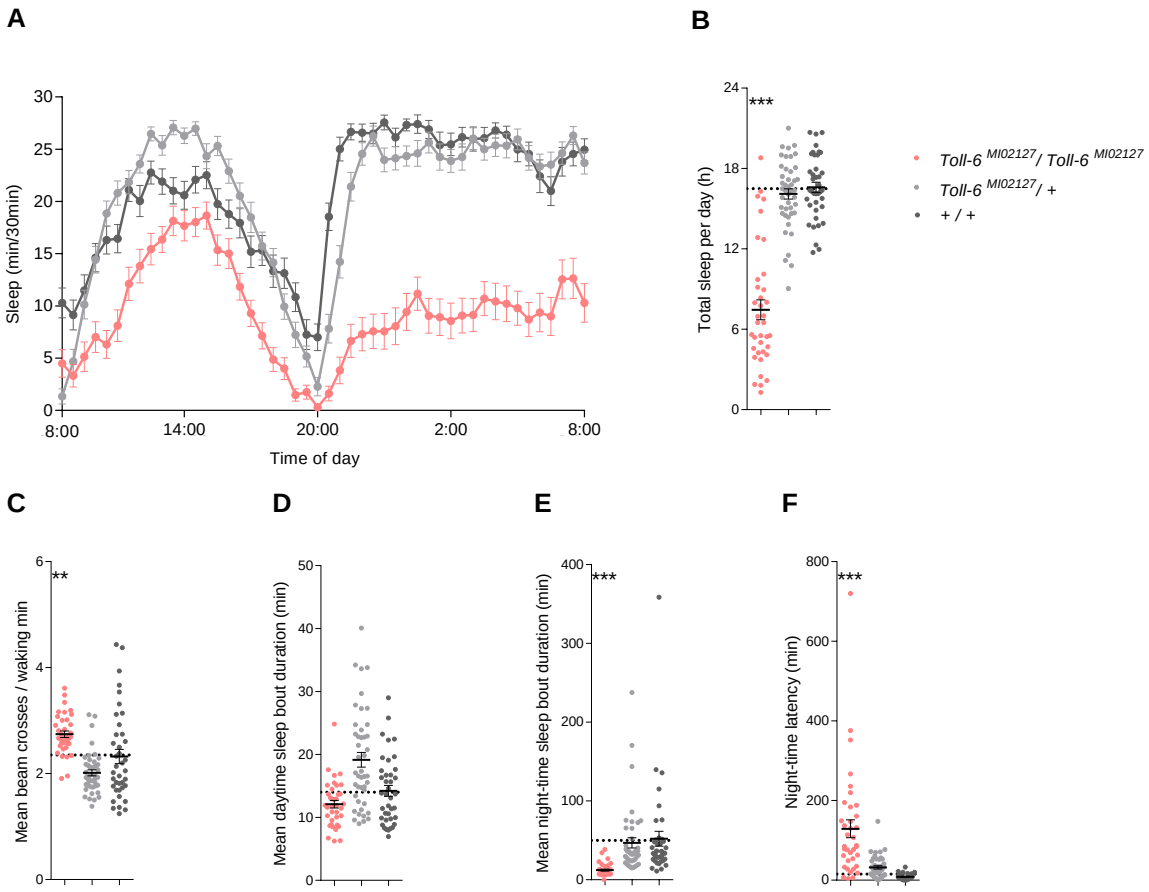

Figure 22: Sleep architecture of *Toll-6^{MI02127}* mutants in the *wt* background (A) Sleep (minutes per 30 minutes) of *Toll-6^{MI02127}* homozygous mutant flies (pink) and of heterozygous (*Toll-6^{MI02127}/+)* and *wt* controls shown in grey and dark grey respectively. **(B)** *Toll-6^{MI02127}* homozygous flies show a reduction in their total amount of sleep compared to controls: $F_{(2, 117)} = 96.48$, $p<0.0001$. **(C)** *Toll-6^{MI02127}* homozygous mutants display a slight hyperactivity compared to both parental controls in the *wt* background: $F_{(2, 117)} = 16.30$, $p<0.0001$. **(D)** Significant differences of the *Toll-6^{MI02127}* homozygous mutants from both controls were not detected in the mean sleep bout duration during daytime, but they were **(E)** during night-time: $F_{(2, 117)} = 9.767$, $p<0.0001$. **(F)** Night-time sleep latencies of *Toll-6^{MI02127}* homozygous flies were increased as well: $F_{(2, 117)} = 26.18$, $p<0.0001$. **(B-F)** One-way ANOVA with *Holm-Sidak's* multiple comparisons test. Asterisks denote significant differences between *Toll-6^{MI02127}* homozygous mutants and both controls. Mean ± SEM, n=37-44.

Toll-6 receptor may act upstream of Cv-c during the sleep-wake cycle

The reduction in sleep in flies lacking the *Toll-6* receptor is reminiscent of the insomniac *cv-c* mutant phenotype in which the dFB neurons are clamped to the OFF state (Donlea et al., 2014). It was therefore natural to ask if these two proteins act in the same pathway. To test this hypothesis, *cv-c/Toll-6* mutant flies were first generated, using two *cv-c* alleles previously characterised for their effects on sleep (Donlea et al., 2014): *cv-c*^{C524} and *cv-c*^{MB03717}.

cv-c/Toll-6 mutant flies (*cv-c*^{C524}*/Toll-6*^{MI02127} or *cv-c*^{MB03717}*/Toll*-6^{MI02127}) suffer a severe disruption in their sleep pattern compared to heterozygous controls carrying only one mutant allele (**Figure 23** and **Figure 24**). More importantly, *cv-c*^{C524}*/Toll-6*^{MI02127} mutants sleep as little as the *cv-c* transheterozygotes (**Figure 23B**). *cv-c*^{MB03717}*/Toll-6*^{MI02127} flies show a milder phenotype (**Figure 24B**); these results might arise due to differences in the penetrance of the *cv-c* mutations. Accordingly, during both daytime and night-time, sleep bout durations were equal in *cv-c*^{C524}*/Toll-6*^{MI02127} flies and *Toll-6* homozygous or *cv-c* mutants, and shorter than those of heterozygous controls (**Figure 23C** and **Figure 23D**). Sleep bout durations were also equal in *cv-c*^{MB03717}*/Toll-6*^{MI02127} and *Toll-6* or *cv-c* mutants and much shorter than heterozygous controls during night-time (**Figure 24E**).

Lastly, compared to the rest of the groups, *Toll-6* homozygous mutants showed increased locomotor activity during waking-periods (**Figure 23C** and **Figure 24C**). However, because flies with dFB-driven *Toll-6*^{RNAi} are not hyperactive (**Figure 18C** and **Figure 19C**), such excess in locomotor activity may be attributed to the organism-wide extent of the mutation.

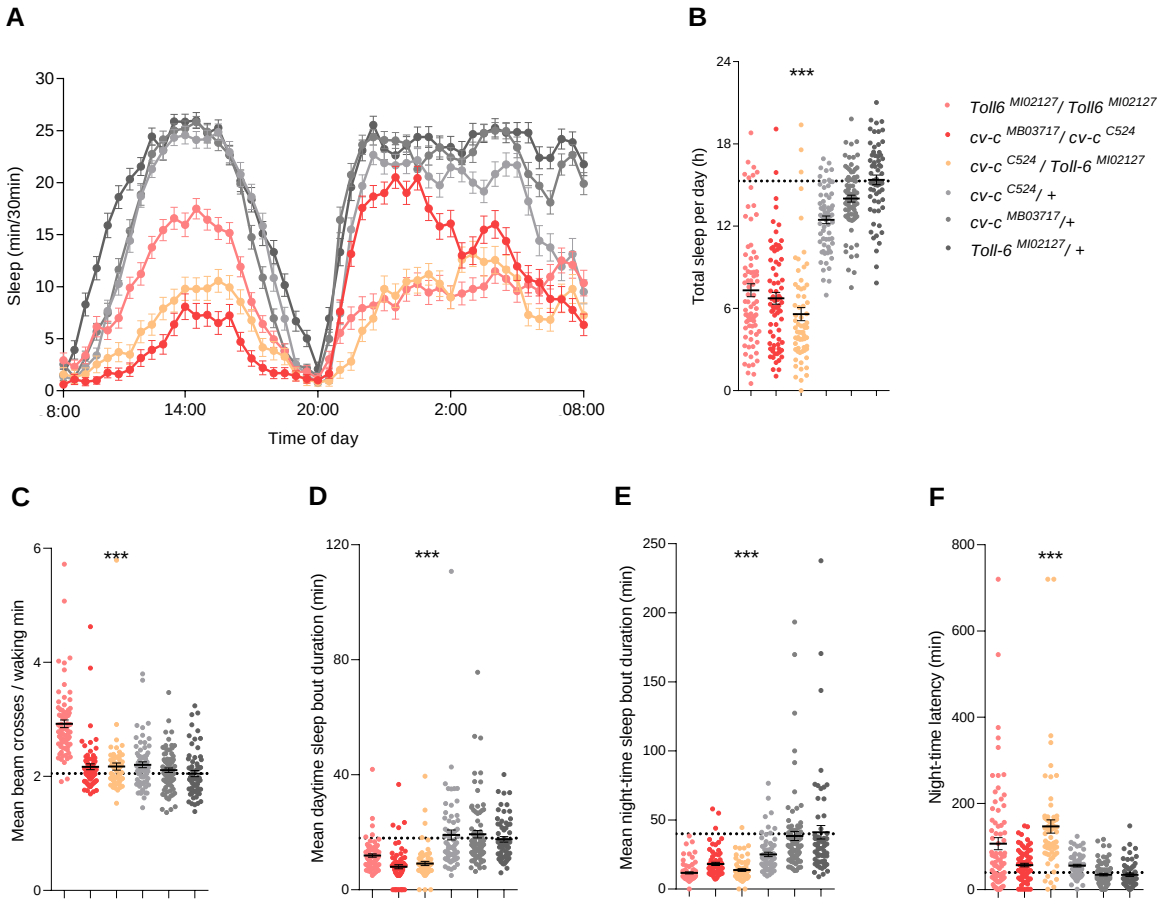

Figure 23: *cv-c^{C524}/Toll-6^{MI02127}* flies are as insomniac as the *cv-c^{MB03717}/cv-c^{C524}* mutants. (A) Sleep (minutes per 30 minutes) of *cv-c^{C524}/Toll-6^{MI02127}* mutant flies (orange), *Toll-6^{MI02127}* homozygous mutant flies (pink), *cv-c^{MB03717}/ cv-c^{C524}* transheterozygous flies (red) and heterozygous controls (*cv-c^{C524}*/+) (*cv-c^{MB03717}*/+) (*Toll-6^{MI02127}*/+) shown in grey. **(B)** Overall, *cv-c^{C524}/Toll-6^{MI02127}* flies sleep as much as the *cv-c^{MB03717}/ cv-c^{C524}* mutants, less than *Toll-6^{MI02127}* homozygous mutants and much less than heterozygous controls: $F_{(5, 421)} = 113.3$, $p<0.0001$. **(C)** The locomotor activity of *cv-c^{C524}/Toll-6^{MI02127}* flies is the same as all other genotypes, apart from the *Toll-6^{MI02127}* homozygous mutants that exhibit increased activity during waking periods: $F_{(5, 421)} = 37.60$, $p<0.0001$. **(D)** and **(E)** The mean sleep bout duration during daytime and night-time is no different in *cv-c^{C524}/Toll-6^{MI02127}* flies from *cv-c^{MB03717}/ cv-c^{C524}* or *Toll-6^{MI02127}* mutant flies and is less than that of heterozygous controls: $F_{(5, 421)} = 23.10$, $p<0.0001$ and $F_{(5, 421)} = 25.71$, $p<0.0001$. **(F)** Lastly, the night-time latency of *cv-c^{C524}/Toll-6^{MI02127}* flies is increased compared to the rest of the groups: $F_{(5, 421)} = 23.91$, $p<0.0001$. **(B-F)** Significant differences were detected by one-way ANOVA with *Holm-Sidak's* multiple comparisons test. Asterisks denote where there are significant differences between *cv-c^{C524}/Toll-6^{MI02127}* flies and any other group. Mean ± SEM, n=62-80.

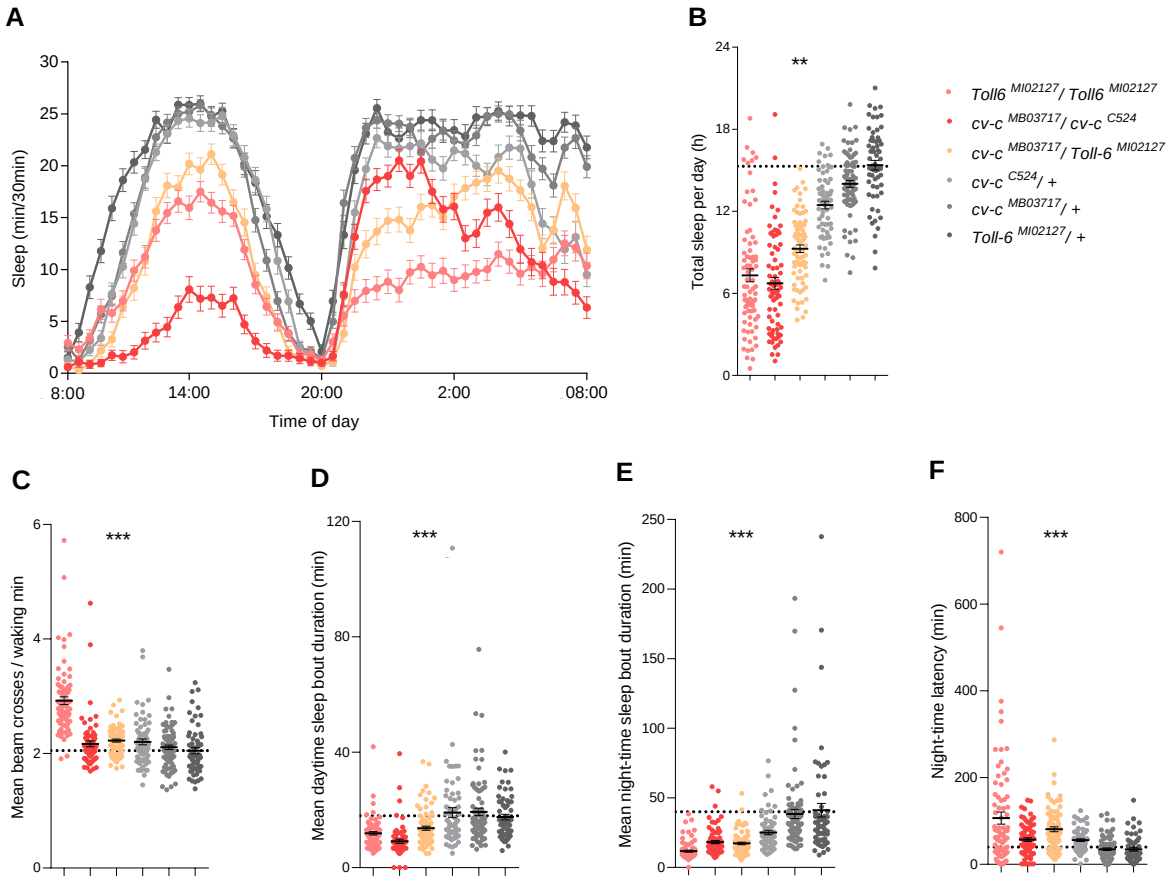

Figure 24: Sleep in *cv-c*^{MB03717}/*Toll-6*^{MI02127} flies is reduced. (A) Sleep (minutes per 30 minutes) of *cv-c*^{MB03717}/*Toll-6*^{MI02127} mutant flies (orange), *Toll-6*^{MI02127} homozygous flies (pink), *cv-c*^{MB03717}/ *cv-c*^{C524} transheterozygous flies (red) and heterozygous controls (*cv-c*^{C524}/+) (*cv-c*^{MB03717}/+) (*Toll-6*^{MI02127}/+) shown in grey. **(B)** *cv-c*^{MB03717}/*Toll-6*^{MI02127} mutant flies sleep less than heterozygous controls but more than *cv-c*^{MB03717}/ *cv-c*^{C524} or *Toll-6*^{MI02127} mutant flies: $F_{(5, 435)}$ = 100.0, p<0.0001. **(C)** Locomotion of *cv-c*^{MB03717}/*Toll-6*^{MI02127} flies does not differ from other genotypes, apart from *Toll-6*^{MI02127} homozygous mutants that are slightly hyperactive: $F_{(5, 435)}$ = 44.46, p<0.0001. **(D)** The mean sleep bout duration during daytime is shorter in *cv-c*^{MB03717}/*Toll-6*^{MI02127} flies and equal to *Toll-6*^{MI02127} mutants but more than that of *cv-c*^{MB03717}/ *cv-c*^{C524} flies: $F_{(5, 435)}$ = 18.60, p<0.0001. **(E)** In contrast, the night-time sleep bout duration does not differ in *cv-c*^{MB03717}/*Toll-6*^{MI02127}, *cv-c*^{MB0371}/ *cv-c*^{C524} or *Toll-6*^{MI02127} mutant flies and is shorter than heterozygous controls: $F_{(5, 435)}$ = 24.76, p<0.0001. **(F)** The night-time latency of *cv-c*^{MB03717}/*Toll-6*^{MI02127} flies is not different to *cv-c*^{MB0371}/ *cv-c*^{C524} mutants and heterozygous controls but is shorter than that of *Toll-6*^{MI02127} mutants**:** $F_{(5, 435)}$ = 15.82, p<0.0001. **(B-F)** Significant differences were detected by one-way ANOVA with *Holm-Sidak's* multiple comparisons test. Asterisks denote where there are significant differences between *cv-c*^{MB03717}/*Toll-6*^{MI02127} flies and any other group. Mean ± SEM, n=62-80.

DNT1 mutation decreases sleep whereas a mutation for *DNT2* increases sleep

Based on the findings above, it was important to next test if and how ligands of Toll-6 receptor affect sleep. Previous studies implicated the spätzle proteins DNT1 and DNT2 as potential ligands for the receptor (Foldi et al., 2017; McIlroy et al., 2013). To identify whether one or the other acts upstream of Toll-6, mutants for the two genes were tested (**Figure 25** and **Figure 26**). *DNT1*^{41} mutants were generated by homologous recombination (Zhu et al., 2008) and *DNT2*^{e03444} mutants by a transposable element insertion.

Notably, mutations in the two ligands had opposing effects on sleep: *DNT1* homozygous mutants sleep less, while *DNT2* homozygous mutants sleep more compared to heterozygous and *wt* controls (**Figure 25** and **Figure 26**). The reduction in sleep in *DNT1* mutants (**Figure 25B**) is associated with shorter sleep bout durations during daytime (**Figure 25D**). In contrast, no differences in the sleep bout duration during daytime (**Figure 26D**) or night-time (**Figure 26E**) were observed in *DNT2* mutants, possibly due to saturation. *DNT1* mutants also take longer to fall asleep as indicated by the prolonged night-time latencies (**Figure 25F**), a finding that was reversed in *DNT2* mutants with short latencies (**Figure 26F**). Thus, an insomniac phenotype is revealed for flies bearing the *DNT1* mutation and a hypersomniac phenotype for flies with the *DNT2* mutation.

In both cases, *DNT1* and *DNT2* homozygous mutants are more active than their respective controls during wakefulness (**Figure 25** and **Figure 26**); therefore, the decrease in sleep observed in *DNT1* mutants might not necessarily be due to a hyper-active phenotype, but rather due to deficits caused by the mutation.

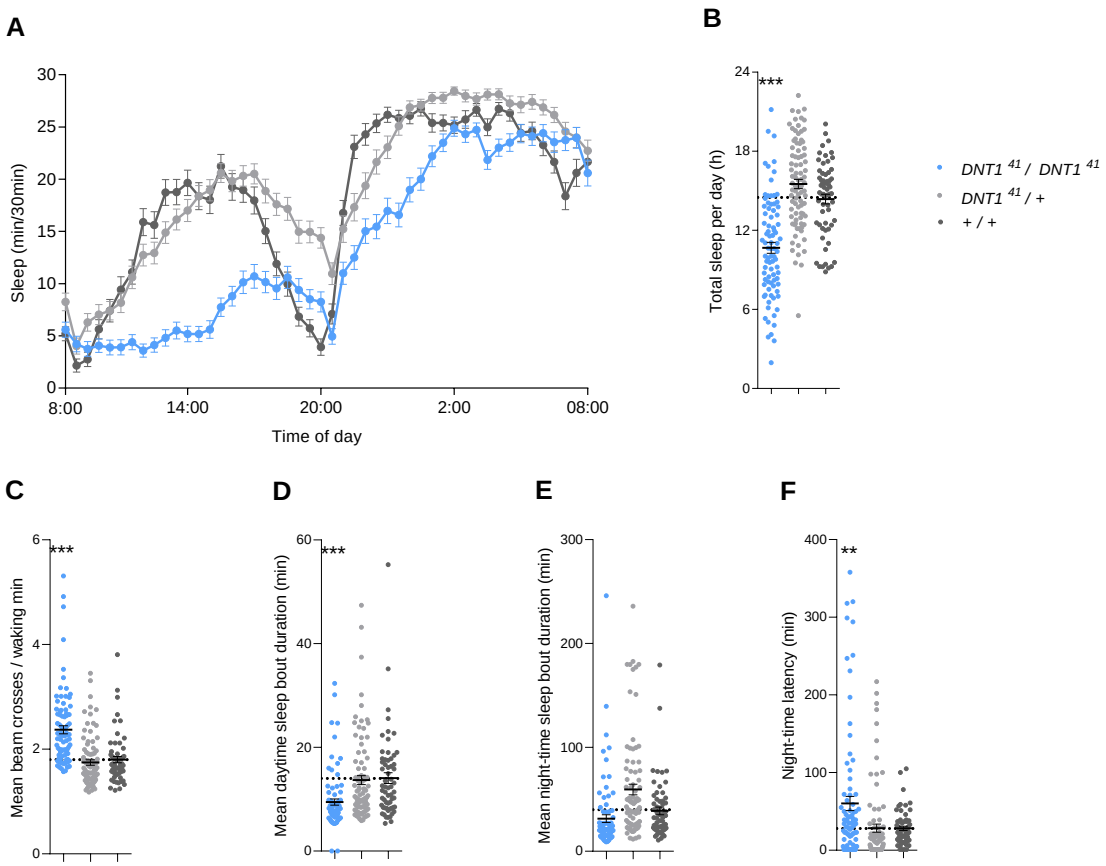

Figure 25: Sleep architecture of *DNT1^{41}* mutants. (A) Sleep (minutes per 30 minutes) of *DNT1^{41}* homozygous mutant flies (blue) and of heterozygous (*DNT1^{41}/+)* and *wt* (+/+) controls shown in grey and dark grey respectively. **(B)** The total amount of sleep in *DNT1^{41}* homozygous mutant flies is reduced compared to controls: $F_{(2, 230)} = 46.70$, $p<0.0001$. **(C)** *DNT1^{41}* mutant flies are more active during wakefulness compared to control flies: $F_{(2, 230)} = 29.80$, $p<0.0001$. **(D)** The duration of sleep bouts is shorter in *DNT1^{41}* homozygous mutants during daytime ($F_{(2, 230)} = 10.03$, $p<0.0001$) while there is no difference during **(E)** night-time. **(F)** *DNT1^{41}* mutant flies also take longer to fall asleep as indicated by the longer sleep latencies of these flies: $F_{(2, 230)} = 7.582$, $p=0.0006$. **(B-F)** One-way ANOVA with *Holm-Sidak's* multiple comparisons test. Asterisks denote differences between *DNT1* homozygous mutants and both controls. Mean ± SEM, n=61-87.

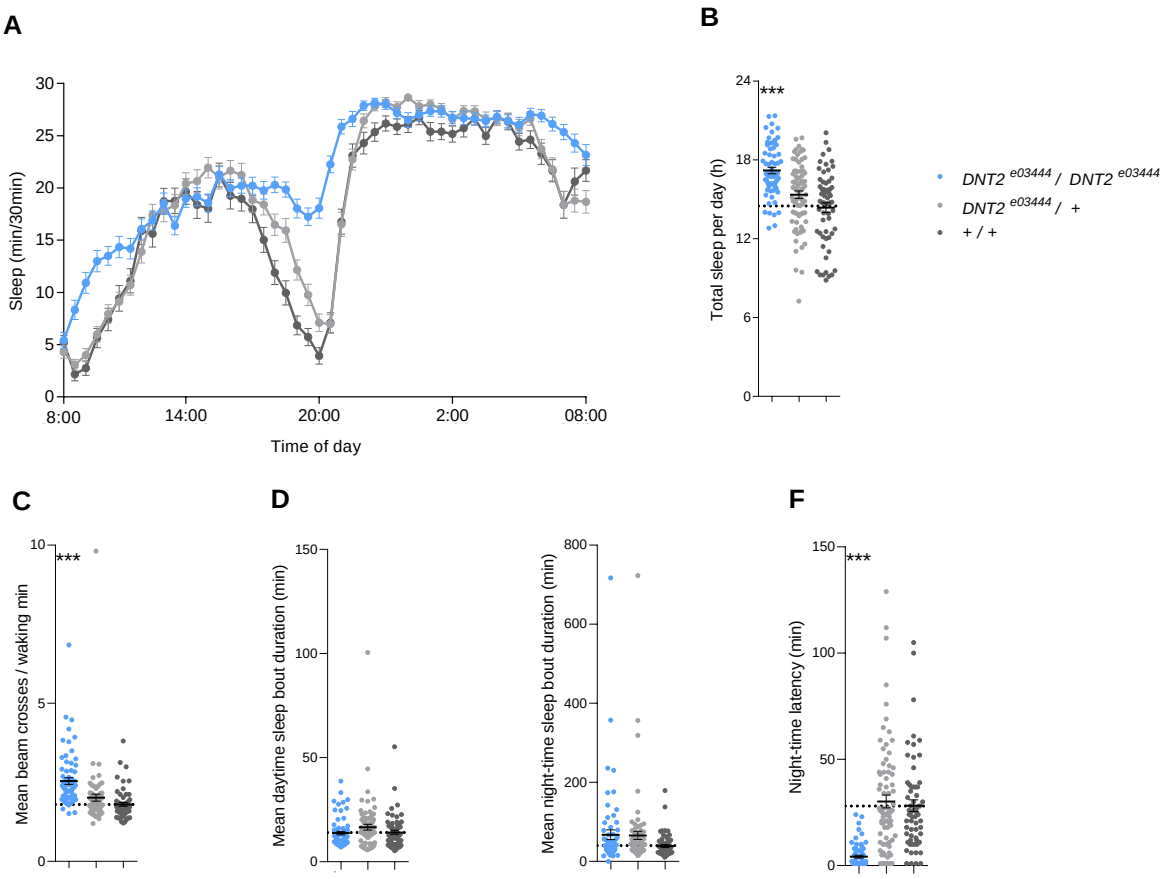

Figure 26: Sleep architecture of *DNT2^{e03444}* mutants. (A) Sleep (minutes per 30 minutes) of *DNT2^{e03444}* homozygous mutant flies (blue) and of heterozygous (*DNT2^{e03444}/+)* and *wt* (+/+) controls shown in grey and dark grey respectively. **(B)** *DNT2^{e03444}* homozygous mutants sleep more compared to controls: ($F_{(2, 203)}$ = 22.42, p<0.0001). **(C)** When awake, *DNT2^{e03444}* mutants are more active than controls: $F_{(2, 203)}$ = 14.15, p<0.0001. **(D)** and **(E)** Sleep bout durations during daytime and night-time are the same among the three genotypes while **(F)** *DNT2^{e03444}* homozygous mutants have much shorter night-time latencies compared to controls: $F_{(2, 203)}$ = 34.14, p<0.0001. **(B-F)** One-way ANOVA with *Holm-Sidak's* multiple comparisons test. Asterisks denote differences between *DNT2* homozygous mutants and both controls. Mean ± SEM, n=61-78.

Depletion of DNT1 from the R5 neurons decreases sleep

An attractive source of neurotrophin release to the dFB neurons is inevitably the R5 neurons of the ellipsoid body (EB), as it is a circuit known to generate sleep pressure that is sensed and discharged by dFB neurons (Liu et al., 2016). The mode of communication between R5 and dFB neurons is unknown and may involve neurotrophins and their receptors. To test this hypothesis, RNAi lines for *DNT1* and *DNT2* were driven in the R5 neurons with a restricted *split GAL4* line (*R58H05-DBD, RG30G03-AD*) (**Figure 27**). Two RNAi lines targeting *DNT1* in the R5 neurons cause flies to sleep less; this result matches the *DNT1* mutant phenotype and the *Toll-6* deficient phenotype. Subsequent experiments have therefore focused on DNT1. Other than the total amount of sleep, the sleep bout durations (**Figure 28D** and **Figure 28E**) and latencies (**Figure 28F**) are not different in R5-driven *DNT1*^{RNAi} flies compared to their parental controls. When *DNT1* is targeted with the 26115GD RNAi line, flies show an increase in their activity compared to one of their parental controls, the *R58H05-DBD, RG30G03-AD/+* (**Figure 28C**). For this reason, the 26116GD line was used for further experiments.

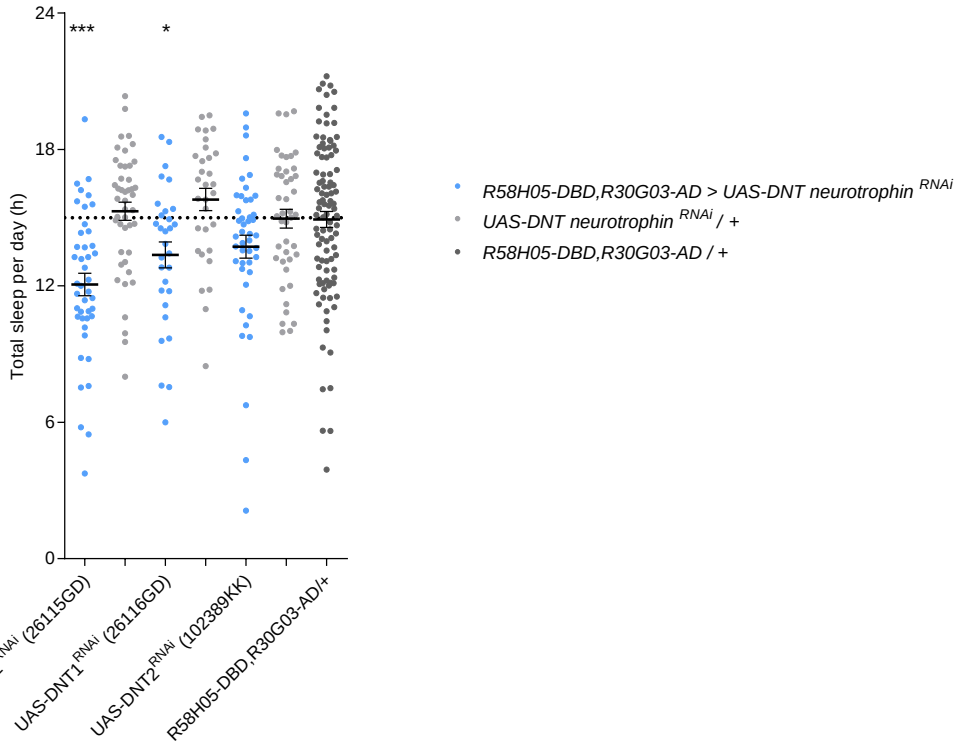

Figure 27: Sleep amount in flies with RNAi lines targeting *DNT1* and *DNT2* in the R5 neurons using *R58H05-DBD, RG30G03-AD split-GAL4*. RNAi lines targeting *DNT1* and *DNT2* were driven in the R5 neurons by the *R58H05-DBD, RG30G03-AD split GAL4* line (blue). The *UAS-DNT neurotrophin/+* and *R58H05-DBD, RG30G03-AD /+* parental controls are shown in grey and dark grey respectively. Flies with RNAi lines targeting *DNT1* in the R5 neurons have reduced amount of sleep compared to parental controls; *UAS-DNT1*^{RNAi} *(26115GD)*: $F_{(2, 126)} = 13.00$, $p<0.0001$ and *UAS-DNT1*^{RNAi} *(26116GD)*: $F_{(2, 128)} = 4.547$, $p=0.0124$. One-way ANOVA with *Holm-Sidak's* multiple comparisons test. Asterisks denote significant differences from both parental controls. Mean ± SEM, n = 27-70.

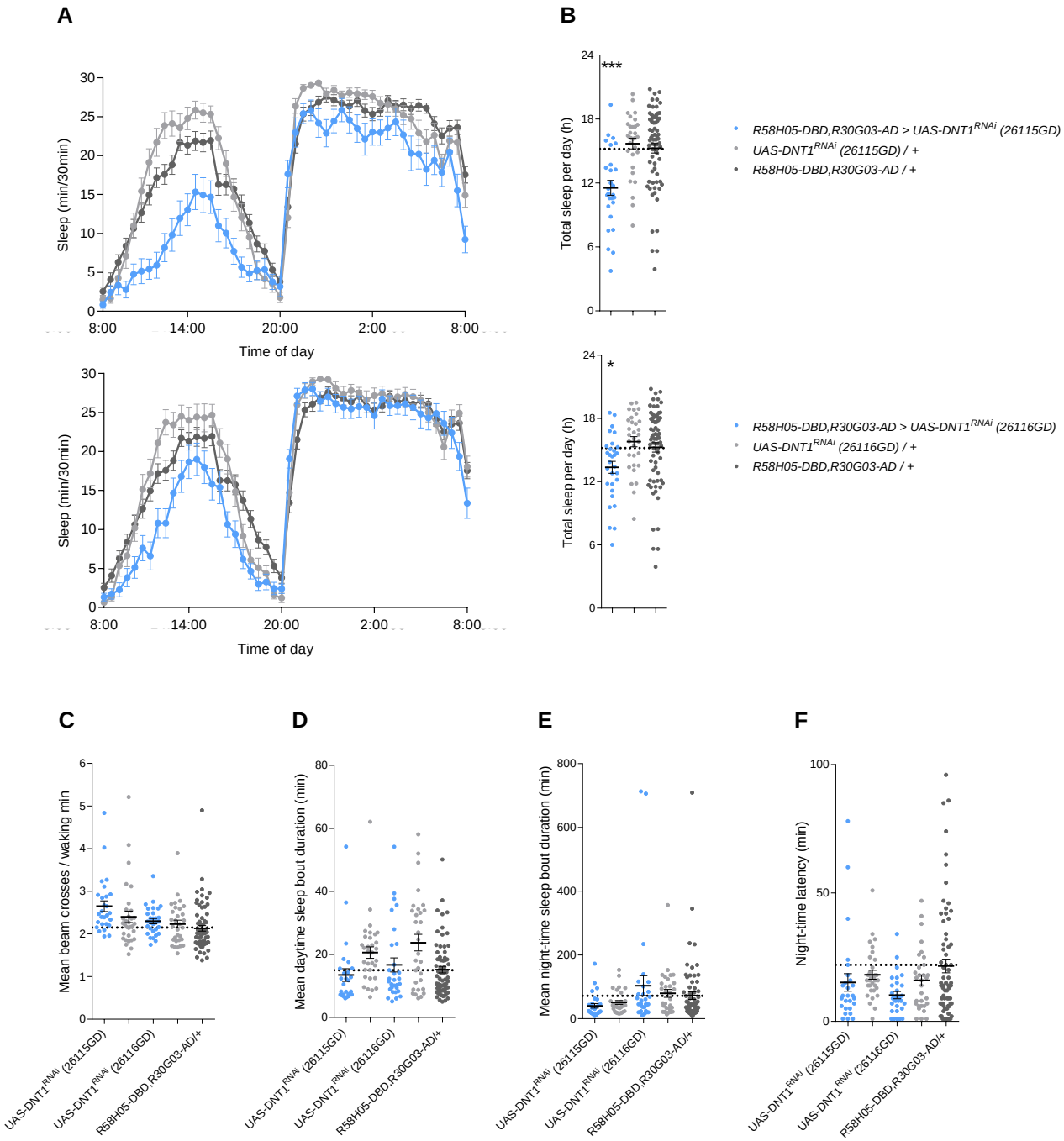

Figure 28: R5-restricted interference with *DNT1* using *R58H05-DBD, RG30G03-AD split GAL4*. (A) Sleep (minutes per 30 minutes) of flies expressing R5-driven RNAi lines targeting *DNT1* (blue) and of *UAS-DNT1 ^{RNAi}/+* and *R58H05-DBD, RG30G03-AD /+* parental controls, shown in grey and dark grey respectively. **(B)** The total amount of sleep in flies expressing R5-driven *DNT1^{RNAi}* is decreased compared to controls; 26115GD: $F_{(2, 126)}$ = 13.00, p<0.0001 and 26116GD: $F_{(2, 128)}$ = 4.547, p=0.0124. **(C)** In flies that *DNT1* knockdown in the R5 neurons was targeted by the 26116GD RNAi line, no differences in activity were detected between driven and undriven controls. However, flies in which *DNT1* knockdown is targeted by the 26115GD RNAi line have increased locomotor activity compared to the *R58H05-DBD, RG30G03-AD/+* control flies. No significant differences were detected in the mean sleep bouts duration during **(D)** daytime or **(E)** night-time and **(F)** in the sleep latency between flies expressing R5-driven *DNT1^{RNAi}* and parental controls. **(B-F)** One-way ANOVA with *Holm-Sidak's* multiple comparisons test. Asterisks denote significant differences between R5-driven RNAi lines for *DNT1* and both parental controls. Mean ± SEM, n = 27-70.

As in the case of the Toll-6 receptor, expression of the RNAi was restricted in adult flies using the *tubP-GAL80^{ts}* suppressor, to exclude that developmental defects in flies with *DNT1* knockdown affect sleep measurements (**Figure 29**). Flies with *DNT1* knockdown in the R5 neurons sleep as much as the *R58H05-DBD, RG30G03-AD/+* control flies at 18°C and much less than both parental when expression of the RNAi was restricted to adulthood (31°C) (**Figure 29A** and **Figure 29B**). The decrease in sleep in DNT1 deficient flies is thus not likely to be due to developmental abnormalities.

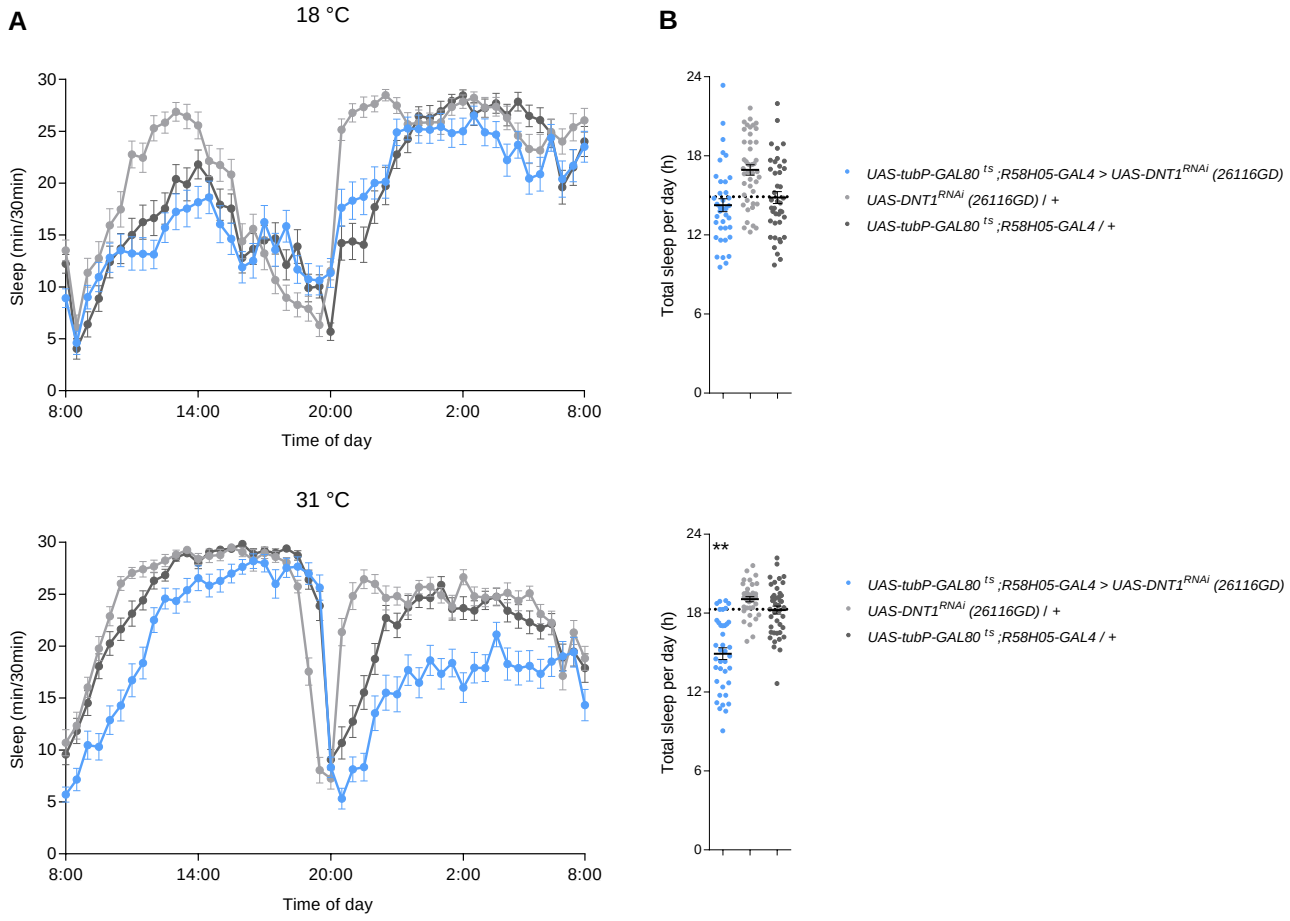

Figure 29: Adult-onset induction of *DNT1^{RNAi}* in the R5 neurons using the temperature-sensitive *GAL80^{ts}* repressor. (A) Sleep (minutes per 30 minutes) of flies expressing *DNT1^{RNAi}* in the R5 neurons (blue) and parental controls, raised at 18°C or 31°C. The *UAS-DNT1^{RNAi}/+* and *UAS-tubP-GAL80^{ts};R58H05-GAL4/+* are shown in grey and dark grey respectively. **(B)** Flies with the R5-driven *DNT1* knockdown sleep less than both parental controls at 31°C. At 18°C they sleep equally to the *UAS-tubP-GAL80^{ts};R58H05-GAL4/+* control flies but less than the *UAS-26116GD^{RNAi}/+* control flies. Two-way ANOVA, interaction of genotype x temperature: $F_{(2, 238)} = 6.102$, p= 0.0026. Mean ± SEM, n=38-44.

Sleep-need encoded by R5 neurons is likely to require DNT1

While thermogenetic activation of dFB neurons acutely induces sleep, activation of R5 neurons increases sleep after a lag which reflects an increase in the sleep need of the flies (Liu et al., 2016). To test whether DNT1 is required for the generation of sleep drive within the circuit, the R5 neurons were thermogenetically activated using the Transient receptor potential cation channel *(TrpA)* in a *DNT1* knockdown ($DNT1^{RNAi}$) background. Following 24h of thermogenetic induction, flies with TrpA-activated R5 neurons slept more, in agreement with previous findings (Liu et al., 2016). In contrast, loss of *DNT1* abolishes "rebound" sleep, implying that this molecule might be important for encoding sleep need in the R5 neurons (**Figure 30**).

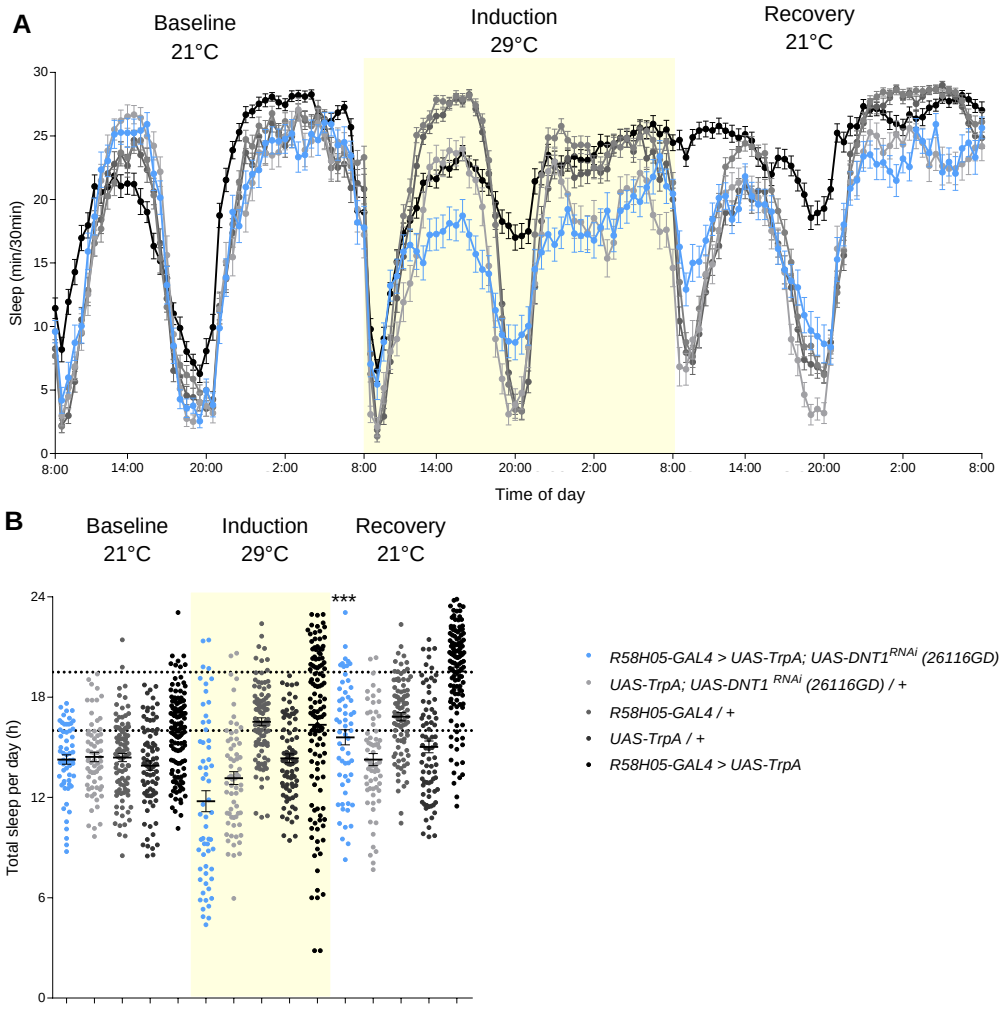

Figure 30: Thermogenetic activation of R5 neurons depleted from *DNT1*. (A) Sleep (minutes per 30 minutes) of the flies over the time-course of the experiment: baseline, thermogenetic induction, and recovery days. Flies with the *TrpA*-activated R5 neurons are indicated in black while flies expressing $DNT1^{RNAi}$ in *TrpA*-activated R5 neurons are shown in blue. Parental controls (*R58H05-GAL4*/+)(*UAS-TrpA*/+) (*UAS-TrpA;UAS-DNT1*^{RNAi}/+) are shown in grey **(B)** The total amount of sleep in *R58H05-GAL4>UAS-TrpA* flies increases compared to baseline and induction days. However, the amount of sleep in flies that the R5 neurons are activated but lack *DNT1* is the same on the recovery and baseline days, and is also much less than that of *R58H05-GAL4>UAS-TrpA* flies during the recovery day. Two-way repeated measures ANOVA, interaction of genotype x temperature: $F_{(8, 702)} = 11.87$, $p<0.0001$. Mean ± SEM, n = 47-104.

3.4 DISCUSSION

Neurotrophic factors have been conjectured to represent a signal of heightened sleep pressure (Brown et al., 2012; Tononi & Cirelli, 2014). In *Drosophila*, two receptors (Toll-6 and Toll-7) with neurotrophic function belong to the Toll family and localise to the fan-shaped body (McIlroy et al., 2013). Given that Cv-c is a Rho-GAP and small GTPases are known to be mediated by the action of neurotrophins, it is conceivable that these receptors act upstream of Cv-c and Sandman to convey sleep pressure in the dFB neurons in an activity-dependent manner.

RNAi-mediated knockdown of Toll receptors in the fan-shaped body revealed that interfering with the function of four receptors (Toll-2, Toll-5 and Toll-6 and Toll-8) reduces the total amount of sleep of flies (**Figure 17**). Because Toll-6 is one of the receptors with neurotrophic function (McIlroy et al., 2013), subsequent studies focused on this receptor. This does not exclude, however, that the other three receptors are also important for sleep regulation or that a synergistic action between the receptors exists. For example, Toll-6 along with Toll-2 and Toll-8 are expressed in a striped fashion in the embryonic epidermis and are the targets of Eve and Runt during convergent extension (Paré et al., 2014). The combined actions of the receptors direct cell intercalation and planar polarity while their disruptions lead to ectopic stripe expression and defects in these procedures (Paré et al., 2014). Alternatively, Toll-6 also forms a dimer with Kek-6, a member of the tyrosine-kinase less receptor family, encoded by the Kekkon family of receptors in *Drosophila* (Ulian-Benitez et al., 2017). Together the dimer binds DNT2 to modulate neuromuscular junction growth (Ulian-Benitez et al., 2017). It will also be interesting to explore in the future whether such synergistic functions exist in sleep-wake regulation.

For further validation that loss of Toll-6 receptor causes a reduction in sleep, experiments with *Toll-6*^{RNAi} lines were repeated using the *R23E10-GAL4* line and an additional *GAL4* line (*R84C10-GAL4*) that also labels the dFB neurons (**Figure 18** and **Figure 19**). A decrease in the total amount of sleep of flies with dFB-driven *Toll-6*^{RNAi} was prominent with both *GAL4* lines used (**Figure 18B** and **Figure 19B**). Due to the crucial role of Toll receptors in development, the expression of the RNAi was restricted in adult flies

using the *tubP-GAL80^{ts}* repressor where a reduction in sleep prevailed in the permissive temperature (**Figure 20A** and **Figure 20B**). *Toll-6* mutant flies showed an even more pronounced fragmented sleep pattern (**Figure 21** and **Figure 22**). The sleep loss of *Toll-6* mutant flies was substantial (**Figure 21B** and **Figure 22B**) and was accompanied by decreased sleep bout durations (**Figure 21E** and **Figure 22E**) and increased sleep latencies (**Figure 21F** and **Figure 22F**) during night-time. Together, the results of *Toll-6* knockdown in the dFB and *Toll-6* mutation suggest the importance of the receptor for a normal sleep-wake cycle. In future experiments, rescuing the sleep loss of *Toll-6* homozygous mutants by overexpressing the receptor in the dFB neurons, will further establish these neurons as the site of action of Toll-6.

To investigate whether the receptor acts upstream of Cv-c, mutants bearing a copy of the *Toll-6^{MI02127}* allele and a copy of either *cv-c^{C524}* or *cv-c^{MB03717}* alleles were generated. The dFB neurons in *cv-c* mutants display reduced excitability which impairs the sleep homeostat and results in an insomniac phenotype (Donlea et al., 2014). *cv-c^{C524} /Toll-6^{MI02127}* mutants display comparable amounts of sleep loss to the *cv-c* mutants, suggesting that Toll-6 is likely to feed into the same pathway. (**Figure 23**). *cv-c^{MB03717} /Toll-6^{MI02127}* mutants also sleep less than heterozygous controls but a reduction in sleep is not as pronounced as in the *cv-c^{C524}/Toll-6^{MI02127}* mutants which may be due to *cv-c^{MB03717}* allele causing a less severe insomniac phenotype (**Figure 24**). Further to these genetic interaction experiments, as there is preliminary evidence that Cv-c and Sandman act in the same pathway (**Chapter 2-Figure 14**), introducing a dFB-specific Sandman knockdown in a *Toll-6^{MI02127}* mutant background will also decipher whether these components act in concert in the same pathway.

To identify the ligand of the Toll-6 receptor, *DNT1* and *DNT2* mutants were tested first. The mutants showed opposing phenotypes: *DNT1* mutants exhibit a substantial reduction in sleep whereas *DNT2* mutants showed a gain in sleep (**Figure 25** and **Figure 26**). To localise the source of neurotrophin release, expression of RNAi lines targeting *DNT1* and *DNT2* was restricted in the R5 neurons of the EB. Previous experiments have shown that the sleep drive encoded by these neurons is conveyed to the dFB neurons; this

led to the hypothesis of a homeostatic operator where R5 neurons constitute the “sensor circuit” and dFB neurons the “effector” circuit (Liu et al., 2016). Because RNAi-mediated interference of *DNT1* in the R5 neurons also reduces sleep (**Figure 27** and **Figure 28**), which resembles the *DNT1* mutant and *Toll-6* deficient phenotypes, subsequent experiments focused on this ligand.

To assess the importance of *DNT1* for the generation of sleep drive in the R5 neurons, these were thermogenetically activated while simultaneously knocking down *DNT1*. *DNT1* depletion from the circuit abolishes the increase in sleep normally observed on the recovery day of the experiment (Liu et al., 2016), suggesting the involvement of the neurotrophin in the encoding of sleep need by the R5 neurons (**Figure 30A** and **Figure 30B**). To exclude the effect of temperature fluctuations in the experiment due to the thermogenetic activation of the neurons, these results will be further validated using an optogenetic approach. To identify whether DNT1 is secreted in response to rising sleep pressure, it will also be important that levels of DNT1 are assessed following baseline sleep and sleep deprivation conditions; it is expected that following the latter, levels of DNT1 will be elevated.

It is, however, possible that neurotrophins are also secreted from other sources. For instance, a recent study linked neuron-glia communication to the signalling of sleep need (Blum et al., 2021). The authors show that secretion of Spz from astroglia is essential for the signalling of sleep need to the R5 neurons through the Toll receptor (Blum et al., 2021). Thus, exploring the differential actions of neurotrophins secreted from various sources could provide critical insights into sleep-related mechanisms. As an additional tool to RNAi, cell-specific CRISPR KO versions of *Toll-6* and *DNT1*, were generated in the same manner described in chapter 2 (**Chapter 2**-**Figure 15**).

To conclude, the results of these experiments set the background for a mechanism whereby sleep pressure accumulates through the activity of R5 neurons, which secrete a DNT1 signal that is conveyed to the effector circuit, the dFB neurons, through the Toll-6 receptor (**Figure 31**). Toll-6 may feed into a small GTPase signalling cascade that enhances the internalisation of Sandman and terminates with the state switching of the dFB

neurons to the ON state promoting sleep. Further elucidating the molecular components of this cascade will be essential to gain an integrated picture of the homeostatic sleep switch.

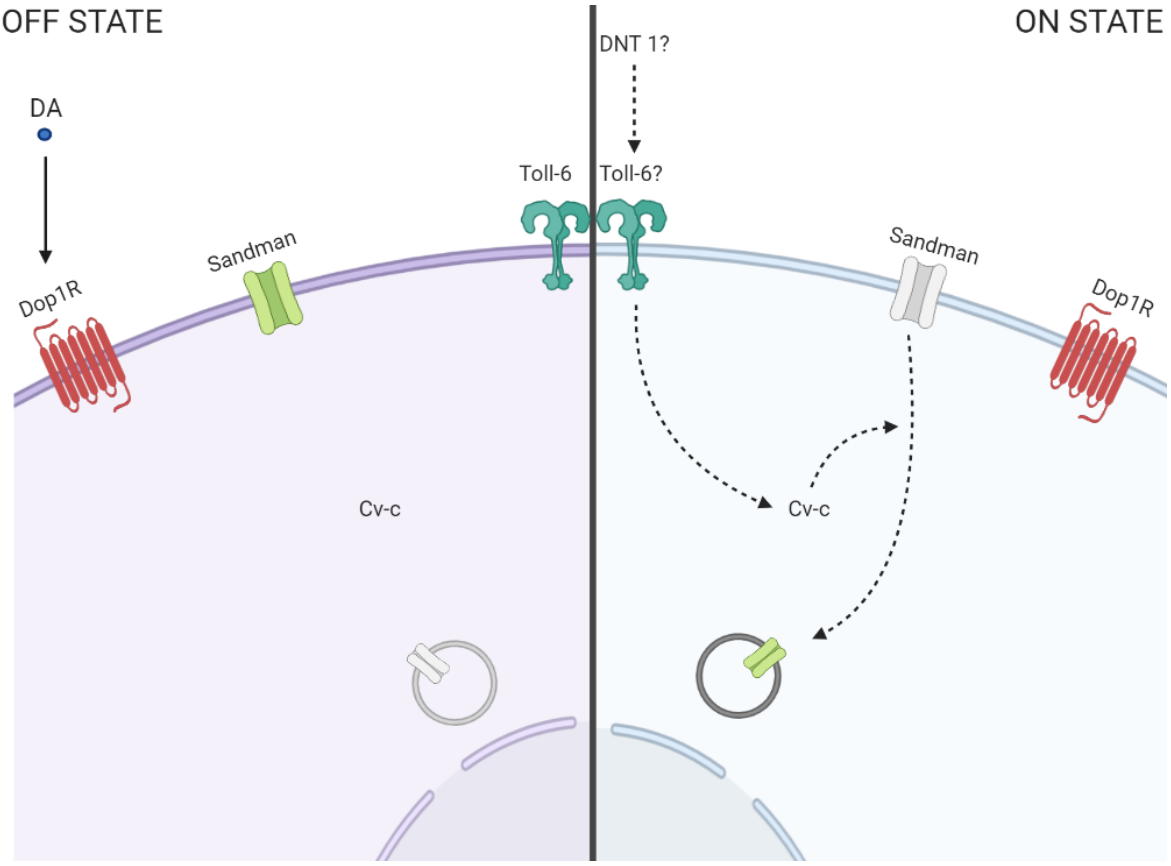

Figure 31: Proposed mechanism by which the dFB neurons promote sleep. During wakefulness, it is hypothesised that generation of sleep pressure within the R5 neurons, elevates DNT1 levels leading to the secretion of the protein. The sleep pressure is relieved by Toll-6 in the dFB neurons whose activation likely employs a downstream pathway that is hypothesised to involve Cv-c and the internalisation of Sandman, switching the neurons ON. Figure created with BioRender.com.

General conclusion

Despite centuries of reseach, the physiological function of sleep remains largely unknown. It has been proposed that sleep enhances the clearance of metabolic products from the brain, the accumulation of which would be toxic (Hablitz et al., 2019; Xie et al., 2013), serves a synaptic homeostasis role (Tononi & Cirelli, 2014, 2020) and is inextricably linked to immunity (Besedovsky et al., 2019).

In the present study, it is proposed that a neurotrophin signal is sleep-inducing (Chapter 3-Figure 15). However, whether this signal is secreted in response to activity-dependent plasticity or drives plastic changes in sleep promoting circuits leading to sleep induction was not identified. It was previously shown that sleep loss is associated with an upregulation of Ca^{2+}, active zones and an NDMAR subunit in the R5 neurons (Liu et al., 2016). Future studies addressing whether DNT1 is required for the upregulation of these plasticity components could aid delineating the mechanism leading to its secretion and sleep. In turn, visualising whether structural plasticity changes occur in the dFB neurons following DNT1 secretion will also provide significant insights on the nature of the beneficial effects arising from the neutorophin-induced sleep.

Due to the cell-restricted manipulations used in this study, it is also predicted that the neurotrophin is secreted from a sleep-promoting population to another rather than its global upregulation. However, it cannot be excluded that the same or other neurotrophins exert somnogenic effects elsewhere in the brain and that perhaps their secretion is context-specific. Interestingly, dFB neurons alter their physiological properties in response to different upstream signals but also in response to their own recent experiences affected by environmental demands (Dissel et al., 2021). Thus, it is evident that tight spatiotemporal control of sleep- and wake-promoting signals within diffrent cell populations is crucial in mediating the differential aspects of sleep. Further uncovering the link between neurotrophism and sleep may illuminate at least one of these apsects and contribute to the understanding of the vital function of sleep.

Chapter 4

METHODS

4.1 CLONING

Generation of *sand-pHluorin* constructs

For the generation of *sand-pHluorin* constructs, overlap extension polymerase chain reaction (OE-PCR) was used (Nelson & Fitch, 2012). In the first step, three fragments were amplified with overlapping ends: the initial part of the *sandman* sequence, the *pHluorin* sequence, and the terminal part of the *sandman* sequence. The *sandman* fragment was obtained from the RE21922 cDNA clone (DGRC #8293) and the *pHluorin* sequence from the pGM87 vector (GenBank accession number #AY533296). For the second step of OE-PCR, DNA was extracted from the amplified sequences using the QIAquick Gel Extraction Kit (QIAGEN #28706X4) and the overlapping fragments were fused together in a second PCR reaction. The final inserts were amplified into the *pJFRC28-10XUAS* vector (Addgene #36431) for fly experiments and the *pCDH-CMV4* vector (Addgene #72284) for mammalian cell culture experiments.

For insertion into the *pJFRC28-10XUAS* vector, the restriction site Acc65I (NEB #R0599) was attached to the forward primer and XbaI (NEB #R0145) to the reverse primer. For insertion into the *pCDH-CMV4* vector, the XbaI site was attached to the forward primer while the Acc65I to the reverse primer. The inserts and the empty vectors were digested and ligated with T4 DNA ligase (NEB #M0202) according to NEB protocols. One Shot™ TOP10 Chemically Competent *E. coli* (ThermoFisher #C404006) cells were transformed with the ligation reactions according to the instructions and colonies were allowed to grow overnight at 37°C degrees in plates with Luria broth (LB) medium supplemented with carbenicillin. DNA was isolated and purified from the colonies using the Macherey-Nagel DNA purification kit (MN #740952.50).

Generation of overexpressing untagged, N-terminal *GFP* and N-terminal *venus* tagged *sandman*

The N-terminal *GFP* and N-terminal *venus* tags were generated using Gateway cloning with the pENTR™ Directional TOPO® cloning kit (ThermoFisher #K2400-20). The *sandman* sequence was amplified from the RE21299 cDNA clone (DGRC #8293) and the CACC sequence was added to the 5' end of the forward primer. The gateway is based on a site-specific recombination strategy and includes two reactions. In the first reaction (TOPO® Cloning reaction), the *sandman* sequence is amplified in an entry clone. Once in the entry clone, the LR Recombination Reaction was used to recombine they entry clone with the *pUASt-GFP* (DGRC #1075) and *pUASt-Venus* (DGRC #1091) destination vectors to create N-terminal tagged versions of *sandman*.

The untagged overexpressing version of *sandman* was generated by amplifying the coding region of *sandman* from the RE21922 cDNA clone with primers carrying the Acc65I and XbaI restriction sites to the forward and reverse primers respectively. The amplified fragment was digested and ligated into the *pJFRC-MUH* vector *(*Addgene #26213) as described above.

Generation of cell-specific *sandman*, *Toll-6,* and *DNT1* CRISPR knockouts

CRISPR knockouts were generated according to the protocol developed by (Port & Bullock, 2016) at www.CRISPRflydesign.org. gRNA sequences for *sandman*, *Toll-6* and *DNT1* were selected using the CHOPCHOP website (chopchop.cbu.uib.no). Using standard primers (www.CRISPRflydesign.org) overlapping fragments between the *pCFD6* vector (Addgene #73915) and tRNA-flanked gRNAs, were amplified using a high-fidelity Phusion polymerase (NEB #M0531). The amplified sequences were extracted using the Macherey Nagel gel extraction kit (MN #740609). Following extraction, the fragments, were mixed together with a BbsI-digested (NEB #R3539) *pCFD6* vector in a Gibson assembly reaction (NEB #E5510). According to the protocol a two-fold molar excess was inserted for every fragment (www.CRISPRflydesign.org). The assembly reactions were subsequently transformed into One Shot™ TOP10 Chemically Competent *E. coli* (ThermoFisher

#C404006) cells and incubated overnight at 37°C in carbenicillin-containing LB plates. DNA was isolated using the Macherey-Nagel DNA purification kit (MN #740952.50) and a colony PCR was used to screen for fragments of the correct size. Subsequently, those with the correct size were purified and verified by sequencing.

Verification and injection

All primers used in this study are listed in table 2. Final constructs were verified by Sanger sequencing (Source Bioscience) and sent for injection at Bestgene (BestGene Inc). *sand-pHluorin* plasmids were injected at the attP40 landing site on the 2nd chromosome using the PhiC31 site-specific integration system (Bischof et al., 2007). gRNA-containing vectors for *sandman*, *Toll-6* and *DNT1* as well as the untagged, overexpressing version of *sandman* were injected at the attP40 and attP2 landing sites on the 2nd and 3rd chromosomes, respectively. Finally, the gateway N-terminal *GFP* and *venus* tagged *sandman* plasmids were injected on the 2nd and 3rd chromosomes using P-element insertion.

4.2 CELL CULTURE

HEK-293T cells were grown in Dulbecco's Modified Eagle Medium (DMEM) supplemented with 10% fetal bovine serum (FBS), streptomycin (10 000 µg/µl) and L-glutamine and were maintained in a humidified incubator at 37°C and 5% CO_2. All constructs were transfected at the recommended concentrations using the Lipofectamine™ 3000 transfection reagent kit (ThermoFisher #L3000001). Before transfection, the DMEM medium was replaced with the Opti-MEM™ I Reduced Serum Medium. The cells were allowed to grow on coverslips overnight before staining and imaging.

4.3 IMMUNOSTAINING

For live imaging, HEK-293 cells were incubated for 1min with 0.1X of the CellMask Deep Red plasma membrane stain solution (ThermoFisher #C10046) and imaged in Opti-MEM™ I medium under the 25X objective using confocal imaging. For the KDEL staining, cells were fixed in 100% ice-cold methanol for 5min at 4°C. Permeabilization was achieved with 0.1% Triton X-100 incubation for 10min and blocking with 10% normal goat serum (NGS) for 1h. Cells were incubated with the primary antibody (Anti-KDEL- Alexa fluor®647 conjugated) (Abcam #214714) at a 1:1000 dilution overnight at 4°C. The following day, cells were washed with phosphate bovine serum (PBS) and mounted with Vectashield (Vector Labs #H-1000-10). For DAPI staining, cells were incubated with 300nM of DAPI staining solution (Merck #D9542) for 5min, washed with PBS and mounted with Vectashield.

For dFB neuron staining, brains were dissected in phosphate buffered saline (PBS) and fixed in 4% paraformaldehyde in PBS for 20min at room temperature. Following fixation, the brains were permeabilised with 0.3% Triton X-100 in PBS and incubated in blocking solution, 10% NGS in 0.3% Triton X-100, for several hours. For immunostaining, brains were incubated with the primary antibody for 48h (1:1,000 rabbit anti-GFP, ThermoFisher #A6455). Following washes with 0.3% Triton X-100 in PBS, the secondary antibody was added for 24h (1:500 goat anti-rabbit antibody conjugated to Alexa Fluor 488; ThermoFisher #A11034). Samples were mounted in Vectashield and imaged on a Leica TCS SP5 confocal microscope using the water immersion (25x) and oil immersion (40x) objectives.

4.4 TWO-PHOTON MICROSCOPY

For two-photon microscopy, flies were head-fixed into a custom mount and a dorsal cranial window was excised for imaging. The brains were superfused continuously with extracellular solution (103 mM NaCl, 3 mM KCl, 5 mM TES, 8 mM trehalose, 10 mM glucose, 7 mM sucrose, 26 mM $NaHCO_3$, 1 mM NaH_2PO_4, 1.5 mM $CaCl_2$, 4 mM $MgCl_2$, pH 7.3) that was equilibrated with carbogen (95% O_2–5% CO_2). Fluorescence was excited with a Ti:Sapphire laser tuned to 920nm (Coherent, Chameleon Ultra II), coupled into a galvo scanning two-photon microscope (Sutter, MOMScope) controlled by ScanImage (Vidrio Technologies), with a water immersion, 20X objective (Zeiss #421452-9800-000). The laser power was set to a maximum of ~ 70 mW measured at the specimen plane. Fluorescence emitted by tdTomato and pHluorin was split into red and green channels using a dichroic beam splitter (Semrock FF562-Di03) and band pass filters (Semrock BrightLine FF02-628/40 (red) and FF01-520/60 (green). GaAsP PMTs (Hamamatsu Photonics H10770-40 SEL) were used for detection.

Images were acquired as Z-stacks (z-step size = 1µm) using a piezoelectric positioner (Physik Instrumente LTD), and with a resolution of 512 x 512 pixels. For the ratiometric analysis, regions of interests (ROIs) were drawn for the somata, dendrites and axons using Fiji software. For both green and red channels, an area of the image where no fluorescence was detected was designated as the background. For each ROI, the max fluroscence value from each stack was selected and the background was substracted from it. The ratio was computed by dividing the remaining values of the red by the green channel.

For dopamine delivery, a glass electrode containing 10mM dopamine in extracellular soluction was positioned at the centre of one of the dFB dentritic tufts. The neurotransmitter was applied in 50ms pulses at 10Hz for 5min using a Picospritzer (Picospritzer III). For testing acidic pH, the normal extracellular solution was replaced in a serial manner with MES-based acidic solutions (pK_a = 6.1) (Sankaranarayanan et al., 2000) of pH 5.5 for 10min and of pH 3.5 for another 10min. Once the lower pH solutions were tested, the brains were superfused again with normal extracellular solution of pH 7.4.

Ammonium chloride solution was prepared by substituting 50 mM NaCl in the extracellular solution with NH_4Cl.

4.5 SLEEP MEASUREMENTS

Female flies (3-5 days old) were individually inserted into 65 mm glass tubes sealed with food on one side and cotton on the other. The tubes were loaded into the TriKinetics *Drosophila* Activity Monitors (DAM) (Trikinetics Inc; Waltham MA, USA) to record the activity of the flies. Immobility lasting for five minutes or longer is classified as sleep (Hendricks et al., 2000; Shaw et al., 2000). The monitors were housed in incubators under 12-hour light/12-hour dark conditions. Trikinetics activity records were analysed using the Sleep and Circadian Analysis MATLAB Program (S.C.A.M.P.) scripts.

4.6 STATISTICAL ANALYSIS

Data were analysed with Prism 6 (GraphPad). For sleep measurements, group means were compared by one- or two-way ANOVA, using repeated measures where appropriate. The *Holm-Šídák's* multiple comparisons test followed where difference was significant. For two-photon imaging, paired t-test and one-way ANOVA were used where appropriate.

4.7 *DROSOPHILA* STRAINS AND CULTURE

Fly strains were cultivated on standard cornmeal agar and maintained under a 12 h light:12 h dark cycle at 25 °C except for flies expressing *tubP-GAL80^{ts}*; those were raised at 18°C. Crosses for thermogenetic experiments were housed at 21°C. Fly stocks were obtained from the Centre for Neural Circuits and Behaviour (CNCB) stock collection, the Vienna Drosophila Resource Centre (VDRC) or the Bloomington Drosophila Stock Centre (BDSC). *DNT1^{41}* and *DNT2^{e03444}* mutants were a gift from Alicia Hidalgo's lab while the *R58H05-DBD, R30G03-AD split GAL4* line a gift from Mark Wu's lab. Strains used in this study are listed in **Table 1**.

Table 1	
Drosophila Strains	**Source**
spz2 (DNT1)^{RNAi}	VDRC # 26115 GD
spz2 (DNT1)^{RNAi}	VDRC # 26116 GD
spz5 (DNT2)^{RNAi}	VDRC # 102389 KK
Toll (Tl)^{RNAi}	VDRC # 100078 KK
Toll-2 (18-wheeler)^{RNAi}	VDRC # 965 GD
Toll-2 (18-wheeler)^{RNAi}	VDRC # 44386 GD
Toll-2 (18-wheeler)^{RNAi}	VDRC # 44387 GD
Toll-3 (Mst-Prox)^{RNAi}	VDRC # 108034KK
Toll-4^{RNAi}	VDRC # 102642 KK
Toll-5 (Tehao)^{RNAi}	VDRC # 839 GD
Toll-5 (Tehao)^{RNAi}	VDRC # 17903 GD
Toll-5 (Tehao)^{RNAi}	VDRC # 109705 KK
Toll-6^{RNAi}	VDRC # 928 GD
Toll-6^{RNAi}	VDRC # 27102 GD
Toll-6^{RNAi}	VDRC # 108907 KK
Toll-7^{RNAi}	VDRC # 39176 GD
Toll-8(Tollo)^{RNAi}	VDRC # 9431 GD
Toll-8(Tollo^{RNAi}	VDRC # 13549 GD
Toll-8(Tollo)^{RNAi}	VDRC # 27099 GD
Toll-9^{RNAi}	VDRC # 924 GD
Toll-9^{RNAi}	VDRC # 36308 GD
Toll-9^{RNAi}	VDRC # 109635 KK
sandman^{RNAi}	VDRC # 47977 GD
UAS-sand:ECL1_1	Generated in this study- Injected at BestGene
UAS-sand:ECL1_2	Generated in this study- Injected at BestGene
UAS-sand:ECL1_3	Generated in this study- Injected at BestGene
UAS-sand:ECL1_4	Generated in this study- Injected at BestGene
UAS-sand:ECL2_1	Generated in this study- Injected at BestGene
UAS-sand:ECL2_2	Generated in this study- Injected at BestGene
UAS-sand:ECL2_3	Generated in this study- Injected at BestGene
UAS-sand:ECL2_4	Generated in this study- Injected at BestGene
UAS-sand:ECL2_5	Generated in this study- Injected at BestGene
UAS-sand:ECL3_1	Generated in this study- Injected at BestGene
UAS-sand:ECL3_3	Generated in this study- Injected at BestGene
UAS-sand:ECL3_4	Generated in this study- Injected at BestGene
UAS-sand:ECL3_6	Generated in this study- Injected at BestGene
UAS-sand:ECL4_1	Generated in this study- Injected at BestGene
UAS-sand:ECL4_2	Generated in this study- Injected at BestGene
UAS-sand:ECL4_3	Generated in this study- Injected at BestGene
UAS-sand:ECL4_4	Generated in this study- Injected at BestGene
UAS-sand:ECL4_5	Generated in this study- Injected at BestGene
UAS-sand	Generated in this study- Injected at BestGene
UAS-$_{GFP}$ sand	Generated in this study- Injected at BestGene
UAS-$_{VENUS}$ sand	Generated in this study- Injected at BestGene
DNT1^{41}	Gift from Hidalgo lab
DNT2^{e03444}	Gift from Hidalgo lab
Toll-6^{MI02127}	BDSC # 34467
cv-c^{MB03717}	BDSC # 24085
cv-c^{C524}	CNCB stock collection
cv-c^{1}	CNCB stock collection
R23E10-GAL4	BDSC # 49032
R84C10-GAL4	BDSC # 48378
R58H05-GAL4	BDSC # 39198
R58H05-DBD,R30G03-AD split GAL4	Gift from Wu lab
UAS-TrpA1	CNCB stock collection
UAS-mCD8::GFP	CNCB stock collection
UAS-CD4-tdTomato	CNCB stock collection
UAS-tubP-GAL80^{ts}	CNCB stock collection
yellow-white (yw)	CNCB stock collection
Canton-S (CS)	CNCB stock collection

Table 2	
List of Primers	
Primers used to generate *UAS*- and *CMV-sand-pHluorin* constructs using OE-PCR	
The primers listed below (FP1-RP1, FP2-RP2, FP3-RP3) were used for the first step of OE-PCR	
FP1 and RP3 primers were used in combination with all RP1 and FP3 primers and contain parts of the initial and terminal parts of the *sandman* sequence	
FP1	ATGTCCTCCCGACGCAGCT
RP3	CTAGGAGGTGCGGCACCG
RP1,FP2,RP2 and FP3 primers contain overlapping sequences between *sandman* and *pHluorin.* The *pHluorin* sequence is indicated in blue colour	
ECL1_p1	
RP1	GACAACTCCAGTGAAAAGTTCTTCTCCTTTACT GATGCTCTGGAATATGAACGC
FP2	GGAGCGTTCATATTCCAGAGCATC AGTAAAGGAGAAGAACTTTTCACTGGAGT
RP2	GAGCCGCTCGTACTCGAAAATCTC TTTGTATAGTTCATCCATGCCATGT
FP3	GGATTACACATGGCATGGATGAACTATACAAA GAGATTTTCGAGTACGAGCGG
ECL1_p2	
RP1	GACAACTCCAGTGAAAAGTTCTTCTCCTTTACT GAAAATCTCGATGCTCTGGAA
FP2	CGTTCATATTCCAGAGCATCGAGATTTTC AGTAAAGGAGAAGAACTTTTCACTGGAGT
RP2	CCGACTTGAGCCGCTCGTACTC TTTGTATAGTTCATCCATGCCATGT
FP3	GGATTACACATGGCATGGATGAACTATACAAA GAGTACGAGCGGCTCAAGTC
ECL1_p3	
RP1	GACAACTCCAGTGAAAAGTTCTTCTCCTTTACT AGCTGCTTTTTCACTATGGC
FP2	AGGGCCATAGTGAAAAAGCAGCT AGTAAAGGAGAAGAACTTTTCACTGGAGT
RP2	GCTCCACGTCGGGTCCCTT TTTGTATAGTTCATCCATGCCATGT
FP3	GGATTACACATGGCATGGATGAACTATACAAA AAGGGACCCGACGTGG
ECL1_p4	
RP1	GACAACTCCAGTGAAAAGTTCTTCTCCTTTACT GTCGGGTCCCTTCAGCT
FP2	AAGCAGCTGAAGGGACCCGAC AGTAAAGGAGAAGAACTTTTCACTGGAGT
RP2	CGGAGAAGCTCCACTGCTCCAC TTTGTATAGTTCATCCATGCCATGT
FP3	GGATTACACATGGCATGGATGAACTATACAAA GTGGAGCAGTGGAGCTTCTC
ECL2_p1	
RP1	GACAACTCCAGTGAAAAGTTCTTCTCCTTTACTAATGTTGGACAGGTAGAGCAAGAA
FP2	GCTGTTCTTGCTCTACCTGTCCAACATTAGTAAAGGAGAAGAACTTTTCACTGGAGT
RP2	AGGACTTGGCCAGGACGTCTCC TTTGTATAGTTCATCCATGCCATGT
FP3	GGATTACACATGGCATGGATGAACTATACAAA GGAGACGTCCTGGCCAAGTC
ECL2_p2	
RP1	GACAACTCCAGTGAAAAGTTCTTCTCCTTTACTGTCTCCAATGTTGGACAGGTAGAGCA
FP2	TGCTCTACCTGTCCAACATTGGAGAC AGTAAAGGAGAAGAACTTTTCACTGGAGT
RP2	CACTTGAAGGACTTGGCCAGGAC TTTGTATAGTTCATCCATGCCATGT
FP3	GGATTACACATGGCATGGATGAACTATACAAA GTCCTGGCCAAGTCCTTCAAGTG
ECL2_p3	
RP1	GACAACTCCAGTGAAAAGTTCTTCTCCTTTACT CAGGACGTCTCCAATGTTGG
FP2	CTGTCCAACATTGGAGACGTCCTG AGTAAAGGAGAAGAACTTTTCACTGGAGT

RP2	CTTCGAGTATATCCACTTGAAGGACTTGGC TTTGTATAGTTCATCCATGCCATGT
FP3	GGATTACACATGGCATGGATGAACTATACAAAGCCAAGTCCTTCAAGTGGATATACTC G
ECL2_p4	
RP1	GACAACTCCAGTGAAAAGTTCTTCTCCTTTACT CTTGGCCAGGACGTCTCCAAT
FP2	ATTGGAGACGTCCTGGCCAAG AGTAAAGGAGAAGAACTTTTCACTGGAGT
RP2	AGGCACACCTTCGAGTATATCCACTTG TTTGTATAGTTCATCCATGCCATGT
FP3	GGATTACACATGGCATGGATGAACTATACAAA TCCTTCAAGTGGATATACTCGAAGGTGTG
ECL2_p5	
RP1	GACAACTCCAGTGAAAAGTTCTTCTCCTTTACT GAAGGACTTGGCCAGGACGTC
FP2	GAGACGTCCTGGCCAAGTCCTTC AGTAAAGGAGAAGAACTTTTCACTGGAGT
RP2	GACATAGGCACACCTTCGAGTATATCCACTT TTTGTATAGTTCATCCATGCCATGT
FP3	GGATTACACATGGCATGGATGAACTATACAAA AAGTGGATATACTCGAAGGTGTGCCTAT
ECL3_p1	
RP1	GACAACTCCAGTGAAAAGTTCTTCTCCTTTACT ACCGAAGAGCAGCGCACC
FP2	GGTGCGCTGCTCTTCGGT AGTAAAGGAGAAGAACTTTTCACTGGAGT
RP2	CAGATAGTTCCAGTCCTCCCAACG TTTGTATAGTTCATCCATGCCATGT
FP3	GGATTACACATGGCATGGATGAACTATACAAA CGTTGGGAGGACTGGAACTATCTG
ECL3_p3	
RP1	GACAACTCCAGTGAAAAGTTCTTCTCCTTTACT GTCCTCCCAACGACCGAAGAG
FP2	CTCTTCGGTCGTTGGGAGGAC AGTAAAGGAGAAGAACTTTTCACTGGAGT
RP2	AGAAGTAGCTCCCATCCAGATAGTTCCA TTTGTATAGTTCATCCATGCCATGT
FP3	GGATTACACATGGCATGGATGAACTATACAAA TGGAACTATCTGGATGGGAGCTACTTCT
ECL3_p4	
RP1	GACAACTCCAGTGAAAAGTTCTTCTCCTTTACT GTTCCAGTCCTCCCAACGACC
FP2	GGTCGTTGGGAGGACTGGAAC AGTAAAGGAGAAGAACTTTTCACTGGAGT
RP2	ATAAGGCAGAAGTAGCTCCCATCCAGATA TTTGTATAGTTCATCCATGCCATGT
FP3	GGATTACACATGGCATGGATGAACTATACAAA TATCTGGATGGGAGCTACTTCTGCCTTAT
ECL3_p6	
RP1	GACAACTCCAGTGAAAAGTTCTTCTCCTTTACT CCCATCCAGATAGTTCCAGTCCTCC
FP2	GGAGGACTGGAACTATCTGGATGGG AGTAAAGGAGAAGAACTTTTCACTGGAGT
RP2	TGCTGAGCGATATAAGGCAGAAGTAGCT TTTGTATAGTTCATCCATGCCATGT
FP3	GGATTACACATGGCATGGATGAACTATACAAA AGCTACTTCTGCCTTATATCGCTCAGCA
ECL4_p1	
RP1	GACAACTCCAGTGAAAAGTTCTTCTCCTTTACT CAGATCGCCAAATCCAATGCTG
FP2	CAGCATTGGATTTGGCGATCTG AGTAAAGGAGAAGAACTTTTCACTGGAGT
RP2	TATCACACGATCGCCTGGCAC TTTGTATAGTTCATCCATGCCATGT
FP3	GGATTACACATGGCATGGATGAACTATACAAA GTGCCAGGCGATCGTGTGATA
ECL4_p2	
RP1	GACAACTCCAGTGAAAAGTTCTTCTCCTTTACT TGGCACCAGATCGCCAAATC
FP2	GATTTGGCGATCTGGTGCCA AGTAAAGGAGAAGAACTTTTCACTGGAGT
RP2	GGCAGTTATCACACGATCGCC TTTGTATAGTTCATCCATGCCATGT

FP3	GGATTACACATGGCATGGATGAACTATACAAA GGCGATCGTGTGATAACTGCC
ECL4_p3	
RP1	GACAACTCCAGTGAAAAGTTCTTCTCCTTTACT ATCGCCTGGCACCAGATCG
FP2	CGATCTGGTGCCAGGCGAT AGTAAAGGAGAAGAACTTTTCACTGGAGT
RP2	CCCTGTCGGCAGTTATCACACG TTTGTATAGTTCATCCATGCCATGT
FP3	GGATTACACATGGCATGGATGAACTATACAAA CGTGTGATAACTGCCGACAGGG
ECL4_p4	
RP1	GACAACTCCAGTGAAAAGTTCTTCTCCTTTACT CACACGATCGCCTGGCAC
FP2	GTGCCAGGCGATCGTGTG AGTAAAGGAGAAGAACTTTTCACTGGAGT
RP2	CCACCTTATCCCTGTCGGCAGTTAT TTTGTATAGTTCATCCATGCCATGT
FP3	GGATTACACATGGCATGGATGAACTATACAAA ATAACTGCCGACAGGGATAAGGTGG
ECL4_p5	
RP1	GACAACTCCAGTGAAAAGTTCTTCTCCTTTACT AGTTATCACACGATCGCCTGGC
FP2	GCCAGGCGATCGTGTGATAACT AGTAAAGGAGAAGAACTTTTCACTGGAGT
RP2	CTCCACCTTATCCCTGTCGGC TTTGTATAGTTCATCCATGCCATGT
FP3	GGATTACACATGGCATGGATGAACTATACAAA GCCGACAGGGATAAGGTGGAG
ECL4_p6	
RP1	GACAACTCCAGTGAAAAGTTCTTCTCCTTTACT GTCGGCAGTTATCACACGATCG
FP2	CGATCGTGTGATAACTGCCGAC AGTAAAGGAGAAGAACTTTTCACTGGAGT
RP2	GAATGAAGCTAACCTCCACCTTATCCCT TTTGTATAGTTCATCCATGCCATGT
FP3	GGATTACACATGGCATGGATGAACTATACAAA AGGGATAAGGTGGAGGTTAGCTTCATTC
Primers used for amplification of the OE-PCR final insert (fused fragment) into the *pJFRC28-10XUAS* vector	
FP	CGGGGTACCATGTCCTCCCGACGCAGCT (Acc65I restriction site)
RP	CTAGTCTAGACTAGGAGGTGCGGCACCG (XbaI restriction site)
Primers used for amplification of the OE-PCR final insert (fused fragment) into the *pCDH-CMV4* vector	
FP	CTAG TCTAGACAAAATGTCCTCCCGACGCAGCT (XbaI restriction site)
RP	CGG GGTACC CTAGGAGGTGCGGCACCG (Acc65I restriction site)
Primers for amplification of *sandman* cDNA in the *pENTR™ TOPO* vector (Gateway cloning)	
FP	CACC ATGTCCTCCCGACGCAGCT
RP	CTAGGAGGTGCGGCACCG
Primers for amplification of the untagged *sandman* fragment into the *pJFRC-MUH* vector	
FP	CGGGGTACCATGTCCTCCCGACGCAGCT (Acc65I restriction site)
RP	CTAGTCTAGACTAGGAGGTGCGGCACCG (XbaI restriction site)
Primers for incorporation of 2,3 or 4 gRNAs into the *pCFD6* vector for the generation of cell-specific CRISPR KO of *sandman*, *Toll-6* and *DNT1*. gRNA sequences are indicated in blue colour	
sandman	
CG8713_4X_F1	CGGCCCGGGTTCGATTCCCGGCCGATGCAGACAGGTAGAGCAAGAACAGGTTTCAGAGCTATGCTGGAAAC
CG8713_4X_R1	CTCGATATCCGAATCAGACTTGCACCAGCCGGGAATCGAACC
CG8713_4X_F2	AGTCTGATTCGGATATCGAGGTTTCAGAGCTATGCTGGAAAC
CG8713_4X_R2	CCGTCAACTCCCATATGCGGTGCACCAGCCGGGAATCGAACC
CG8713_4X_F3	CCGCATATGGGAGTTGACGGGTTTCAGAGCTATGCTGGAAAC

CG8713_4X_R3	ATTTTAACTTGCTATTTCTAGCTCTAAAACCACAGGATATACCTTTATTTTGCACCAGCC GGGAATCGAACC
CG8713_3X_F1	CGGCCCGGGTTCGATTCCCGGCCGATGCAGACAGGTAGAGCAAGAACAGGTTTCAGA GCTATGCTGGAAAC
CG8713_3X_R1	CTCGATATCCGAATCAGACTTGCACCAGCCGGGAATCGAACC
CG8713_3X_F2	AGTCTGATTCGGATATCGAGGTTTCAGAGCTATGCTGGAAAC
CG8713_3X_R2	ATTTTAACTTGCTATTTCTAGCTCTAAAACCCGTCAACTCCCATATGCGGTGCACCAGC CGGGAATCGAACC
CG8713_2X_F1	CGGCCCGGGTTCGATTCCCGGCCGATGCAGACAGGTAGAGCAAGAACAGGTTTCAGA GCTATGCTGGAAAC
CG8713_2X_R1	ATTTTAACTTGCTATTTCTAGCTCTAAAACCGTGGATATTCAGTACACCGTGCACCAGC CGGGAATCGAACC
Toll-6	
CG7250_4X_F1	CGGCCCGGGTTCGATTCCCGGCCGATGCAGGTGTTCTTATCGATCCAGGGTTTCAGA GCTATGCTGGAAAC
CG7250_4X_R1	CCGTGAATATGTACGCCACATGCACCAGCCGGGAATCGAACC
CG7250_4X_F2	TGTGGCGTACATATTCACGGGTTTCAGAGCTATGCTGGAAAC
CG7250_4X_R2	CGATGAATAATCTGCACACGTGCACCAGCCGGGAATCGAACC
CG7250_4X_F3	CGTGTGCAGATTATTCATCGGTTTCAGAGCTATGCTGGAAAC
CG7250_4X_R3	ATTTTAACTTGCTATTTCTAGCTCTAAAACCCCGGGTCAGATTGGTTTTGTGCACCAGC CGGGAATCGAACC
CG7250_3X_F1	CGGCCCGGGTTCGATTCCCGGCCGATGCAGGTGTTCTTATCGATCCAGGGTTTCAGA GCTATGCTGGAAAC
CG7250_3X_R1	CCGTGAATATGTACGCCACATGCACCAGCCGGGAATCGAACC
CG7250_3X_F2	TGTGGCGTACATATTCACGGGTTTCAGAGCTATGCTGGAAAC
CG7250_3X_R2	ATTTTAACTTGCTATTTCTAGCTCTAAAACCCCGGGTCAGATTGGTTTTGTGCACCAGC CGGGAATCGAACC
CG7250_2X_F1	CGGCCCGGGTTCGATTCCCGGCCGATGCAGGTGTTCTTATCGATCCAGGGTTTCAGA GCTATGCTGGAAAC
CG7250_2X_R1	ATTTTAACTTGCTATTTCTAGCTCTAAAACCCCGGGTCAGATTGGTTTTGTGCACCAGC CGGGAATCGAACC
DNT1	
CG42576_F1	CGGCCCGGGTTCGATTCCCGGCCGATGCAAAGTCCATCAGCTCATCGTGTTTCAGA GCTATGCTGGAAAC
CG42576_R1	CAGTAGAGACCTTTTTTGGC TGCACCAGCCGGGAATCGAACC
CG42576_F2	GCCAAAAAAGGTCTCTACTG GTTTCAGAGCTATGCTGGAAAC
CG42576_R2	CCCAAAAGTTGCTGCTCGGT TGCACCAGCCGGGAATCGAACC
CG42576_F3	ACCGAGCAGCAACTTTTGGG GTTTCAGAGCTATGCTGGAAAC
CG42576_R3	ATTTTAACTTGCTATTTCTAGCTCTAAAAC CGGCGCTGTTTCTTTGCAGA TGCACCAGCCGGGAATCGAACC
CG42576_3X_F1	CGGCCCGGGTTCGATTCCCGGCCGATGCAAAGTCCATCAGCTCATCGTGTTTCAGA GCTATGCTGGAAAC
CG42576_3X_R1	CAGTAGAGACCTTTTTTGGC TGCACCAGCCGGGAATCGAACC
CG42576_3X_F2	GCCAAAAAAGGTCTCTACTGGTTTCAGAGCTATGCTGGAAAC
CG42576_3X_R2	ATTTTAACTTGCTATTTCTAGCTCTAAAAC CGGCGCTGTTTCTTTGCAGA TGCACCAGCCGGGAATCGAACC
CG42576_2X_F1	CGGCCCGGGTTCGATTCCCGGCCGATGCAAAGTCCATCAGCTCATCGTGTTTCAGA GCTATGCTGGAAAC
CG42576_2X_R1	ATTTTAACTTGCTATTTCTAGCTCTAAAAC CCCAAAAGTTGCTGCTCGGTTGCACCAGCCGGGAATCGAACC

Primers for verification of transgenes by sequencing	
sandman_seq 1	ATGTCCTCCCGACGC
sandman_seq 2	ACTGCCGACAGGGAT
pHluorin_seq	AGTAAAGGAGAAGAACTT
GFP_seq	GGAGTACAACTACACAGCC
Venus_seq	GTGAGCAAGGGCGAGGAGC
pUASt_seq	CGAAAGAACCTGGTACATC
pJFRC28-10XUAS_seq	CGAAAGAACCTGGTACATC
pJFRC-MUH	CGAAAGAACCTGGTACATC
CMV_seq	CAGGAAACAGCTATGACC
pCFD6_seq	GTAGACATCAAGCATCGGTGG

References

The Alliance of Genome Resources: Building a Modern Data Ecosystem for Model Organism Databases. (2019). *Genetics*, *213*(4), 1189-1196. https://doi.org/10.1534/genetics.119.302523

Andretic, R., van Swinderen, B., & Greenspan, R. J. (2005). Dopaminergic modulation of arousal in Drosophila. *Curr Biol*, *15*(13), 1165-1175. https://doi.org/10.1016/j.cub.2005.05.025

Ashby, M. C., Ibaraki, K., & Henley, J. M. (2004). It's green outside: tracking cell surface proteins with pH-sensitive GFP. *Trends Neurosci*, *27*(5), 257-261. https://doi.org/10.1016/j.tins.2004.03.010

Aston-Jones, G., & Bloom, F. E. (1981). Activity of norepinephrine-containing locus coeruleus neurons in behaving rats anticipates fluctuations in the sleep-waking cycle. *J Neurosci*, *1*(8), 876-886. https://doi.org/10.1523/jneurosci.01-08-00876.1981

Bachmann, V., Klein, C., Bodenmann, S., Schafer, N., Berger, W., Brugger, P., & Landolt, H. P. (2012). The BDNF Val66Met polymorphism modulates sleep intensity: EEG frequency- and state-specificity. *Sleep*, *35*(3), 335-344. https://doi.org/10.5665/sleep.1690

Benington, J. H., & Heller, H. C. (1995). Restoration of brain energy metabolism as the function of sleep. *Prog Neurobiol*, *45*(4), 347-360. https://doi.org/10.1016/0301-0082(94)00057-o

Besedovsky, L., Lange, T., & Haack, M. (2019). The Sleep-Immune Crosstalk in Health and Disease. *Physiol Rev*, *99*(3), 1325-1380. https://doi.org/10.1152/physrev.00010.2018

Bianco, A., Townsley, F. M., Greiss, S., Lang, K., & Chin, J. W. (2012). Expanding the genetic code of Drosophila melanogaster. *Nature Chemical Biology*, *8*(9), 748-750. https://doi.org/10.1038/nchembio.1043

Bischof, J., Maeda, R. K., Hediger, M., Karch, F., & Basler, K. (2007). An optimized transgenesis system for Drosophila using germ-line-specific C31 integrases. *Proceedings of the National Academy of Sciences*, *104*(9), 3312-3317. https://doi.org/10.1073/pnas.0611511104

Blum, I. D., Keles, M. F., Baz, E. S., Han, E., Park, K., Luu, S., Issa, H., Brown, M., Ho, M. C. W., Tabuchi, M., Liu, S., & Wu, M. N. (2021). Astroglial Calcium Signaling Encodes Sleep Need in Drosophila. *Curr Biol*, *31*(1), 150-162 e157. https://doi.org/10.1016/j.cub.2020.10.012

Borbély, A. A. (1982). A two process model of sleep regulation. *Human Neurobiology*, *1*(3), 195-204.

Borbély, A. A., Daan, S., Wirz-Justice, A., & Deboer, T. (2016). The two-process model of sleep regulation: a reappraisal. *J Sleep Res*, *25*(2), 131-143. https://doi.org/10.1111/jsr.12371

Brown, R. E., Basheer, R., McKenna, J. T., Strecker, R. E., & McCarley, R. W. (2012). Control of Sleep and Wakefulness. *Physiological Reviews*, *92*(3), 1087-1187. https://doi.org/10.1152/physrev.00032.2011

Bushey, D., Huber, R., Tononi, G., & Cirelli, C. (2007). Drosophila Hyperkinetic Mutants Have Reduced Sleep and Impaired Memory. *Journal of Neuroscience*, *27*(20), 5384-5393. https://doi.org/10.1523/jneurosci.0108-07.2007

Campbell, S. S., & Tobler, I. (1984). Animal sleep: a review of sleep duration across phylogeny. *Neurosci Biobehav Rev*, *8*(3), 269-300. https://doi.org/10.1016/0149-7634(84)90054-x

Chatterjee, A., Guo, J., Lee, H. S., & Schultz, P. G. (2013). A Genetically Encoded Fluorescent Probe in Mammalian Cells. *Journal of the American Chemical Society*, *135*(34), 12540-12543. https://doi.org/10.1021/ja4059553

Cirelli, C., Bushey, D., Hill, S., Huber, R., Kreber, R., Ganetzky, B., & Tononi, G. (2005). Reduced sleep in Drosophila Shaker mutants. *Nature*, *434*(7037), 1087-1092. https://doi.org/10.1038/nature03486

Cirelli, C., Pompeiano, M., & Tononi, G. (1996). Neuronal gene expression in the waking state: a role for the locus coeruleus. *Science*, *274*(5290), 1211-1215. https://doi.org/10.1126/science.274.5290.1211

Cirelli, C., & Tononi, G. (2000). Gene expression in the brain across the sleep-waking cycle. *Brain Res*, *885*(2), 303-321. https://doi.org/10.1016/s0006-8993(00)03008-0

Citri, A., & Malenka, R. C. (2008). Synaptic Plasticity: Multiple Forms, Functions, and Mechanisms. *Neuropsychopharmacology*, *33*(1), 18-41. https://doi.org/10.1038/sj.npp.1301559
Crocker, A., & Sehgal, A. (2008). Octopamine Regulates Sleep in Drosophila through Protein Kinase A-Dependent Mechanisms. *Journal of Neuroscience*, *28*(38), 9377-9385. https://doi.org/10.1523/jneurosci.3072-08a.2008
Crocker, A., Shahidullah, M., Levitan, I. B., & Sehgal, A. (2010). Identification of a neural circuit that underlies the effects of octopamine on sleep:wake behavior. *Neuron*, *65*(5), 670-681. https://doi.org/10.1016/j.neuron.2010.01.032
Daan, S., Beersma, D. G., & Borbely, A. A. (1984). Timing of human sleep: recovery process gated by a circadian pacemaker. *American journal of physiology. Regulatory, integrative and comparative physiology*, *246*(2), 161-183. https://doi.org/10.1152/ajpregu.1984.246.2.R161
De Vivo, L., Bellesi, M., Marshall, W., Bushong, E. A., Ellisman, M. H., Tononi, G., & Cirelli, C. (2017). Ultrastructural evidence for synaptic scaling across the wake/sleep cycle. *Science*, *355*(6324), 507-510. https://doi.org/10.1126/science.aah5982
DeLotto, Y., & DeLotto, R. (1998). Proteolytic processing of the Drosophila Spatzle protein by easter generates a dimeric NGF-like molecule with ventralising activity. *Mech Dev*, *72*(1-2), 141-148. https://doi.org/10.1016/s0925-4773(98)00024-0
Diering, G. H., Nirujogi, R. S., Roth, R. H., Worley, P. F., Pandey, A., & Huganir, R. L. (2017). Homer1a drives homeostatic scaling-down of excitatory synapses during sleep. *Science*, *355*(6324), 511-515. https://doi.org/10.1126/science.aai8355
Dissel, S., Klose, M. K., van Swinderen, B., Cao, L., & Shaw, P. J. (2021). Sleep promoting neurons remodel their response properties to calibrate sleep drive with environmental demands. *bioRxiv*, 2021.2011.2005.467459. https://doi.org/10.1101/2021.11.05.467459
Donlea, J. M., Pimentel, D., & Miesenbock, G. (2014). Neuronal machinery of sleep homeostasis in Drosophila. *Neuron*, *81*(4), 860-872. https://doi.org/10.1016/j.neuron.2013.12.013
Donlea, J. M., Pimentel, D., Talbot, C. B., Kempf, A., Omoto, J. J., Hartenstein, V., & Miesenbock, G. (2018). Recurrent Circuitry for Balancing Sleep Need and Sleep. *Neuron*, *97*(2), 378-389 e374. https://doi.org/10.1016/j.neuron.2017.12.016
Donlea, J. M., Thimgan, M. S., Suzuki, Y., Gottschalk, L., & Shaw, P. J. (2011). Inducing sleep by remote control facilitates memory consolidation in Drosophila. *Science*, *332*(6037), 1571-1576. https://doi.org/10.1126/science.1202249
Dubowy, C., & Sehgal, A. (2017). Circadian Rhythms and Sleep in Drosophila melanogaster. *Genetics*, *205*(4), 1373-1397. https://doi.org/10.1534/genetics.115.185157
Eijk, P. J. V. d., & Hulskamp, M. (2019). Éditions de la Sorbonne. In: Éditions de la Sorbonne.
Enyedi, P., & Czirják, G. (2010). Molecular Background of Leak K+ Currents: Two-Pore Domain Potassium Channels. *Physiological Reviews*, *90*(2), 559-605. https://doi.org/10.1152/physrev.00029.2009
Faraguna, U., Vyazovskiy, V. V., Nelson, A. B., Tononi, G., & Cirelli, C. (2008). A Causal Role for Brain-Derived Neurotrophic Factor in the Homeostatic Regulation of Sleep. *Journal of Neuroscience*, *28*(15), 4088-4095. https://doi.org/10.1523/jneurosci.5510-07.2008
Foldi, I., Anthoney, N., Harrison, N., Gangloff, M., Verstak, B., Nallasivan, M. P., Alahmed, S., Zhu, B., Phizacklea, M., Losada-Perez, M., Moreira, M., Gay, N. J., & Hidalgo, A. (2017). Three-tier regulation of cell number plasticity by neurotrophins and Tolls in Drosophila. *Journal of Cell Biology*, *216*(5), 1421-1438. https://doi.org/10.1083/jcb.201607098
Hablitz, L. M., Vinitsky, H. S., Sun, Q., Stæger, F. F., Sigurdsson, B., Mortensen, K. N., Lilius, T. O., & Nedergaard, M. (2019). Increased glymphatic influx is correlated with high EEG delta power and low heart rate in mice under anesthesia. *Sci Adv*, *5*(2), eaav5447. https://doi.org/10.1126/sciadv.aav5447
Halassa, M. M., Florian, C., Fellin, T., Munoz, J. R., Lee, S.-Y., Abel, T., Haydon, P. G., & Frank, M. G. (2009). Astrocytic modulation of sleep homeostasis and cognitive consequences of sleep loss. *Neuron*, *61*(2), 213-219. https://doi.org/10.1016/j.neuron.2008.11.024
Hendricks, J. C., Finn, S. M., Panckeri, K. A., Chavkin, J., Williams, J. A., Sehgal, A., & Pack, A. I. (2000). Rest in Drosophila is a sleep-like state. *Neuron*, *25*(1), 129-138. https://doi.org/10.1016/s0896-6273(00)80877-6

Hill, V. M., O'Connor, R. M., Sissoko, G. B., Irobunda, I. S., Leong, S., Canman, J. C., Stavropoulos, N., & Shirasu-Hiza, M. (2018). A bidirectional relationship between sleep and oxidative stress in Drosophila. *PLoS Biology*, *16*(7), e2005206. https://doi.org/10.1371/journal.pbio.2005206

Huang, S., Piao, C., Beuschel, C. B., Gotz, T., & Sigrist, S. J. (2020). Presynaptic Active Zone Plasticity Encodes Sleep Need in Drosophila. *Curr Biol*, *30*(6), 1077-1091 e1075. https://doi.org/10.1016/j.cub.2020.01.019

Huber, R., Felice Ghilardi, M., Massimini, M., & Tononi, G. (2004). Local sleep and learning. *Nature*, *430*(6995), 78-81. https://doi.org/10.1038/nature02663

Huber, R., Ghilardi, M. F., Massimini, M., Ferrarelli, F., Riedner, B. A., Peterson, M. J., & Tononi, G. (2006). Arm immobilization causes cortical plastic changes and locally decreases sleep slow wave activity. *Nature Neuroscience*, *9*(9), 1169-1176. https://doi.org/10.1038/nn1758

Huber, R., Tononi, G., & Cirelli, C. (2007). Exploratory behavior, cortical BDNF expression, and sleep homeostasis. *Sleep*, *30*(2), 129-139. https://doi.org/10.1093/sleep/30.2.129

Hulse, B. K., Haberkern, H., Franconville, R., Turner-Evans, D. B., Takemura, S., Wolff, T., Noorman, M., Dreher, M., Dan, C., Parekh, R., Hermundstad, A. M., Rubin, G. M., & Jayaraman, V. (2020). A connectome of the Drosophila central complex reveals network motifs suitable for flexible navigation and context-dependent action selection. *bioRxiv*, 2020.2012.2008.413955. https://doi.org/10.1101/2020.12.08.413955

Ishimori, K. (1909). True cause of sleep: a hypnogenic substance as evidenced in the brain of sleep-deprived animals. *Tokyo Igakkai Zasshi*, *23*, 429-457.

Jaaro, H., Beck, G., Conticello, S. G., & Fainzilber, M. (2001). Evolving better brains: a need for neurotrophins? *Trends Neurosci*, *24*(2), 79-85. https://doi.org/10.1016/s0166-2236(00)01690-8

Jinek, M., Chylinski, K., Fonfara, I., Hauer, M., Doudna, J. A., & Charpentier, E. (2012). A Programmable Dual-RNA-Guided DNA Endonuclease in Adaptive Bacterial Immunity. *Science*, *337*(6096), 816-821. https://doi.org/10.1126/science.1225829

Keene, A. C., & Duboue, E. R. (2018). The origins and evolution of sleep. *Journal of Experimental Biology*, *221*(11), jeb159533. https://doi.org/10.1242/jeb.159533

Kempf, A., Song, S. M., Talbot, C. B., & Miesenböck, G. (2019). A potassium channel β-subunit couples mitochondrial electron transport to sleep. *Nature*, *568*(7751), 230-234. https://doi.org/10.1038/s41586-019-1034-5

Koh, K., Evans, J. M., Hendricks, J. C., & Sehgal, A. (2006). A Drosophila model for age-associated changes in sleep:wake cycles. *Proc Natl Acad Sci U S A*, *103*(37), 13843-13847. https://doi.org/10.1073/pnas.0605903103

Kubota, K. (1989). Kuniomi Ishimori and the first discovery of sleep-inducing substances in the brain. *Neurosci Res*, *6*(6), 497-518. https://doi.org/10.1016/0168-0102(89)90041-2

Kume, K. (2005). Dopamine Is a Regulator of Arousal in the Fruit Fly. *Journal of Neuroscience*, *25*(32), 7377-7384. https://doi.org/10.1523/jneurosci.2048-05.2005

Legendre, R., & Piéron, H. (1907). *Les rapports entre les conditions physiologiques et les modifications histologiques des cellules cérébrales dans l'insomnie expérimentale*. Masson et Cie, éditeurs.

Liu, Q., Liu, S., Kodama, L., Maria, & Mark. (2012). Two Dopaminergic Neurons Signal to the Dorsal Fan-Shaped Body to Promote Wakefulness in Drosophila. *Current Biology*, *22*(22), 2114-2123. https://doi.org/10.1016/j.cub.2012.09.008

Liu, S., Liu, Q., Tabuchi, M., & Wu, M. N. (2016). Sleep Drive Is Encoded by Neural Plastic Changes in a Dedicated Circuit. *Cell*, *165*(6), 1347-1360. https://doi.org/10.1016/j.cell.2016.04.013

Lucretius Carus, T., Rouse, W. H. D., & Smith, M. F. (1924). *On the nature of things* (New ed. ed.). Harvard University Press.

Mao, Z., & Davis, R. L. (2009). Eight different types of dopaminergic neurons innervate the Drosophila mushroom body neuropil: anatomical and physiological heterogeneity. *Front Neural Circuits*, *3*, 5. https://doi.org/10.3389/neuro.04.005.2009

Mathie, A., Rees, K. A., El Hachmane, M. F., & Veale, E. L. (2010). Trafficking of neuronal two pore domain potassium channels. *Curr Neuropharmacol*, *8*(3), 276-286. https://doi.org/10.2174/157015910792246146

McIlroy, G., Foldi, I., Aurikko, J., Wentzell, J. S., Lim, M. A., Fenton, J. C., Gay, N. J., & Hidalgo, A. (2013). Toll-6 and Toll-7 function as neurotrophin receptors in the Drosophila melanogaster CNS. *Nature Neuroscience*, *16*(9), 1248-1256. https://doi.org/10.1038/nn.3474

Miesenböck, G., De Angelis, D. A., & Rothman, J. E. (1998). Visualizing secretion and synaptic transmission with pH-sensitive green fluorescent proteins. *Nature*, *394*(6689), 192-195. https://doi.org/10.1038/28190

Mizuguchi, K., Parker, J. S., Blundell, T. L., & Gay, N. J. (1998). Getting knotted: a model for the structure and activation of Spatzle. *Trends Biochem Sci*, *23*(7), 239-242. https://doi.org/10.1016/s0968-0004(98)01216-x

Nelson, M. D., & Fitch, D. H. A. (2012). Overlap Extension PCR: An Efficient Method for Transgene Construction. In (pp. 459-470). Humana Press. https://doi.org/10.1007/978-1-61779-228-1_27

Ni, J. D., Gurav, A. S., Liu, W., Ogunmowo, T. H., Hackbart, H., Elsheikh, A., Verdegaal, A. A., & Montell, C. (2019). Differential regulation of the Drosophila sleep homeostat by circadian and arousal inputs. *eLife*, *8*. https://doi.org/10.7554/elife.40487

Paré, A. C., Vichas, A., Fincher, C. T., Mirman, Z., Farrell, D. L., Mainieri, A., & Zallen, J. A. (2014). A positional Toll receptor code directs convergent extension in Drosophila. *Nature*, *515*(7528), 523-527. https://doi.org/10.1038/nature13953

Pimentel, D., Donlea, J. M., Talbot, C. B., Song, S. M., Thurston, A. J. F., & Miesenböck, G. (2016). Operation of a homeostatic sleep switch. *Nature*, *536*(7616), 333-337. https://doi.org/10.1038/nature19055

Port, F., & Bullock, S. L. (2016). Augmenting CRISPR applications in Drosophila with tRNA-flanked sgRNAs. *Nature Methods*, *13*(10), 852-854. https://doi.org/10.1038/nmeth.3972

Port, F., Strein, C., Stricker, M., Rauscher, B., Heigwer, F., Zhou, J., Beyersdörffer, C., Frei, J., Hess, A., Kern, K., Lange, L., Langner, N., Malamud, R., Pavlović, B., Rädecke, K., Schmitt, L., Voos, L., Valentini, E., & Boutros, M. (2020). A large-scale resource for tissue-specific CRISPR mutagenesis in Drosophila. *eLife*, *9*. https://doi.org/10.7554/elife.53865

Raccuglia, D., Huang, S., Ender, A., Heim, M. M., Laber, D., Suárez-Grimalt, R., Liotta, A., Sigrist, S. J., Geiger, J. R. P., & Owald, D. (2019). Network-Specific Synchronization of Electrical Slow-Wave Oscillations Regulates Sleep Drive in Drosophila. *Current Biology*, *29*(21), 3611-3621.e3613. https://doi.org/10.1016/j.cub.2019.08.070

Ran, F. A., Hsu, P. D., Wright, J., Agarwala, V., Scott, D. A., & Zhang, F. (2013). Genome engineering using the CRISPR-Cas9 system. *Nature Protocols*, *8*(11), 2281-2308. https://doi.org/10.1038/nprot.2013.143

Reichardt, L. F. (2006). Neurotrophin-regulated signalling pathways. *Philos Trans R Soc Lond B Biol Sci*, *361*(1473), 1545-1564. https://doi.org/10.1098/rstb.2006.1894

Reimund, E. (1994). The free radical flux theory of sleep. *Med Hypotheses*, *43*(4), 231-233. https://doi.org/10.1016/0306-9877(94)90071-x

Roos, A., & Boron, W. F. (1981). Intracellular pH. *Physiol Rev*, *61*(2), 296-434. https://doi.org/10.1152/physrev.1981.61.2.296

Rubin, G. M., Yandell, M. D., Wortman, J. R., Gabor Miklos, G. L., Nelson, C. R., Hariharan, I. K., Fortini, M. E., Li, P. W., Apweiler, R., Fleischmann, W., Cherry, J. M., Henikoff, S., Skupski, M. P., Misra, S., Ashburner, M., Birney, E., Boguski, M. S., Brody, T., Brokstein, P., . . . Lewis, S. (2000). Comparative genomics of the eukaryotes. *Science*, *287*(5461), 2204-2215. https://doi.org/10.1126/science.287.5461.2204

Sankaranarayanan, S., De Angelis, D., Rothman, J. E., & Ryan, T. A. (2000). The Use of pHluorins for Optical Measurements of Presynaptic Activity. *Biophysical Journal*, *79*(4), 2199-2208. https://doi.org/10.1016/s0006-3495(00)76468-x

Sankaranarayanan, S., & Ryan, T. A. (2000). Real-time measurements of vesicle-SNARE recycling in synapses of the central nervous system. *Nat Cell Biol*, *2*(4), 197-204. https://doi.org/10.1038/35008615

Saper, C. B., Fuller, P. M., Pedersen, N. P., Lu, J., & Scammell, T. E. (2010). Sleep state switching. *Neuron*, *68*(6), 1023-1042. https://doi.org/10.1016/j.neuron.2010.11.032

Shaw, P. J., Cirelli, C., Greenspan, R. J., & Tononi, G. (2000). Correlates of sleep and waking in Drosophila melanogaster. *Science*, *287*(5459), 1834-1837. https://doi.org/10.1126/science.287.5459.1834

Sherin, J. E., Elmquist, J. K., Torrealba, F., & Saper, C. B. (1998). Innervation of Histaminergic Tuberomammillary Neurons by GABAergic and Galaninergic Neurons in the Ventrolateral Preoptic Nucleus of the Rat. *The Journal of Neuroscience*, *18*(12), 4705-4721. https://doi.org/10.1523/jneurosci.18-12-04705.1998

Siegel, J. M. (2005). Clues to the functions of mammalian sleep. *Nature*, *437*(7063), 1264-1271. https://doi.org/10.1038/nature04285

Singh, P., & Donlea, J. M. (2020). Bidirectional Regulation of Sleep and Synapse Pruning after Neural Injury. *Curr Biol*, *30*(6), 1063-1076 e1063. https://doi.org/10.1016/j.cub.2019.12.065

Stanhope, B. A., Jaggard, J. B., Gratton, M., Brown, E. B., & Keene, A. C. (2020). Sleep Regulates Glial Plasticity and Expression of the Engulfment Receptor Draper Following Neural Injury. *Curr Biol*, *30*(6), 1092-1101 e1093. https://doi.org/10.1016/j.cub.2020.02.057

Svoboda, P. (2020). Key Mechanistic Principles and Considerations Concerning RNA Interference. *Front Plant Sci*, *11*, 1237. https://doi.org/10.3389/fpls.2020.01237

Tononi, G., & Cirelli, C. (2003). Sleep and synaptic homeostasis: a hypothesis. *Brain Res Bull*, *62*(2), 143-150. https://doi.org/10.1016/j.brainresbull.2003.09.004

Tononi, G., & Cirelli, C. (2014). Sleep and the Price of Plasticity: From Synaptic and Cellular Homeostasis to Memory Consolidation and Integration. *Neuron*, *81*(1), 12-34. https://doi.org/10.1016/j.neuron.2013.12.025

Tononi, G., & Cirelli, C. (2020). Sleep and synaptic down-selection. *European Journal of Neuroscience*, *51*(1), 413-421. https://doi.org/10.1111/ejn.14335

Ueno, T., Tomita, J., Tanimoto, H., Endo, K., Ito, K., Kume, S., & Kume, K. (2012). Identification of a dopamine pathway that regulates sleep and arousal in Drosophila. *Nature Neuroscience*, *15*(11), 1516-1523. https://doi.org/10.1038/nn.3238

Ulian-Benitez, S., Bishop, S., Foldi, I., Wentzell, J., Okenwa, C., Forero, M. G., Zhu, B., Moreira, M., Phizacklea, M., McIlroy, G., Li, G., Gay, N. J., & Hidalgo, A. (2017). Kek-6: A truncated-Trk-like receptor for Drosophila neurotrophin 2 regulates structural synaptic plasticity. *PLOS Genetics*, *13*(8), e1006968. https://doi.org/10.1371/journal.pgen.1006968

Vaccaro, A., Kaplan Dor, Y., Nambara, K., Pollina, E. A., Lin, C., Greenberg, M. E., & Rogulja, D. (2020). Sleep Loss Can Cause Death through Accumulation of Reactive Oxygen Species in the Gut. *Cell*, *181*(6), 1307-1328.e1315. https://doi.org/10.1016/j.cell.2020.04.049

Vyazovskiy, V. V., Cirelli, C., Pfister-Genskow, M., Faraguna, U., & Tononi, G. (2008). Molecular and electrophysiological evidence for net synaptic potentiation in wake and depression in sleep. *Nature Neuroscience*, *11*(2), 200-208. https://doi.org/10.1038/nn2035

Wang, L., Brock, A., Herberich, B., & Schultz, P. G. (2001). Expanding the Genetic Code of Escherichia coli. *Science*, *292*(5516), 498-500. https://doi.org/10.1126/science.1060077

Xie, K., Minkenberg, B., & Yang, Y. (2015). Boosting CRISPR/Cas9 multiplex editing capability with the endogenous tRNA-processing system. *Proceedings of the National Academy of Sciences*, *112*(11), 3570-3575. https://doi.org/10.1073/pnas.1420294112

Xie, L., Kang, H., Xu, Q., Chen, M. J., Liao, Y., Thiyagarajan, M., O'Donnell, J., Christensen, D. J., Nicholson, C., Iliff, J. J., Takano, T., Deane, R., & Nedergaard, M. (2013). Sleep drives metabolite clearance from the adult brain. *Science*, *342*(6156), 373-377. https://doi.org/10.1126/science.1241224

Yamauchi, J., Chan, J. R., & Shooter, E. M. (2003). Neurotrophin 3 activation of TrkC induces Schwann cell migration through the c-Jun N-terminal kinase pathway. *Proceedings of the National Academy of Sciences*, *100*(24), 14421-14426. https://doi.org/10.1073/pnas.2336152100

Yamauchi, J., Chan, J. R., & Shooter, E. M. (2004). Neurotrophins regulate Schwann cell migration by activating divergent signaling pathways dependent on Rho GTPases. *Proceedings of the*

National Academy of Sciences, *101*(23), 8774-8779. https://doi.org/10.1073/pnas.0402795101

Zhu, B., Pennack, J. A., McQuilton, P., Forero, M. G., Mizuguchi, K., Sutcliffe, B., Gu, C.-J., Fenton, J. C., & Hidalgo, A. (2008). Drosophila Neurotrophins Reveal a Common Mechanism for Nervous System Formation. *PLoS Biology*, *6*(11), e284. https://doi.org/10.1371/journal.pbio.0060284

Zuniga, L., & Zuniga, R. (2016). Understanding the Cap Structure in K2P Channels. *Front Physiol*, *7*, 228. https://doi.org/10.3389/fphys.2016.00228